Universidad
Rey Juan Carlos

Departamento de Biología y Geología, Física y Química Inorgánica

TESIS DOCTORAL

Unpredictability and Fractality in Nonlinear Dynamics

Álvar Daza Esteban
Universidad Rey Juan Carlos

May, 2016

Miguel Ángel Fernández Sanjuán, Catedrático de Física y
Alexandre Wagemakers, Profesor Contratado Doctor de Física

CERTIFICAN:

Que la presente memoria de tesis doctoral, titulada *"Unpredictability and Fractality in Nonlinear Dynamics"*, ha sido realizada bajo nuestra dirección por Álvar Daza Esteban para optar al grado de Doctor por la Universidad Rey Juan Carlos.

Y para que conste que la citada tesis reune todos los requisitos necesarios para su defensa y aprobación, firmamos el presente certificado en Móstoles a veinte de mayo de dos mil dieciséis.

Móstoles, 20 de mayo de 2016

Fdo. Miguel Ángel Fernández Sanjuán
Catedrático de Física
Universidad Rey Juan Carlos

Fdo. Alexandre Wagemakers
Profesor Contratado Doctor de Física
Universidad Rey Juan Carlos

A mis padres, que me enseñaron a dudar y, al mismo tiempo, me dieron las certezas más firmes.

Agradecimientos

Esta tesis doctoral es la suma (no lineal) de los esfuerzos de muchas personas, a quienes quiero dar las gracias en estas líneas.

Primeramente, a mis directores de tesis los Profs. *Miguel Ángel Fernández Sanjuán* y *Alexandre Wagemakers*, que con su trabajo han sabido encauzar los míos de la mejor manera posible. Cada uno a su modo, ambos me han enseñado muchas lecciones valiosas sobre ciencia, investigación y docencia, así como otras lecciones que considero aún más importantes y que no pertenecen a ninguna de las categorías anteriores.

Quiero expresar también mi más sincero agradecimiento a los Profs. *Bertrand Georgeot* y *David Guéry-Odelin* por haberme ofrecido la oportunidad única de aprender con ellos durante mi estancia en el Institut de Recherche sur les Systèmes Atomiques et Moléculaires Complexes, de la Université Paul Sabatier de Toulouse. El fructífero intercambio de ideas desde diferentes perspectivas que tuvo lugar durante aquellos meses propició algunos de los resultados más interesantes de esta tesis: merci beaucoup.

No puede faltar un agradecimiento muy especial para mi compañero y hermano en esta empresa, *Álvaro García López.* Sin él esta tesis no habría sido lo que es hoy y, sobre todo, el camino habría sido mucho más aburrido. Espero que sigamos siendo eternos becarios, aunque sea de espíritu.

Gracias también a todos mis compañeros del grupo de Dinámica No lineal, Teoría del Caos y Sistemas Complejos de la URJC. Gracias por su apoyo constante, por las impagables discusiones y por hacer estimulante lo cotidiano. En particular, la bibliografía de esta tesis no habría sido posible sin la ayuda de *Juan Sabuco.* Muchas gracias por ayudarme con tu tiempo a ahorrar el mío.

Por supuesto, a quien más tengo que dar las gracias es a mi familia, en especial a mis padres *Juan* y *Elisa* y a mi tía *Inés*, por todo lo que han hecho por mí, no sólo durante la tesis, sino en cada uno de los pasos que me han llevado hasta ella. No obstante, quizá por lo que más agradecido les estoy es porque sé que no hace falta que se lo agradezca.

Siguiendo con los agradecimientos a las personas que son más importantes para mí, es turno de dar las gracias a *Marta.* Baste decir que algunas cosas se entienden solamente como parte de algo más amplio, y así esta tesis no podría concebirse sin ella.

Aunque es imposible agradecer aquí a todas las demás personas que de alguna manera han contribuido a esta tesis, quiero acordarme de mis amigos (San Martín

de Rubiales fue la cuna de algunas discusiones que aparecen en la tesis), compañeros (ojalá hubiera podido leer tu tesis *Diego*) y profesores (a los buenos por enseñarme, a los no tan buenos por enseñarme a perseverar).

Por último, es obligado mencionar que las investigaciones llevadas a cabo en esta tesis se han realizado bajo la financiación de los proyectos FIS2009-098981 del Ministerio de Ciencia e Innovación y FIS2013-40653-P del Ministerio de Economía y Competitividad. Además, la estancia de investigación en el Institut de Recherche sur les Systèmes Atomiques et Moléculaires Complexes, de la Université Paul Sabatier en Toulouse fue posible gracias a los fondos del Programme Investissements d'Avenir bajo los programas ANR-11-IDEX-0002-02 y ANR-10-LABX-0037-NEXT.

Mayo, 2016
Álvar Daza Esteban

Preface

"Communication across the revolutionary divide is inevitably partial."
-Thomas S. Kuhn, *The structure of scientific revolutions*

This thesis has been developed during the years in the research group on Nonlinear Dynamics, Chaos Theory and Complex Systems of the URJC. Its main purpose is the study of the unpredictability in chaotic dynamics. Despite the utilization of specific dynamical systems, one of the ambitions of the present thesis has been to find global results and techniques useful for a broad community of scientists. After an introductory chapter preparing the general framework, my investigations are collected in chapters that correspond to different research articles. This thesis is eminently nonlinear, both in its content and in its structure. The different topics are interwoven, connected by feedback loops in such a way that the contents does not follow a straight path, but a dendritic growth conveys a more accurate picture of its development. Here is a brief summary of each chapter:

Chapter 1. Introduction
The introductory chapter lays the foundations for the thesis. First, the limits imposed by scientific knowledge are discussed and the history of unpredictability in the Physics of the 20th century is revised. Afterwards, concepts like chaos, fractals, delayed systems and dissipative structures are briefly introduced. These ideas are constantly invoked and revisited along the whole thesis.

Chapter 2. Vibrational resonance in a time-delayed genetic toggle switch
The second chapter is devoted to study the effects of external periodic perturbations in a nonlinear system with applications to *systems biology*. In particular, we investigate the *vibrational resonance* in a genetic network motif known as toggle switch, considering also the possible delays. We show how a low-frequency external signal can be enhanced by means of a high-frequency perturbation provoking the effect known as *vibrational resonance*. The role of different parameters is analyzed, as

well as their importance in the biological context. The delay, which arises naturally as a consequence of the biochemical processes involved, plays a fundamental role in the dynamics of the system. Some of the early results concerning delay and basins of attraction paved the way for the investigations presented in subsequent chapters.

Chapter 3. Ultrasensitive vibrational resonance

In *vibrational resonance*, the enhancement of the low-frequency signal is possible thanks to a high-frequency perturbation with a large amplitude, which in most of the cases is even larger than the signal itself. We present a novel phenomenon called *ultrasensitive vibrational resonance*, where a very small perturbation is able to amplify the signal in a striking manner. We first found this resonance mechanism in systems with delay, but the final cause of this behavior is related to fractal basins of attraction. The fractal structures in phase space provoke a fractal pattern of resonances and allow such small perturbations to increase the response exceptionally.

Chapter 4. Testing for Wada basins

Fractal objects allow inconceivable situations for Euclidean geometry. This is the case of Wada boundaries, where three or more sets share the same boundary. At first, this could seem a topological curiosity, but Wada boundaries are very common in escape basins and basins of attraction of chaotic dynamical systems. Small perturbations near Wada boundaries can drive the system to any of the possible final states, which implies a special case of unpredictability. In this chapter, we introduce a new quantitative method to test the Wada property, that also enables the classification of partial Wada basins. Examples of application and computational features are detailed as well.

Chapter 5. Wada property in systems with delay

As announced in previous chapters, delay can induce fractal basins of attraction. These basins are infinite dimensional because delay differential equations need history functions that account for the past states of the system. We show that, in these infinite dimensional basins of attraction, delay can induce not only fractal structures, but also the Wada property. At the same time, delayed systems provide a great example of application of our method to test Wada basins, introduced in Chapter 4.

Chapter 6. Basin entropy

Wada basins are often said to be more unpredictable than fractal basins which do not have the Wada property, but how can we measure the *unpredictability* of the basins? We try to answer this simple question by introducing the concept of *basin entropy*, which is the result of the application of information entropy to the basins. Making some simple assumptions we are able to dissect the different factors that contribute to the unpredictability of dynamical systems, compare the unpredictability for different parameter values and even detect fractal boundaries at a given scale with the $\log 2$ criterion.

Chapter 7. Chaotic dynamics of propagating matter waves

The theory developed in Chapter 6 is applied to a model used in the context of propagating matter waves. We illustrate how we could prove both fractality and the Wada property in real experiments using the basin entropy. Other techniques used in nonlinear dynamics, like basin stability and survival probability, also give useful information concerning the experimental setup.

Chapter 8. Conclusions.

The thesis ends with a schematic discussion of the main results in English and then in Spanish. The different chapters are summarized and the methodology is briefly explained.

Contents

Chapter 1
Introduction

"It is wrong to think that the task of physics is to find out how nature is. Physics concerns what we can say about nature."

-Niels Bohr

1.1 Edge of science

In the task of naming, humans have chosen to designate ourselves by the term *homo sapiens* (man that knows), and sometimes also *homo sapiens sapiens* (man that knows that knows). This is as much as to say that we define ourselves through knowledge. We are proud of being self-conscious matter; knowledge is our best advantage to survive and we consider it as our most distinctive feature. But as it usually happens with most of the fundamental concepts, knowledge is hard to define. Allow me to turn to the literature and use a classification scheme of knowledge devised by the Spanish physicist Jorge Wagensberg.

Jorge Wagensberg defines knowledge as every mental representation of reality that can be transmitted to others by non-genetic means. Attending to how it is obtained, knowledge can be classified into three groups: revealed, artistic and scientific. Revealed knowledge assumes the existence of *someone* or *something* that possesses all knowledge, and also assumes that sometimes part of this knowledge is somehow communicated to us. This is the kind of knowledge provided by religion or superstition. Artistic knowledge is based on the belief that some infinite complexities can be transmitted through finite representations, as a painting or a sculpture. Scientific knowledge, for its part, lays on the prosecution of three goals: objectivity, intelligibility and dialectic experimentation. Each kind of knowledge is fundamental to understand the essence of humanity and its history. This thesis aims to be considered itself as a contribution to scientific knowledge and, at the same time, it is devoted to the exploration of some of the limits of the scientific knowledge itself.

Figure 1.1. Solvay conference of 1911. Some of the scientists that revolutionized our perception of nature, like Planck, Einstein and Poincaré, are photographed.

A differential characteristic of science with respect to art or religion is its ability to provide models of behavior of nature. Those scientific models and their predictions are successfully tested everyday. Thanks to scientific knowledge we are able to forecast the weather, anticipate the position of celestial bodies or understand the behavior of microscopic particles. A kind of knowledge completely inaccessible to religion or art. Nevertheless, weather forecasts often fail, the information of celestial bodies must be constantly updated and corrected and microscopic particles exhibit erratic movements. This contradiction is only apparent: the failure of some predictions do not mean the failure of the scientific method, but the practice of science sets the boundary between what is known and the unknown.

Probably we often focus into the rigorous methods of science to put into relief the different nature of scientific knowledge with respect to the artistic and revealed means of acquiring knowledge. We praise the unique power of science to explain reality, to predict it and to transform it using technology. Doubtlessly, some of the greatest achievements of humanity have been reached thanks to scientific knowledge. But science is wise enough to know that it cannot know everything, and brave enough to explore its own limits. The best proof of that is the development of Physics in the 20th century.

In the history of Physics, the last century will be remembered, among other breakthroughs, for the birth of quantum mechanics, relativity and chaos theory. Three huge revolutions for our comprehension of reality. But also three revolutions in our conception of predictability. These theories allowed us to grasp the behavior of nature at levels never seen before. However, every time that science sheds light into nature revealing its hidden shapes, the shadow of our ignorance gets longer.

Quantum mechanics, along with nuclear, atomic and particle physics unveiled the behavior of matter at tiny scales. Thanks to its advances we managed the power of the atoms, changing the world forever. However, one of the pillars of

quantum mechanics is the haphazard nature of matter in the microscopic world. The description of the particles requires probability functions instead of state variables. Another major aspect of the theory is the importance of the interaction between observer and experiment, which finds its maximum expression in the uncertainty principle of Heisenberg. We learned that we cannot measure with an arbitrarily high precision two conjugate variables at the same time, like position and momentum. Therefore, quantum mechanics augmented our knowledge of the surrounding reality and, at the same time, it revealed new restrictions to this knowledge.

If the world of the minuscule suffered a revolution in the last century, a comparable situation took place at the astronomic scale. Special relativity first, and general relativity later, changed our vision of the universe and its geometry. Einstein showed the intimate relation of space and time, and how both are shaped by gravity. The development of cosmology allowed us to infer the history of the universe until its very beginning (or almost). Nevertheless, a key idea of relativity is that the speed of light is finite, imposing an upper limit to how fast information can be transmitted. Once again, as science deepens into nature we find physical limitations.

The case of chaos theory is even more evident. It provided a new perspective for a plethora of different phenomena, from meteorology to population dynamics, showing how simple rules can give birth to extraordinary complex behaviors. One of the key revelations of chaos is that even in classical mechanics, the evolution of dynamical systems is often unpredictable. Further explanations on this topic are postponed.

At the light of the previous exposition, we can conclude that scientific knowledge is a double-edged sword. On the one hand, science opens new paths to master the surrounding reality. On the other hand, every time that a new path is found, others are closed. This thesis is devoted to the study of one of this limits, the unpredictability in Nonlinear Dynamics. As we will see, there is much to learn about this frontier of science and, surprisingly (or maybe not) we can also use it in our own benefit.

1.2 Scientific context

Once the general framework has been set, we will continue introducing briefly some of the concepts that will be used and developed along this thesis.

Chaos Theory

Among the three revolutions that happened in Physics in the previous century, chaos theory is probably the most recent. The pioneer work on the three-body problem by the French scientist Henri Poincaré dates back to 1890 [1], but it was not until the development of the first computers that we started to devise the physical consequences of this mathematical theory, namely thanks to the American meteorologist Edward Lorenz and his investigations on the atmospheric dynamics of 1963 [2]. The name of this emerging science was coined by two mathematicians, the Chinese-American

Tien-Yien Li and the American James A. Yorke, in their famous paper *Period three implies chaos* of 1975 [3]. Despite its novelty in science, the idea of chaos has ancient roots, as this text of Giordano Bruno of 1584 shows: "Now more than ever I realize that the smallest error in the beginning causes a maximum difference and fatal error at the end; one little drawback is countlessly multiplied branching infinitely, as from a small root arise large bulks and innumerable branches", (traslated from [4]). When James A. Yorke received the Japan Prize for his contributions to Chaos Theory with Benoît Mandelbrot in 2003, he also dedicated some words to remark that scientists were probably the last community to recognize the role of chaos in nature, since every single person knows that the world around us is chaotic and that small changes can provoke huge effects.

Nowadays, chaos still admits several technical definitions with slight differences[1]. However, a key underlying idea is common to them all: small uncertainties lead to large uncertainties in chaotic dynamics. This idea can be manifested in many different ways. For example, a common approach to chaotic dynamics is the use of Lyapunov exponents [6]. This mathematical tool measures the divergence of two nearby trajectories as time evolves. In chaotic dynamics, these divergences grow exponentially with time, so small uncertainties in the determination of the initial conditions lead to huge differences in the trajectories in a very short time.

Fractal Geometry

Another facet of chaos are fractal structures. The word fractal was first coined by the mathematician Benoît Mandelbrot [7], and it was no coincidence that the development of fractal geometry took place also in the 20th century. Technically, fractals are defined as geometrical objects with a Hausdorff-Besicovitch dimension larger than their topological dimension. Intuitively, the name fractal refers to broken or fractured objects, in contrast with the smooth shapes of Euclidean geometry.

Fractals exhibit the property of self-similarity[2], which implies that they show a great complexity at every scale of magnification. This is one of the final causes of uncertainty in nonlinear dynamics and it will be thoroughly studied along the present thesis. It is also important to remark that since the beginning of fractal geometry, its applications have pervaded all branches of science.

Dissipative Systems

Fractal structures are especially relevant in dissipative systems. From the perspective of Thermodynamics, dissipative systems are those which exchange matter-energy with their environments. Strictly speaking, all systems are dissipative since there are no perfectly isolated systems, with the possible exception of the whole universe. In practical terms, we can consider some simple systems as isolated, but

[1] The most recent definition of chaos is based on the concept of expansion entropy [5].

[2] The concept of self-similarity needs to be carefully defined. For an exhaustive discussion on this topic see Ref. [8].

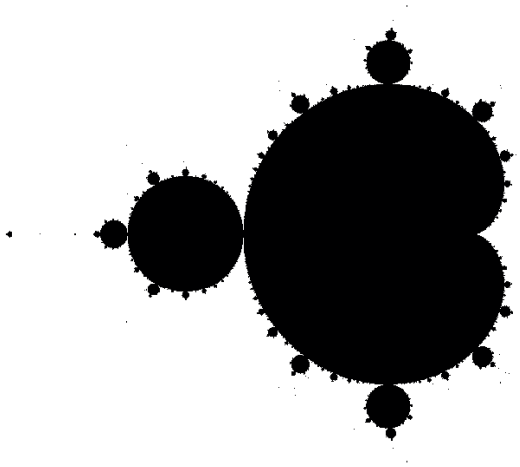

Figure 1.2. Mandelbrot set. This is a paradigmatic example of fractal geometry, with deep connections to chaos theory too.

many others, like living organisms, must necessarily be considered as dissipative systems in order to reflect their complexity. Therefore, dissipative systems are not only ubiquitous in nature, but they are also especially appealing.

In the terminology of dynamical systems the adjective "dissipative" acquires a broader sense, so the systems can exchange any generalized energy with their environment. A crucial feature of these systems is that they often present several asymptotic states. Ilya Prigogine, Nobel Prize in Chemistry in 1977, wrote: "Far from equilibrium, equations are no longer linear; there are many possible properties, many possible states, which are the different accessible dissipative structures", (translated from [9]).

Basins of Attraction or Escape Basins

In dissipative dynamical systems and open Hamiltonian systems, many final states can be possible. A fundamental idea that will be used repeatedly along this thesis is the concept of *basins of attraction* or *escape basins*. Dynamical systems are described by a set of rules that determine the evolution of the system. The set of initial conditions leading to some asymptotic final state is called *basin of attraction* in dissipative systems or *escape basin* in the case of open Hamiltonian systems. A crucial feature of these basins is that they often show fractal structures, hindering the final state predictability [10]. The study of fractal basins and their consequences will be one of the major goals of this thesis.

Delay Differential Equations

Among the three revolutionary theories that changed modern physics, probably it is in relativity where it is hardest to appreciate the appearance of restrictions to our knowledge. The key idea governing relativity is that information has a finite limiting speed, which is the speed of light. This inevitably introduces a new element that should be considered in dynamical systems, the delay between causes and effects. In words of Thomas Erneux [11]: "time delay arises because a finite time is required to sense information and then react to it". Oftentimes, these delays are so small that it is unnecessary to include them explicitly in the equations. Nonetheless, there are many situations where delay plays a fundamental role and must be included to reflect the dynamics.

Delay differential equations are a useful mathematical tool to treat this kind of problems. In these equations, the future of the system is described in terms of its present and past states. The past states are called the system's *history*, and they play a similar role to initial conditions in ordinary differential equations. Delay differential equations are irreversible, and present some specific features that will be developed along the present work. They are widely used in the modeling of biological systems because of the different time scales involved in biological processes. Delayed feedbacks have also interesting applications in meteorology, engineering and many other branches of science [11], [12].

Perturbations and Resonances

As mentioned before, real systems are not isolated, but they are inevitably subjected to external perturbations. Nonlinear systems can respond surprisingly to these external perturbations, exhibiting resonances [13]. The first two chapters of this thesis are devoted to the study of *vibrational resonance*, which can be defined as the enhancement of a low frequency periodic signal by means of a high frequency periodic perturbation. The effects of these perturbations can also be analyzed by means of basins of attraction, which is especially interesting in the case of fractal basins. Studying the coupling of periodic perturbations is particularly meaningful in biological processes, because of the great variety of cyclic processes with different frequencies that occur in life.

Nonlinear Dynamics and Multidisciplinarity

As argued before, the 20th century has been the century of quantum mechanics, relativity and chaos theory. But it has also been the century of molecular biology, neuroscience, genetics, and computer science among others. The keyword in the science of the early twenty-first century is *multidisciplinary*.

Along the history of science, nature has been splitted into many parts for a better understanding. Now, the different areas must interact to complete their descriptions and better comprehend the surrounding reality. In this respect, Nonlinear Dynamics must perform a fundamental role. Playing with the famous beginning of Léon

Tolstói's Ana Karenina, it is often said that *all linear systems are alike, but every nonlinear system is nonlinear in its own way*. This means that Nonlinear Dynamics can cover a wide variety of phenomena in all branches of science [14], but with a unique perspective and proper techniques suitable for each particular case.

Following this multidisciplinary spirit, the present thesis deals with apparently distant topics. We start studying the effects of periodic perturbations in a model appearing in molecular biology, then we explore the effects of delay in a mathematical model related to the phenomenon of El Niño, we study fractal structures in systems with applications to galactic dynamics and engineering and the final chapter is devoted to the dynamics of cold atoms guided by two crossing laser beams. Despite the diversity of topics treated, they all are studied under the unique light of nonlinear dynamics, showing that concepts like fractality, delay, or nonlinear resonances are ubiquitous in nature.

The purpose of my investigations has always been to find widely applicable results and develop useful tools for the whole scientific community. I am not an expert in genetics neither in climatology nor quantum mechanics, but hopefully my work can contribute to reveal unexpected aspects of these and other areas. As James C. Maxwell said: "There is nothing more practical than a good theory".

Bibliography

[1] H. Poincaré, "Sur le problème des trois corps et les équations de la dynamique", *Acta Math.* **13**, A3–A270 (1890).

[2] E. N. Lorenz, "Deterministic nonperiodic flow", *J. Atmos. Sci.* **20**, 130–141 (1963).

[3] T.-Y. Li and J. A. Yorke, "Period three implies chaos", *Am. Math. Mon.* **82**, 985–992 (1975).

[4] G. Bruno, *Del infinito: el universo y los mundos*. Madrid: Alianza, 1993.

[5] B. R. Hunt and E. Ott, "Defining chaos", *Chaos* **25**, 097618 (2015).

[6] K. T. Alligood, T. D. Sauer, and J. A. Yorke, *Chaos: an introduction to dynamical systems*. New York: Springer, 1996.

[7] B. B. Mandelbrot, *Fractal geometry of nature*. San Francisco: Henry Holt & Company, 1982.

[8] H.-O. Peitgen, H. Jürgens, and D. Saupe, *Chaos and fractals*. New York: Springer, 2004.

[9] I. Prigogine, *El nacimiento del tiempo*. Barcelona: Tusquets Editores S.A., 1991.

[10] J. Aguirre, R. L. Viana, and M. A. F. Sanjuán, "Fractal structures in nonlinear dynamics", *Rev. Mod. Phys.* **81**, 333–386 (2009).

[11] T. Erneux, *Applied delay differential equations*. New York: Springer, 2009.

[12] M. Lakshmanan and D. V. Senthilkumar, *Dynamics of nonlinear time-delay systems*. Berlin: Springer, 2011.

[13] S. Rajasekar and M. A. F. Sanjuán, *Nonlinear resonances*. New York: Springer, 2016.

[14] S. H. Strogatz, *Nonlinear dynamics and chaos: with applications to physics, biology, chemistry, and engineering*. Cambridge: Westview Press, 2001.

Chapter 2
Vibrational resonance in a time-delayed genetic toggle switch

"Cells are matter that dance."

-Uri Alon, *An introduction to systems biology*

As stated in the introduction, the science of this century is eminently multidisciplinary. Nonlinear dynamics and biology are a prolific couple with a long tradition and promising future. As a matter of fact, some of the milestones in dynamical systems like the logistic map, the Lotka-Volterra model or the Hodgkin-Huxley equations have biological roots. This is so, because even simple biological processes are strongly nonlinear. Furthermore, biological systems are also nice examples of open dissipative systems, since they are always subject to environmental changes and drain the surrounding resources.

This chapter exemplifies that philosophy. We study a simple model called the time-delayed genetic toggle switch, which is a synthetic gene-regulatory network. This network motif can be tested in a laboratory under controlled conditions and is also ubiquitous in nature. Besides its biological importance, the toggle-switch presents the advantage of being a rather simple nonlinear model.

Our study is focused on the effects produced by periodic perturbations of very different frequencies, e.g., circadian and seasonal variations of temperature. Namely, we study how a low-frequency signal can be enhanced or depressed by a high-frequency perturbation. When the coupling induces optimal enhancement, the phenomenon is known as *vibrational resonance*. As discussed previously, the modeling of biological systems also requires the study of possible delays. From the dynamical point of view, delays play a fundamental role introducing instabilities.

2.1 Introduction

The concept of resonance in physics generally refers to a large increase in the amplitude of the oscillations provoked by a particular external forcing or perturbation. In nonlinear systems there are many types of resonance, depending on which are the sources that cause them. When the resonance is induced by noise, it is called

stochastic resonance [1]. In the case that the resonance is produced by a chaotic signal, we say that the system presents a chaotic resonance [2], and finally if the forcing is a high-frequency periodic signal then the phenomenon is called *vibrational resonance* (VR) [3]. The role of resonances in different biological processes is paramount. For example, stochastic resonance, which has drawn much attention in the past few years, has been found in neural systems [4], crayfish mechanoreceptor cells [5] or the feeding behavior of paddle-fish [6]. However, though VR has been widely studied in physical systems such as lasers [7] and electronic devices [8], only recent attention has been paid to this phenomenon in biology [9]–[11].

In this chapter, we study VR in a time-delayed genetic network, which is a recurrent control motif in nature [12]. It has been reported that delay is fundamental in processes such as the creation of patterns via quorum sensing [13], the modulation of immunologic pathways [14] or the enhancement of oscillations in circadian clocks [15]. Additionally, nonlinear time-delayed systems have been reported to display a wide variety of dynamical phenomena such as phase synchronization [16], excitation regeneration [17], amplitude death [18], or multiresonances [19], [20], etc. Therefore, the study of delayed systems is interesting both from the biological and dynamical points of view.

Motivated by the preceding ideas, we present a theoretical and computational study of VR in a time-delayed toggle switch. This chapter is organized as follows. In Sec. 2.2 we explain the main features of the time-delayed toggle switch. First, the original model of the toggle switch is presented. Then, we introduce the delays and analyze its implications. Section 2.3 is a description of the usual treatment of VR in dynamical systems and how we apply it to our model. In Sec. 2.4 we examine the mechanism inducing the VR. Next, we vary the periodic forcings in Sec. 2.5 and show the effects of the delay on resonance in Sec. 2.6. Finally, in Sec. 2.7 we summarize our findings and discuss the role of VR in biological systems.

2.2 Model description

The genetic toggle switch is a synthetic gene-regulatory network designed to have two possible stable states [21], in other words, it is a bistable system. It is constructed from two repressible promoters in a mutually inhibitory network, that can be modeled through the following dimensionless differential equations

$$\begin{aligned} \frac{\mathrm{d}u}{\mathrm{d}t} &= \frac{\alpha_1}{1+v^{\beta_1}} - u \\ \frac{\mathrm{d}v}{\mathrm{d}t} &= \frac{\alpha_2}{1+u^{\beta_2}} - v. \end{aligned} \tag{2.1}$$

The variables u and v represent the concentrations of the two transcription factors involved, and their evolution is governed by a repressional nonlinear term and linear degradation. For each protein, the repressional term is modeled by Hill functions depending on the concentration of the other protein. The Hill coefficients β_1, β_2 are usually interpreted as the number of subunits composing the protein. For example,

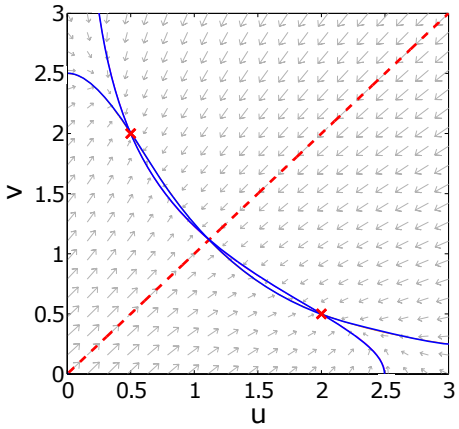

Figure 2.1. Phase diagram of the toggle switch. The picture corresponds to the system without delay, that is to Eq. 2.1. The two red crosses (0.5, 2) and (2, 0.5) are for the two stable equilibria. The dashed red line is the unstable separatrix $u = v$. The blue curves are for the nullclines $\dot{u} = 0$ and $\dot{v} = 0$. Arrows show the vector field in each point.

homodimers have Hill coefficient equal to two. The linear degradation term implies an exponential decay of the level of both proteins in the absence of repression or production. We have assumed unit degradation rates for both proteins.

For the sake of simplicity, we will also assume equal promoter strengths $\alpha_1 = \alpha_2 = \alpha$ for both variables and equal repressional cooperativity coefficients $\beta_1 = \beta_2 = \beta$. As it is shown in Ref. [21], it is needed that the cooperativity coefficient $\beta \geq 2$ to have a bistable system. There are some restrictions on the values of α too, so by choosing $\alpha = 2.5$ and $\beta = 2$ we get a bistable toggle switch (see Appendix A for further details). This election of the parameters will be kept throughout the study. Therefore, the present system can flip between high and low levels of concentration of the repressors: when one is high the other one is low, and vice versa. The phase space is depicted in Fig. 2.1, where we can see the two symmetric fixed points in (0.5, 2) and (2, 0.5) and the separatrix $u = v$ dividing the phase space.

Nevertheless, the previous equations do not take into account that each of the molecular processes involved in this genetic network require some time to be completed: the production of new protein requires transcription, translation and assemble operations [22], the degradation machinery also needs several time-consuming phosphorylation steps as reported in Ref. [15]. In order to reflect these molecular steps, we can modify the previous ordinary differenatial equations into delay

differential equations:

$$\begin{aligned}\frac{\mathrm{d}u}{\mathrm{d}t} &= \frac{\alpha}{1+v(t-\tau_r)^2} - u(t-\tau_d)\\ \frac{\mathrm{d}v}{\mathrm{d}t} &= \frac{\alpha}{1+u(t-\tau_r)^2} - v(t-\tau_d),\end{aligned} \tag{2.2}$$

where we have supposed equal time delays for the production of both proteins τ_r and their degradation τ_d. From a biological point of view, the production delay τ_r has the same or even greater importance than the degradation delay τ_d. However, concerning the dynamics, a linear stability analysis (see Appendix A) shows that the delay in the repressional term τ_r can induce only damped oscillations, whereas the delay τ_d can induce damped and sustained oscillations for values $\tau_d > \tau_{crit}$ via a subcritical Hopf bifurcation. Thus, studying the effects of τ_d is sufficient to understand the dynamics of the system. Moreover, the original work, where VR was first reported [3], was carried out on a bistable damped oscillator. Thereby the time-delayed toggle switch is an extraordinary candidate to make a first study of VR in genetic networks.

2.3 Methods on VR

Vibrational resonance consists of the optimization of the response of the system to a low-frequency (LF) signal of amplitude A and frequency ω due to a high-frequency (HF) perturbation of amplitude B and frequency $\Omega \gg \omega$. For the time-delayed toggle switch one can think the forcing as a thermal bath with oscillating temperature, or an experimental setting with biharmonic variation of the concentration of chemical inductor, for instance. Our present purpose is to search numerically the phenomenon of VR, so we introduce these two forcings to one of the proteins and look at the response of the other one. The system of delay differential equations that we have to solve is:

$$\begin{aligned}\frac{\mathrm{d}u}{\mathrm{d}t} &= \frac{\alpha}{1+v^\beta} - u\left(t-\tau\right) + A\sin\omega t + B\sin\Omega t,\\ \frac{\mathrm{d}v}{\mathrm{d}t} &= \frac{\alpha}{1+u^\beta} - v\left(t-\tau\right).\end{aligned} \tag{2.3}$$

The response for the frequency ω is usually defined as the amplitude of the sine and cosine components of the output signal, yielding

$$C_s = \frac{2}{nT}\int_0^{nT} v(t)\,\sin\omega t\mathrm{d}t \tag{2.4}$$

$$C_c = \frac{2}{nT}\int_0^{nT} v(t)\,\cos\omega t\mathrm{d}t, \tag{2.5}$$

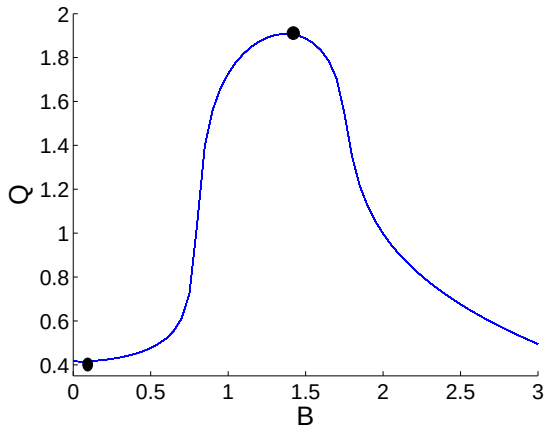

Figure 2.2. VR for the time-delayed genetic toggle switch. The response of the system Q is plotted vs the amplitude of the HF perturbation B. The parameters of equations (2.3) are chosen to be $\alpha = 2.5$, $\beta = 2$, $\tau = 0.5$, $A = 0.1$, $\omega = 0.1$ and $\Omega = 5$. These will be the standard parameters along this work if not specified.

where n is the number of complete oscillations of the LF signal and $T = (2\pi/\omega)$ is its period. The numerical values of C_S and C_C are related to the Fourier spectrum of the time series of the variable v computed at the frequency ω. Then, the relation between the output and the forcings provides an idea of how the LF signal is being amplified by the HF perturbation. This is commonly defined by means of the Q factor:

$$Q = \frac{\sqrt{C_s^2 + C_c^2}}{A} \,. \tag{2.6}$$

The usual procedure to search for VR is to compute Q for different amplitudes B of the HF periodic perturbation [3]. If there is a value of B that maximizes Q, then the VR occurs. This means that there is a particular value of the HF periodic perturbation that optimizes the response of the system to the weak LF periodic signal.

Our algorithm, developed in MATLAB, accomplish several computational tasks. The different steps are:

- First, we solve the delayed differential equations of the system with the external forcings (Eqs. 2.3) using *dde23* [23]. The histories are chosen to be equal to one of the two symmetric equilibrium states, and the external forcings are applied to the protein at the higher level. This is completely equivalent to solve the delayed differential equations in the absence of external forcings with some random initial histories, and then apply the two periodic forcings after the transient has vanished.

- After solving the Eqs. (2.3) and discarding the transient, we compute the factor Q for a range of different values of the HF intensity B.

- Finally a graph of Q vs B is plotted and, if the parameters are properly chosen, a bell-shaped curve is found (Fig. 2.2). The maximum of this curve is the optimal match between the LF and HF signals, that is the VR.

2.4 Explanation of the mechanism inducing VR

So far, we have seen that it is possible to find VR after having chosen the appropriate parameters. However, it would be interesting to understand why the amplitude is increased and to know what the levels of protein are actually doing. To answer these two questions it is convenient to represent the phase diagram. In this kind of diagram the coordinates give the concentrations of each protein, in such a way that every point represents a state of the system at a given time. In Fig. 2.3 we can see the trajectories of the system in three different cases. For small values of B the concentration of the protein only oscillates around the low expression state ($B = 0.1$, red line), for very large values of B the low state becomes unstable and the concentration of the protein oscillates around the high expression state ($B = 2.2$, green line). However, for intermediate values of B the concentration of the protein oscillates between the high and the low states, reaching a maximum amplitude for some optimal value of the amplitude $B_{opt} = 1.5$ (blue line). When the system explores both states the amplitude is much larger, thus unveiling an appearance of the VR. In other words, resonance occurs when the concentrations of both proteins switch (oscillate) between the low and the high state. These examples are directly connected to the Fig. 2.2, where the response amplitude Q of the oscillations is represented as a function of B. The two plotted dots correspond to the simulations for $B = 0.1$ and $B = 1.5$.

Of course we can also plot directly the concentration of the protein vs time (Fig. 2.4). When the amplitude of the HF forcing is $B_{opt} = 1.5$, then the oscillations increase their amplitude about four times keeping the same global period. This is in agreement with Fig. 2.2 too.

2.5 Effects of LF/HF signals on VR

To study the dependence of the resonance with the LF signal we can vary its amplitude A and its frequency ω. When we increase the amplitude A the resonance increases as well and the bell-shaped curve gets wider (Fig. 2.5). There is an upper limit for A, above which the maximum of the response Q is lost, producing an effect sometimes called resonance without tuning [24]. Changing the frequency ω of the LF signal changes the width of the peak too, but just in the opposite way: for decreasing values of ω the value of Q grows and so does its width. In this case there is a lower limit for ω and below this limit resonance without tuning also occurs (Fig. 2.6). From these results we can infer that, in general, resonance will be easily achieved for signals with small frequencies and large amplitudes.

The variation of the HF perturbation changes resonance in a very different manner. Increasing frequencies Ω lead to increasing values of B_{opt} too (Fig. 2.7). This

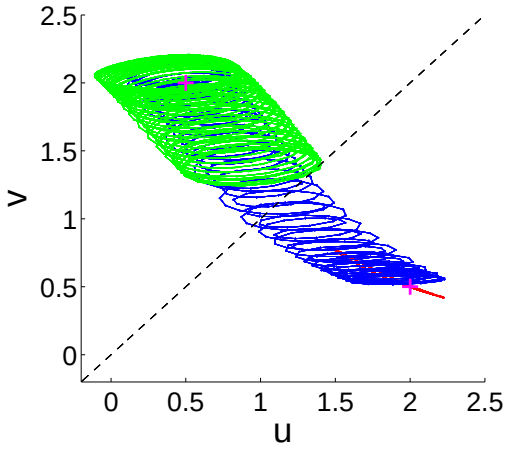

Figure 2.3. Explanation of the VR mechanism. The dashed line represents the separatrix ($u = v$) and the magenta crosses are the two equilibria states ($e_1 = (0.5, 2)$, $e_2 = (2, 0.5)$). In red $B = 0.1$, only one region below the separatrix is explored; in blue $B = 1.5$, both regions are explored making the amplitude higher (VR); in green $B = 2.2$, only the region above the separatrix is explored.

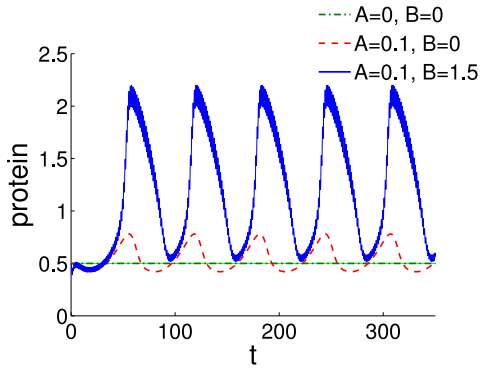

Figure 2.4. Time series. The evolution of the protein levels before introducing any external signal are plotted in green dotted line ($A = 0$, $B = 0$), after introducing the LF signal in red dashed line ($A = 0.1$, $B = 0$), when both LF and HF signals are introduced in blue solid line ($A = 0.1$, $B = 1.5$). The amplitude of the oscillations is highly increased when $B = B_{opt}$. The concentrations are given in arbitrary units and the time is given in hours.

is important since resonance can be achieved with smaller amplitudes B of the HF force, if its frequency Ω is decreased.

Delving deeper into the effects of the HF perturbation, we have observed that there is a linear relation between Ω^2 and B_{opt} (Fig. 2.8). This result can be better understood recalling that the solution of a driven linear oscillator is proportional to F_0/Ω^2. This can be very useful since once we have fixed the parameters of the

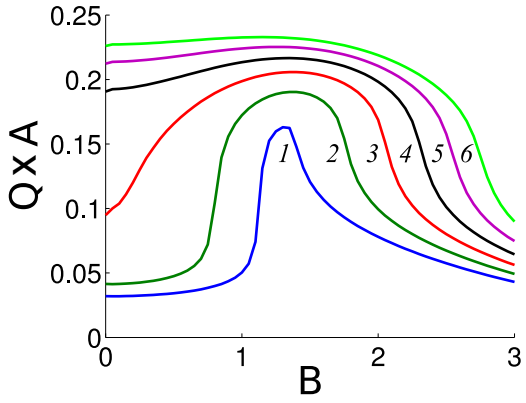

Figure 2.5. Effects of the LF signal's amplitude. The resonance curves are plotted for different amplitudes of the LF periodic signal $A = 0.09$, 0.1, 0.11, 0.12, 0.13, 0.14 (curves 1-6 respectively). Note that here we plot $Q \times A$ for clarity of the plot, to avoid crossings of the curves. The shape of the curves remains unaltered, so we can appreciate how the peaks are widened. Above some threshold ($A \gtrsim 0.15$) resonance without tuning occurs.

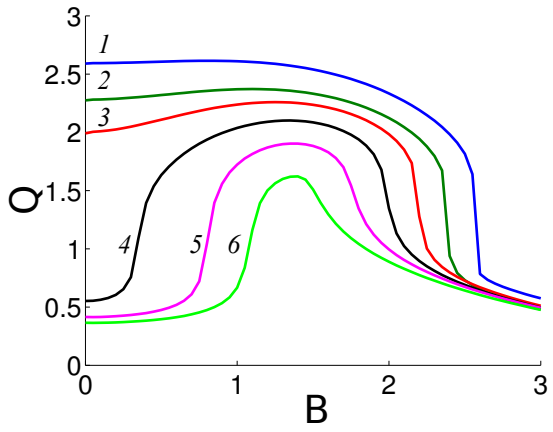

Figure 2.6. Effect of the LF signal's frequency. Response of the system Q when the low frequency ω is varied, ω =0.02, 0.04, 0.06, 0.08, 0.10, 0.12 for curves 1-6 respectively. Below the threshold ($\omega \lesssim 0.02$) there is resonance without tuning.

system, we can tune the amplitude B_{opt} at which VR takes place by tuning the high frequency Ω.

2.6 Effects of the delay

So far, we have kept the delay τ constant. However, the strong effect of the delay in the oscillations of the system can also be exploited. When the delay is in a range of values far from the autonomous regime ($\tau < \tau_{crit}$), the variation of τ has qualitatively similar effects to the variation of the amplitude of the slow signal A:

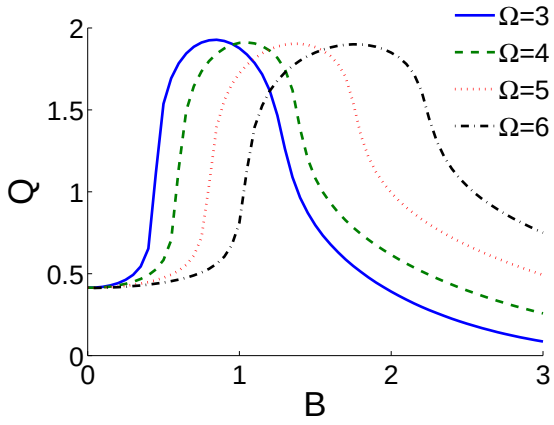

Figure 2.7. Effect of the HF signal's frequency. In this plot Ω is varied keeping the other parameters constant. The VR curve presents a shift in the amplitude of the HF perturbation B at which resonance occurs. However, the maximum value of Q is barely changed.

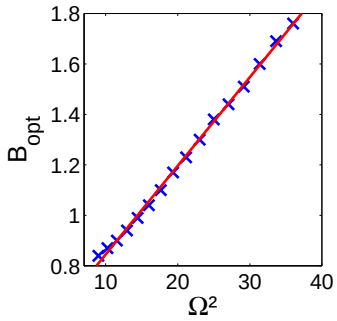

Figure 2.8. Relation between B and Ω. A relation of the type $B_{opt} \propto \Omega^2$ appears when Ω is varied, keeping the other parameters constant. In this plot 16 points from resonance curves (blue crosses) are fitted to a straight-line (red solid line), with a correlation coefficient r =0.9992.

over some value of τ the maximum of the curve Q vs B disappears, and VR without tuning is found (Fig. 2.9).

A more complicated situation appears for values of the delay close to the Hopf bifurcation ($\tau \sim \tau_{crit}$). In Fig. 2.10, we study the basins of attraction of the delayed toggle switch without forcings. We see that as the delay grows the basins of attraction start to mix increasing the sensitivity of the system: small perturbations can drive the system into any of the two possible final states. These results deserve to be carefully investigated. A thorough study on the effects of the periodic signals in this situation is accomplished in Chapter 3, while Chapter 5 is dedicated to study how the delay can dramatically enhance the sensitivity of a system.

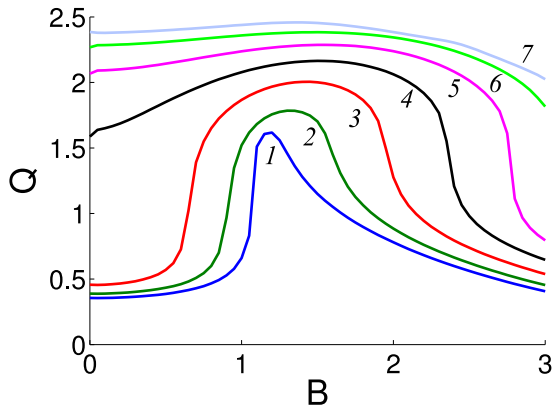

Figure 2.9. Effects of the delay. System response when the delay is far from the Hopf bifurcation, that is $\tau < 1$. For the curves 1-7, $\tau = 0.35, 0.45, 0.55, 0.65, 0.75, 0.85, 0.95$. For $\tau > 1$ autonomous oscillations occur.

2.7 Discussion

In the present chapter of this thesis, it has been shown that under certain conditions LF oscillations can be greatly amplified by a HF perturbation in a time-delayed toggle switch. It has been reported that oscillations underlay in the heart of many cell processes [25], and the timing involved can vary from minutes [26], [27] to days [28], so it is of great importance to know how these low and fast oscillations may couple among them.

Here we have also analyzed the different effects of the LF and HF signals on the resonance. The variation of the high frequency Ω produces a shift of the intensity B at which resonance occurs. This is very remarkable since tuning the high frequency allows similar resonances with smaller variations in the concentrations of the proteins. Furthermore, it has been demonstrated that there is a linear dependence between B_{opt} and Ω^2, making it possible to predict the value of the amplitude B_{opt} at which VR will take place. On the other hand, we have seen that the variation of the LF signal changes the width of the peak of resonance. Moreover, we have shown that variations in the amplitude A and variations in the frequency ω had opposite effects on the resonance: for increasing values of A the resonance increases, but for increasing ω it decreases. This led to a higher (lower) limit for the values of A and ω respectively, and we have seen that above (below) these limits the VR without tuning occurred. In this time-delayed toggle switch, the variation of the delay τ produces a variation in the damping of the system, inducing strong effects on resonance.

When the system is far from the autonomous oscillations regime ($\tau < \tau_{crit}$), the effect of the delay on VR is similar to the effect produced by the variation of the amplitude of the LF signal A, including the higher limit above which resonance without tuning is found. However, when the system is close to the Hopf bifurcation,

it becomes very sensitive to external perturbations. This situation is especially interesting as we will see in subsequent chapters.

The most appealing characteristics of the VR are that it can be externally controlled, and that it can induce collective behaviors [8], what makes it attractive for both biologists and physicists.

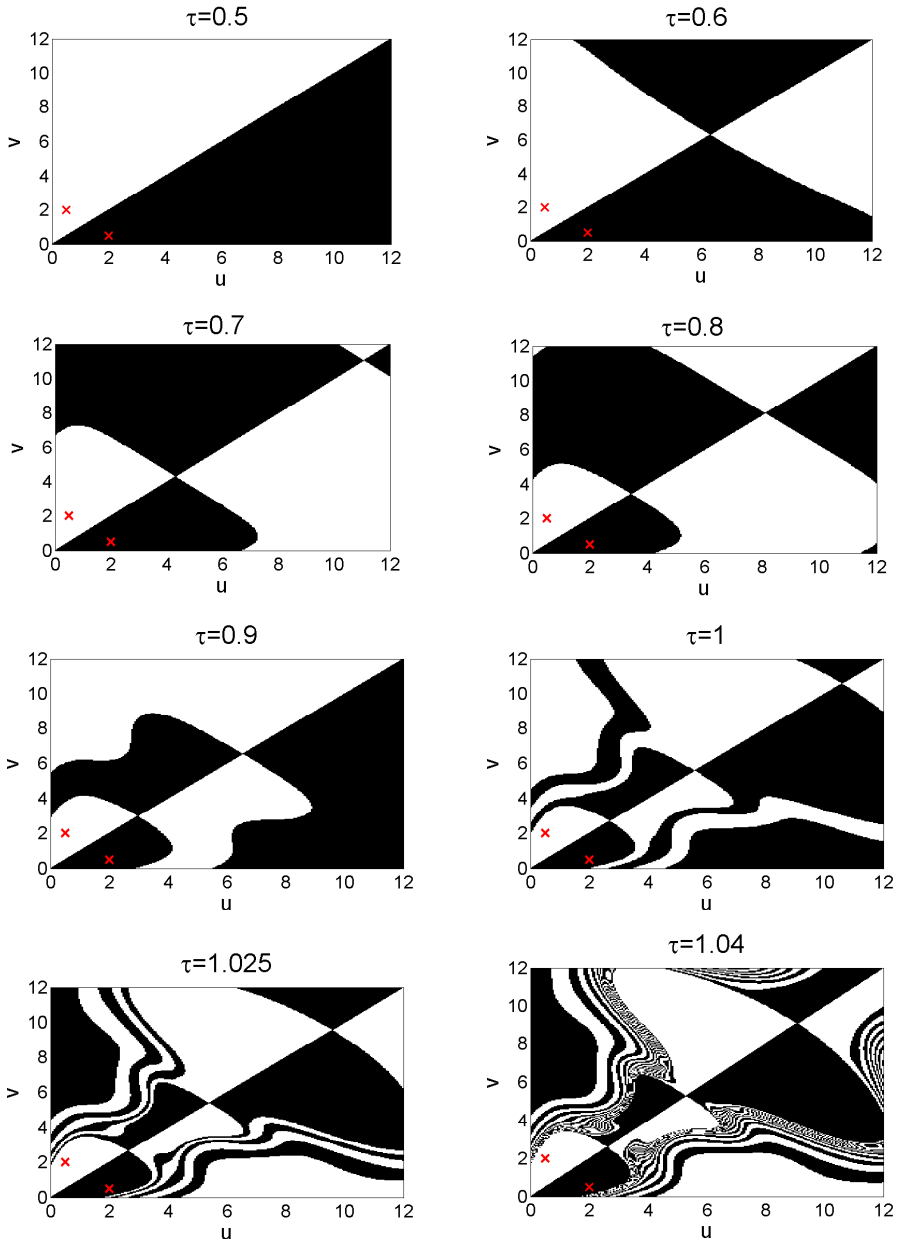

Figure 2.10. Delay provokes sensitivity of the system. These are the basins of attraction for the time-delayed toggle switch (Eqs. 2.3) without the periodic forcings $A = B = 0$. White pixels represent constant values of the histories leading to (0.5, 2), the equilibrium point represented by the upper red cross. Black pixels represent the constant histories leading to (2, 0.5), the equilibrium point represented by the lower red cross. For small delays ($\tau = 0.5$) the basins are not affected by the delayed terms. As τ is increased the basins get mixed, making the system more sensitive as we approach the Hopf bifurcation.

Bibliography

[1] L. Gammaitoni, P. Hänggi, P. Jung, and F. Marchesoni, "Stochastic resonance", *Rev. Mod. Phys.* **70**, 223–287 (1998).

[2] S. Zambrano, J. M. Casado, and M. A. F. Sanjuán, "Chaos-induced resonant effects and its control", *Phys. Lett. A* **366**, 428–432 (2007).

[3] P. S. Landa and P. V. E. McClintock, "Vibrational resonance", *J. Phys. A: Math. Gen.* **33**, L433 (2000).

[4] A. Bulsara, E. W. Jacobs, T. Zhou, F. Moss, and L. Kiss, "Stochastic resonance in a single neuron model: theory and analog simulation", *J. Theor. Biology* **152**, 531–555 (1991).

[5] J. K. Douglass, L. Wilkens, E. Pantazelou, and F. Moss, "Noise enhancement of information transfer in crayfish mechanoreceptors by stochastic resonance", *Nature* **365**, 337–340 (1993).

[6] D. F. Russell, L. A. Wilkens, and F. Moss, "Use of behavioural stochastic resonance by paddle fish for feeding", *Nature* **402**, 291–294 (1999).

[7] V. N. Chizhevsky, E. Smeu, and G. Giacomelli, "Experimental evidence of "vibrational resonance" in an optical system", *Phys. Rev. Lett.* **91**, 220602 (2003).

[8] E. Ullner, A. Zaikin, J. García-Ojalvo, R. Báscones, and J. Kurths, "Vibrational resonance and vibrational propagation in excitable systems", *Phys. Lett. A* **312**, 348–354 (2003).

[9] B. Deng, J. Wang, X. Wei, K. M. Tsang, and W. L. Chan, "Vibrational resonance in neuron populations", *Chaos* **20**, 013113 (2010).

[10] J. Shi, C. Huang, T. Dong, and X. Zhang, "High-frequency and low-frequency effects on vibrational resonance in a synthetic gene network", *Phys. Biol.* **7**, 036006 (2010).

[11] S. Rajasekar, J. Used, A. Wagemakers, and M. A. F. Sanjuán, "Vibrational resonance in biological nonlinear maps", *Commun. Nonlinear Sci.* **17**, 3435–3445 (2012).

[12] U. Alon, *An introduction to systems biology: design principles of biological circuits*. Boca Raton: Chapman and Hall/CRC, 2006.

[13] S. Basu, Y. Gerchman, C. H. Collins, F. H. Arnold, and R. Weiss, "A synthetic multicellular system for programmed pattern formation", *Nature* **434**, 1130–1134 (2005).

[14] M. W. Covert, T. H. Leung, J. E. Gaston, and D. Baltimore, "Achieving stability of lipopolysaccharide-induced NF-kB activation", *Science* **309**, 1854–1857 (2005).

[15] D. Bratsun, D. Volfson, L. S. Tsimring, and J. Hasty, "Delay-induced stochastic oscillations in gene regulation", *P. Natl. Acad. Sci. USA* **102**, 14593–14598 (2005).

[16] D. V. Senthilkumar, M. Lakshmanan, and J. Kurths, "Phase synchronization in time-delay systems", *Phys. Rev. E* **74**, 035205 (2006).

[17] B. Kelleher, C. Bonatto, P. Skoda, S. P. Hegarty, and G. Huyet, "Excitation regeneration in delay-coupled oscillators", *Phys. Rev. E* **81**, 036204 (2010).

[18] D. V. Ramana Reddy, A. Sen, and G. L. Johnston, "Time delay induced death in coupled limit cycle oscillators", *Phys. Rev. Lett.* **80**, 5109–5112 (1998).

[19] J. H. Yang and X. B. Liu, "Controlling vibrational resonance in a multistable system by time delay", *Chaos* **20**, 033124 (2010).

[20] C. Jeevarathinam, S. Rajasekar, and M. A. F. Sanjuán, "Theory and numerics of vibrational resonance in Duffing oscillators with time-delayed feedback", *Phys. Rev. E* **83**, 066205 (2011).

[21] T. S. Gardner, C. R. Cantor, and J. J. Collins, "Construction of a genetic toggle switch in Escherichia coli", *Nature* **403**, 339–342 (2000).

[22] J. Lewis, "Autoinhibition with transcriptional delay: a simple mechanism for the zebrafish somitogenesis oscillator", *Curr. Biol.* **13**, 1398–1408 (2003).

[23] S. Thompson and L. F. Shampine, "A friendly Fortran DDE solver", *Appl. Numer. Math.*, Selected Papers, The Third International Conference on the Numerical Solutions of Volterra and Delay Equations**, 56**, 503–516 (2006).

[24] J. J. Collins, C. C. Chow, and T. T. Imhoff, "Stochastic resonance without tuning", *Nature* **376**, 236–238 (1995).

[25] K. Kruse and F. Jülicher, "Oscillations in cell biology", *Current Op. Cell Biol.* **17**, 20–26 (2005).

[26] O. Pourquié, "The segmentation clock: converting embryonic time into spatial pattern", *Science* **301**, 328–330 (2003).

[27] G. Lahav, N. Rosenfeld, A. Sigal, N. Geva-Zatorsky, A. J. Levine, M. B. Elowitz, and U. Alon, "Dynamics of the p53-Mdm2 feedback loop in individual cells", *Nat. Genet.* **36**, 147–150 (2004).

[28] J. C. Dunlap, "Molecular bases for circadian clocks", *Cell* **96**, 271–290 (1999).

Chapter 3
Ultrasensitive vibrational resonance

"One can confer motion upon even a heavy pendulum which is at rest by simply blowing against it; by repeating these blasts with a frequency which is the same as that of the pendulum one can impart considerable motion."

-Galileo Galilei, *Discourses and mathematical demonstrations relating to two new sciences*

In the previous chapter, we have studied the effects of a nonlinear system perturbed by two harmonic forcings of different frequencies. The slow forcing drives the system into an oscillatory regime, while the fast perturbation enhances the effect of the slow periodic drive. The *vibrational resonance* occurs when the enhancement is optimal, and this usually takes place when the fast perturbation has an amplitude much larger than the slow periodic forcing. We have also seen that the delay can drive the system into a sensitive regime where small perturbations can change the final destination of trajectories. In the present chapter, we show that under these circumstances the *vibrational resonance* can happen for amplitudes of the fast perturbation far below the amplitude of the slow periodic forcing. Furthermore, this resonance presents a fractal pattern, extremely susceptible to small variations of the fast perturbation. We explore here this phenomenon that we call *ultrasensitive vibrational resonance*.

3.1 Introduction

As we have explained in the previous chapter, *vibrational resonance* (VR) occurs when the response of a nonlinear system with a low frequency oscillatory signal is optimized by means of a high frequency perturbation [1]. The VR has been thouroughly studied analytically, numerically and experimentally in a variety of nonlinear systems [2]–[6]. Among these studies, the analysis of the effect of delay on the VR is receiving increasing attention [7]–[12].

In this context, and motivated by the results obtained for the time-delayed genetic toggle switch, we have explored the VR in the vicinity of a Hopf bifurcation induced by a delayed feedback. Delay differential equations, though very complicated from an analytical point of view, are very easily simulated numerically and display a variety of outstanding phenomena. It is well known that among other interesting effects on the VR, time lags can induce multi resonance responses [9], [11]. However, we did not expect to find infinite resonances displaying a fractal pattern, as it happened. Moreover, this resonance takes place for values of the amplitude of the high frequency perturbation smaller than the amplitude of the low frequency signal. This is a unique feature that previous studies on VR have been missing out.

According to this unusual pattern of the resonance curve, we call the phenomenon *ultrasensitive vibrational resonance* (UVR). This resonance is extremely sensitive to slight variations of the amplitude of the high frequency perturbation. Actually, the resonance curves present very sharp and narrow peaks arranged in a fractal pattern, in such a way that it might be possible to find two peaks of resonance arbitrarily close. This is far different from the usual continuous bell shape curve observed in the *vibrational resonance* where the amplitude of the second forcing spans a large interval of values.

Investigating the origin of this extreme sensitivity, we found that the key underlying property which gives rise to the UVR is the appearance of fractal structures in the phase space. We believe that this kind of structures and the presence of attractors of different amplitude are the basic ingredients of the UVR. Small perturbations in a fractal phase space can lead the system from a small attractor to an attractor of large amplitude, therefore the resonance is induced. To check this hypothesis we analyze a nonlinear system without delay but with a *highly fractalized* phase space, and we show that this system is also able to display the phenomenon of UVR.

3.2 Usual vibrational resonance

As a starting point, we reproduce the results of [11], where VR in a Duffing oscillator with a linear delayed feedback is studied. The Duffing oscillator is a paradigmatic model to search for VR as it was the model chosen in the original article of Landa and McClintock [1]. Thus, the model for our study can be formulated as follows

$$\ddot{x} + \gamma\dot{x} + \alpha x + \beta x^3 + cx(t-\tau) = A\cos\omega t + B\cos\Omega t, \tag{3.1}$$

where all the coefficients $\gamma > 0, \alpha < 0, \beta > 0, c < 0, \tau > 0, A > 0, B > 0, \Omega > 0, \omega > 0$, and $\Omega \gg \omega$ are real constants. This model is the usual Duffing oscillator, with two periodic forcings of different frequencies $\Omega \gg \omega$ and a time-delayed feedback $cx(t-\tau)$. The method used to investigate VR is the same described in the previous chapter. First, we integrate the delayed differential equations using a (5,6) pair of Runge-Kutta formulas [13]. Like in the previous chapter, we choose constant histories set onto a point of equilibrium, so for every $t \in [-\tau, 0]$ we set $x = \pm\sqrt{(\alpha-\gamma)/c}$. After getting rid off the transients, we calculate the amplitude response Q (the value of the Fourier transform at the frequency ω) for different intensities of the high-frequency

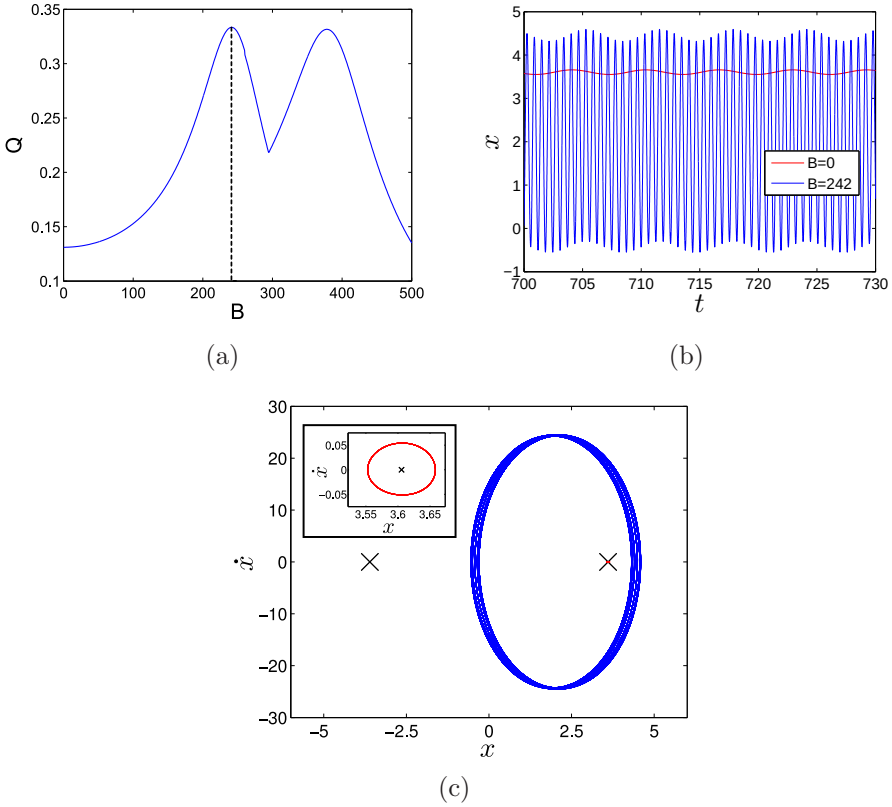

Figure 3.1. Usual vibrational resonance. (a) The typical VR curve for a time-delayed system, as it appears in Ref. [11]. The amplitude response of the system Q varies smoothly when the amplitude of the high frequency perturbation B is varied and the two maxima correspond to the *vibrational resonance*. Equation (3.1) has been solved with the following parameters $\ddot{x} + 0.5\dot{x} - x + 0.1x^3 - 0.3x(t-1) = 0.1\cos t + B\cos 10t$ and histories $x = \dot{x} = 0$ for $t \in [-\tau, 0]$. Notice the wide range of values of the high frequency amplitude B compared to the value of the low frequency amplitude. (b) The time series in red corresponds to $B = 0$ and the time series in blue corresponds to the first maximum of panel (a) marked with a dashed line, which is the usual *vibrational resonance*. (c) We can see the same time series represented in phase space $(x, \dot{x})$. The apparent thickness of the trajectory is a consequence of the high period regime (actually several lines may appear when we zoom in). The trajectory for the case $B = 0$ is plotted in the inset because it is very small compared to the resonant trajectory. This does not mean that the system presents a great resonance, in the sense of great amplification with a small external action, but this is a consequence of such a large difference between the amplitudes of both periodic signals.

perturbation B. The maxima of this curve, if any, correspond to the VR, that is an optimal match between the low frequency and high frequency signals.

The Duffing oscillator with time-delayed feedback, Eq. (3.1), can present two resonances corresponding to the two maxima of the Q vs B curve, (Fig. 3.1(a)), for

certain parameters [11]. It is remarkable that in this case the range of values of the amplitude of the high frequency perturbation B is several orders of magnitude larger than the amplitude of the low frequency signal A. Indeed, the analysis of the theoretical approach of Q includes the assumption $A \ll 1$ [11], i.e., $B \gg A$.

In these conditions, it is still fair to talk about resonance since the high frequency perturbation enhances the response amplitude Q, but probably one would not expect the cause of the resonance to be much larger than the signal itself. Additionally, the time series at the resonance resembles the high frequency perturbation acting as an enhancer, and the low frequency signal is completely eclipsed (Figs. 3.1(b)-3.1(c)). Therefore, it seems desirable to amplify the low frequency signal by means of smaller amplitudes of the secondary high frequency perturbation. As we found out, this is in fact happening for the Eq. (3.1) when the system is on the edge of stability giving rise to the UVR.

3.3 Ultrasensitive vibrational resonance

The UVR consists in a series of sharp and narrow peaks of resonance that appear for very small values of the amplitude of the high frequency signal, as shown in Fig. 3.2(a). Moreover, and unlike the common VR presented in the previous section, the UVR occurs for values of the high frequency amplitude B which are smaller than the low frequency amplitude A. Furthermore, the final time series are not completely disturbed by the high frequency perturbation as in the VR. In the UVR, the resonant time series resembles the low frequency signal but with a much larger amplitude as can be observed in Figs. 3.2(b)-3.2(c). According to this, the UVR fits better the idea of resonance as a big oscillation amplitude driven by a sufficiently small external action.

Another specific feature of this phenomenon is the fractal pattern displayed by the peaks of resonance. This means that when the resolution in B is increased the amplitude response Q presents more and more maxima. Every peak is actually composed of many peaks and valleys that form a fractal curve, making the resonance extremely sensitive to small changes in the parameters. The height of the peaks of Q is almost constant as it is intimately related to the size of the attractors, which do not vary for such small perturbations. A computation of the box-counting dimension is carried out in order to quantify the fractalization of the resonance curve, leading to a non integer dimension of $d = 0.94$ (see Fig. 3.2(d)).

The Duffing oscillator with time-delayed feedback of Eq. (3.1) is able to present the usual VR as shown earlier, but it can also display the UVR if the appropriate parameters are chosen. Research in other models of similar characteristics show that when the delay takes values just before the Hopf bifurcation, very small periodic perturbations induce the UVR. Moreover, this phenomenon occurs when the low frequency signal has a frequency similar to the natural oscillations of the system, as it happens in the resonance of linear systems. Delving deeper into the causes, we found that the key element for the appearance of UVR is the fractalization of the phase space that occurs for this set of parameters.

The phenomenon of UVR is better understood examining the phase space. One procedure to examine the phase space in a delayed system consists in choosing the history as a function with two parameters, and then compute the 2D basin of attraction varying these parameters. Among all the possible functions that can play the role of history [1] for the Duffing oscillator with delay, here we choose the histories as constants values of x and $\dot{x}$ for $t \in [-\tau, 0]$. For every pair of chosen constant histories $(x, \dot{x})$ we integrate the system and plot the basin of attraction, as shown in Fig. 3.3. This subspace of the infinite phase space of the delayed system, is sufficient to show that fractal structures appear for this particular choice of parameters. Fractal structures associated to transient chaos are an outstanding feature very common in time delay systems [14]–[17]. In this case, we can see in Fig. 3.3 that the equilibrium point chosen as constant history lies very close to the fractal boundary where three different basins coexist. Because of the low frequency signal, the equilibrium point turns into a stable periodic orbit, whose basin is very close to another basin that can be reached using very small amplitudes of the high frequency perturbation. In particular, the system can be driven to an attractor of large amplitude oscillations, that is the ultimate cause of the *ultrasensitive vibrational resonance*.

To prove the validity of this interpretation, i.e., that actually the effect of the high frequency perturbation is to drive the trajectory to a larger amplitude attractor, we chose another set of parameters for the same model without delay, so we can extend the results to other kind of systems. Here we consider the Duffing oscillator with the following parameters:

$$\ddot{x} + 0.15\dot{x} - x + x^3 = 0.245 \cos t. \tag{3.2}$$

In this system there is no delay at all, but the phase space is *highly fractalized* [2] [18], as shown in the basin of attraction of Fig. 3.4(a). In this case the system presents three periodic attractors, two of them of period 1 with small amplitudes and one of period 3 of larger amplitude. Now we introduce the second harmonic perturbation and we have the equation

$$\ddot{x} + 0.15\dot{x} - x + x^3 = 0.245 \cos t + B \cos 10t. \tag{3.3}$$

If we choose the initial conditions to be in a fractal boundary and then compute the response amplitude Q (see Fig. 3.4(b)), the UVR takes place with the same characteristics described before. Once again, the high frequency perturbation is able to drive the system to an attractor of large amplitude producing the resonance. This confirms our conviction that the appearance of fractal structures in phase space is the ultimate cause of the UVR. Furthermore, it explains why in both cases, with and without delay, the amplitude response Q takes almost constant values, since the attractor remains almost unchanged for these small perturbations.

[1] Different kinds of history functions and their physical meaning are presented in Appendix C.

[2] A comprehensive discussion about the unique unpredictability of Wada basins is made in Chapters 3, 4 and 5.

3.4 Discussion

In this chapter we have presented a new phenomenon called ultrasensitive *vibrational resonance*. UVR is a particular case of vibrational resonance with some specific characteristics that make it especially interesting.

Originally, the vibrational resonance was considered as a kind of stochastic resonance [19] interchanging the role of the high frequency perturbation with noise. Probably one would not expect the noise to be larger than the signal, and the same reasoning would be applicable to the high frequency perturbation in VR. In fact in many situations, stochastic resonance occurs on the edge of stability. However, in the previous literature on vibrational resonance [7]–[12] the high frequency perturbation typically has a larger amplitude than the low frequency signal. This is not the case in the *ultrasensitive vibrational resonance*, which can be achieved with very small amplitudes of the high frequency perturbation, even smaller than the amplitude of the low frequency signal.

Besides the small amplitude of the high frequency needed to achieve the resonance, another striking feature of this phenomenon is the fractal pattern of sharp and narrow peaks of resonance. As we zoom in the response amplitude Q, more and more peaks are found as in a fractal curve. We have also computed the box-counting dimension showing that it is not an integer, which confirms its fractal nature.

As shown in the previous chapter, the delay could increase the sensitivity in a genetic toggle switch. In this chapter, we have observed that a similar phenomenon happens for the Duffing oscillator with a time-delayed feedback. A thorough examination on the mechanisms relating delay and fractal structures will be provided in Chapter 5. This fractalization of the phase space is the ultimate cause for the particularities of UVR. When the initial condition lies on a fractal boundary or very close to it, the high frequency perturbation can drive the trajectory to different attractors. If one of these attractors is of similar frequency than the low frequency signal but with a larger amplitude, then the UVR is possible. This explains the high sensitivity to small variations and also the fractal pattern of the peaks of resonance, which is due to the fractal nature of the phase space. Furthermore, to check this hypothesis, we have studied the same system without delay for a choice of parameters where the basin of attraction is *highly fractalized*. We have reproduced the same results for the response amplitude Q, proving that the fractal nature of the phase space is at the heart of this phenomenon. This opens the range of dynamical systems susceptible of presenting UVR.

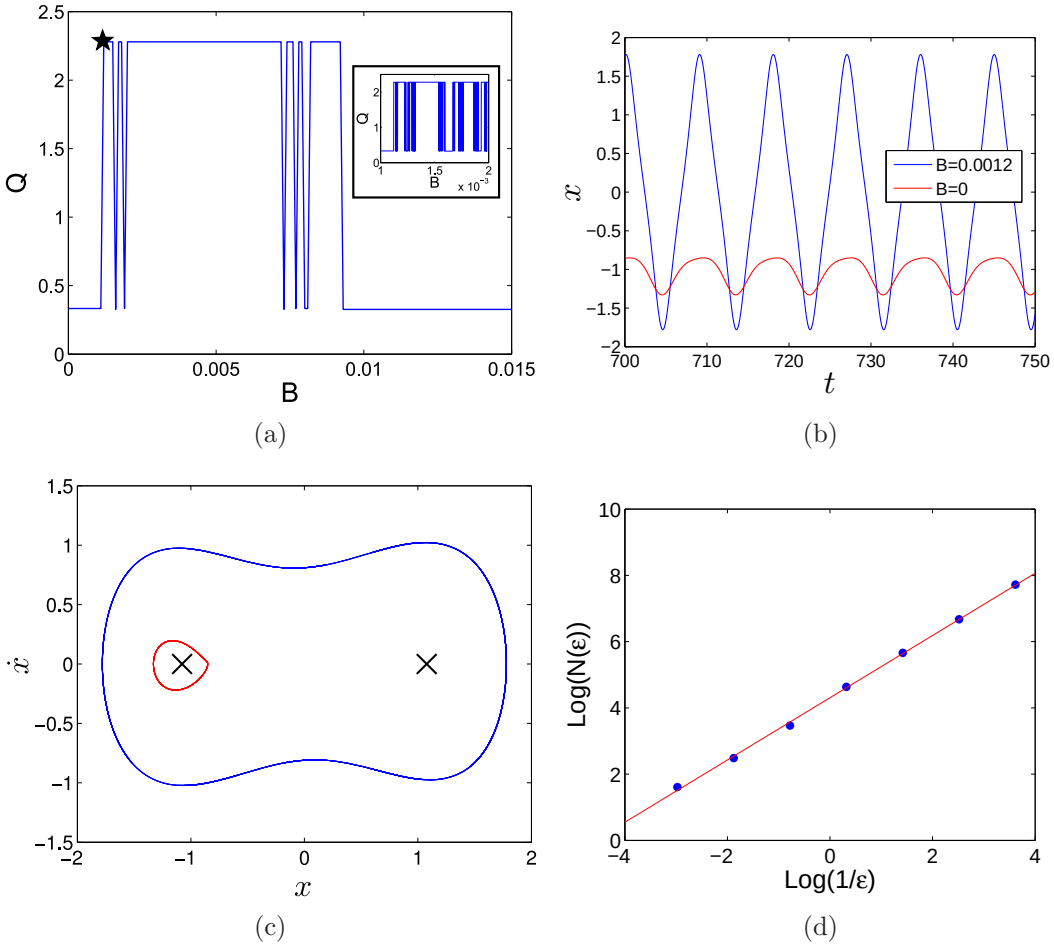

Figure 3.2. Ultrasensitive vibrational resonance. (a) The UVR curve for equation $\ddot{x}+0.1\dot{x}-0.5x+0.5x^3-0.08x(t-6.3)=0.174\cos 0.7t+B\cos 3t$. The amplitude response of the system Q varies in a sharp manner when the amplitude of the high frequency perturbation B is slightly modified. The inset is a zoom of the first apparent peak, revealing that it is composed of more peaks in a fractal-like structure. The height of Q remains almost constant, as it is very closely related to the amplitude of the attractor, which does not vary appreciably for this short range of B. (b) Time series for $B=0.0012$, marked with a star in panel (a). Here the resonant series resembles the non resonant series, but with a larger amplitude. (c) We can see the same time series represented in phase space $(x,\dot{x})$. Notice that we get a strong amplification of the signal, i.e., a high resonance for a very small amplitude of the high frequency perturbation. (d) Computation of the box-counting dimension for the curve of resonance shown in panel (a). The slope of the loglog plot indicates a non integer box-counting dimension of $d=0.93965\pm 0.00016$, which confirms that the curve is fractal.

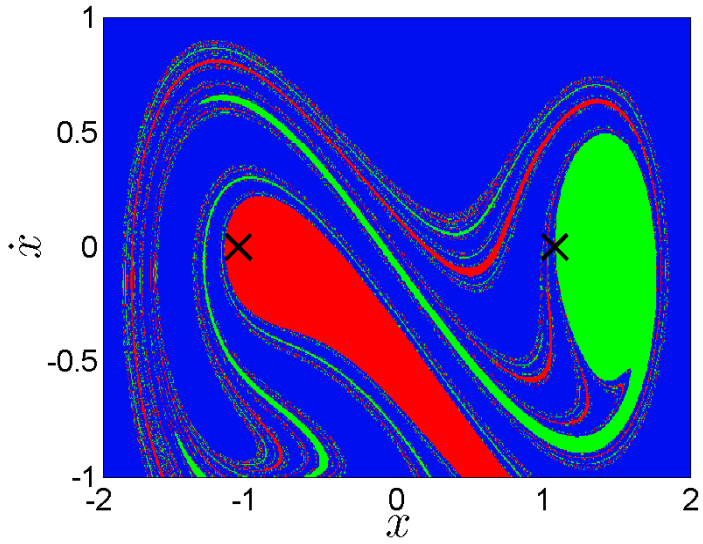

Figure 3.3. Fractal basin of the delayed Duffing oscillator. This basin of attraction in the history function space is for the Duffing oscillator with time-delayed feedback given by $\ddot{x}+0.1\dot{x}-0.5x+0.5x^3-0.08x(t-6.3) = 0.174\cos 0.7t$. This corresponds to Eq. (3.1) with $B = 0$, that is, before the high frequency perturbation is introduced. Histories have been chosen as constants. We can see a fractalization of the projection of the phase space (the actual phase space is infinite-dimensional due to the delay). Perturbations of small amplitude, such as those produced by the high frequency forcing, may drive the system to different attractors.

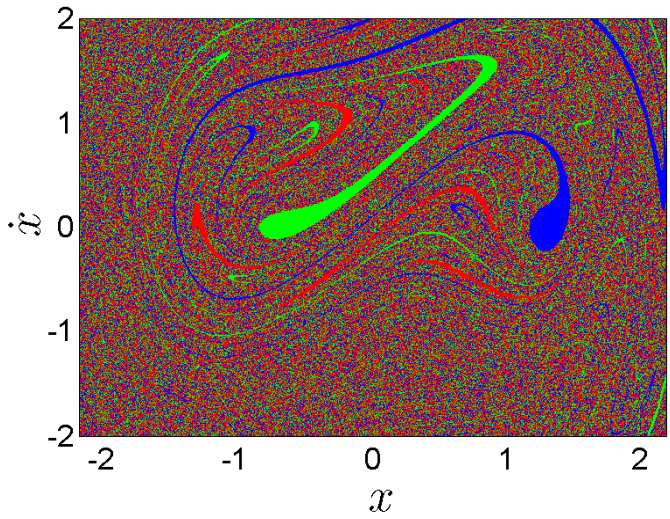

(a)

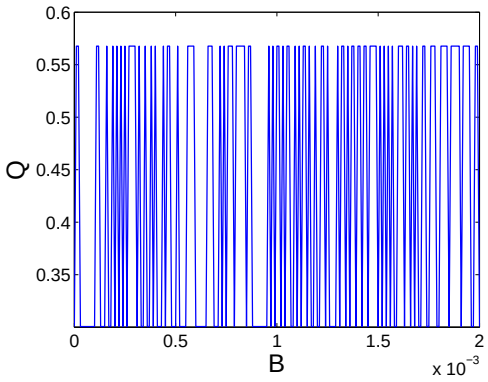

(b)

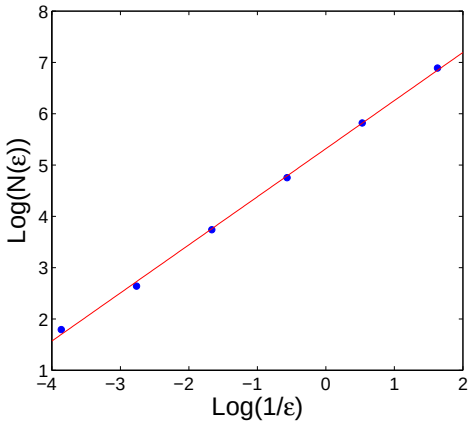

(c)

Figure 3.4. Fractal structures are responsible for UVR. The Duffing oscillator without delay is able to show UVR for this particular choice of parameters: $\ddot{x}+0.15\dot{x}-x+x^3 = 0.245\cos t$. (a) This figure shows the basin of attraction where we can observe that the phase space is *highly fractalized*, indeed this basin has the Wada property [18]. (b) Plot of the *ultrasensitive vibrational resonance* when we introduce the second harmonic perturbation and then the equation becomes $\ddot{x}+0.15\dot{x}-x+x^3 = 0.245\cos t + B\cos 10t$. The peaks of resonance follow a fractal-like structure due to the fractalization of the phase space. As in the case with delay of Fig. 3.2, the height of Q remains almost constant. This is related with the amplitude of the largest attractor of the system. (c) Computation of the box-counting dimension of the curve Q shown in panel (b). The slope of the loglog plot is 0.93737 ± 0.00024, thus the resonance curve has a non-integer dimension.

Bibliography

[1] P. S. Landa and P. V. E. McClintock, "Vibrational resonance", *J. Phys. A: Math. Gen.* **33**, L433 (2000).

[2] V. N. Chizhevsky, E. Smeu, and G. Giacomelli, "Experimental evidence of "vibrational resonance" in an optical system", *Phys. Rev. Lett.* **91**, 220602 (2003).

[3] E. Ullner, A. Zaikin, J. García-Ojalvo, R. Báscones, and J. Kurths, "Vibrational resonance and vibrational propagation in excitable systems", *Phys. Lett. A* **312**, 348–354 (2003).

[4] B. Deng, J. Wang, X. Wei, K. M. Tsang, and W. L. Chan, "Vibrational resonance in neuron populations", *Chaos* **20**, 013113 (2010).

[5] J. Shi, C. Huang, T. Dong, and X. Zhang, "High-frequency and low-frequency effects on vibrational resonance in a synthetic gene network", *Phys. Biol.* **7**, 036006 (2010).

[6] S. Rajasekar, J. Used, A. Wagemakers, and M. A. F. Sanjuán, "Vibrational resonance in biological nonlinear maps", *Commun. Nonlinear Sci.* **17**, 3435–3445 (2012).

[7] J. H. Yang and X. B. Liu, "Controlling vibrational resonance in a multistable system by time delay", *Chaos* **20**, 033124 (2010).

[8] J. H. Yang and X. B. Liu, "Delay induces quasi-periodic vibrational resonance", *J. Phys. A: Math. Theor.* **43**, 122001 (2010).

[9] J. H. Yang and X. B. Liu, "Controlling vibrational resonance in a delayed multistable system driven by an amplitude-modulated signal", *Phys. Scr.* **82**, 025006 (2010).

[10] J. H. Yang and X. B. Liu, "Delay-improved signal propagation in globally coupled bistable systems", *Phys. Scr.* **83**, 065008 (2011).

[11] C. Jeevarathinam, S. Rajasekar, and M. A. F. Sanjuán, "Theory and numerics of vibrational resonance in Duffing oscillators with time-delayed feedback", *Phys. Rev. E* **83**, 066205 (2011).

[12] A. Daza, A. Wagemakers, S. Rajasekar, and M. A. F. Sanjuán, "Vibrational resonance in a time-delayed genetic toggle switch", *Commun. Nonlinear Sci.* **18**, 411–416 (2013).

[13] S. Thompson and L. F. Shampine, "A friendly Fortran DDE solver", *Appl. Numer. Math.*, Selected Papers, The Third International Conference on the Numerical Solutions of Volterra and Delay Equations**, 56**, 503–516 (2006).

[14] J. M. Aguirregabiria and J. R. Etxebarria, "Fractal basin boundaries of a delay-differential equation", *Phys. Lett. A* **122**, 241–244 (1987).

[15] J. Losson, M. C. Mackey, and A. Longtin, "Solution multistability in first?order nonlinear differential delay equations", *Chaos* **3**, 167–176 (1993).

[16] H.-W. Yin, J.-H. Dai, and H.-J. Zhang, "Fractal basin boundaries and transversal heteroclinic intersections in a hybrid optical bistable system", *Phys. Lett. A* **206**, 370–376 (1995).

[17] S. R. Taylor and S. A. Campbell, "Approximating chaotic saddles for delay differential equations", *Phys. Rev. E* **75**, 046215 (2007).

[18] J. Aguirre and M. A. F. Sanjuán, "Unpredictable behavior in the Duffing oscillator: Wada basins", *Physica D* **171**, 41–51 (2002).

[19] L. Gammaitoni, P. Hänggi, P. Jung, and F. Marchesoni, "Stochastic resonance", *Rev. Mod. Phys.* **70**, 223–287 (1998).

Chapter 4
Testing for Wada basins

"Nature's imagination far surpasses our own."

-Richard P. Feynman, *The character of physical law*

In our quest for a better understanding of the uncertainty in nonlinear dynamics, the Wada property is an indispensable subject of study. We have seen that fractal boundaries can give rise to striking effects. Now we focus on Wada basins, a special kind of fractals, which exhibit the most entangled boundaries that one can imagine. Basins of attraction are said to be Wada when a single boundary separates three or more different basins, making initial conditions near that boundary even more unpredictable. Many physical systems of interest with this topological property appear in the literature. However, so far the only approach to study Wada basins has been restricted to two-dimensional phase spaces. In the present chapter, we develop a simple algorithm whose purpose is to look for the Wada property in any given dynamical system, widening its scope of applicability. Another benefit of this procedure is the possibility to classify and study intermediate situations known as *partially* Wada boundaries.

4.1 Introduction

Sometimes a physical property can be labeled with different discrete values depending on parameters. Suppose a space has $N_A \geq 3$ disjoint regions S_j where each S_j represents a different value or state. For example, the sets might be basins of attraction in the phase space of a dynamical system. Numerical and experimental investigations of the property in question can be intricate when the boundaries between the sets are fractal. It may be difficult to predict the state transition of the system as the initial condition is disturbed. This unpredictability increases when the boundaries of S_j are not only fractal but also possess the *Wada property*; that is, each point on the boundary of any of these regions is in fact on the boundary of all of them. In other words, the sets share the same boundary.
This situation emerges for a variety of systems of high interest in physics such as

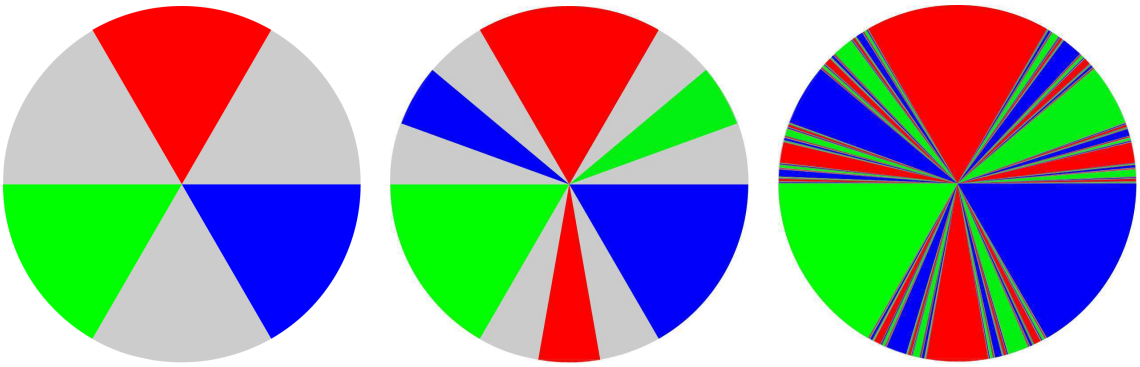

(a) (b) (c)

Figure 4.1. Disconnected Wada set. Three different stages to build a Wada set using three disconnected regions. The basins (colors) share the same boundary but each colored set is disconnected.

the basins of the forced damped pendulum [1], escapes in tokamaks [2], dyes in open hydrodynamical flows [3], the Duffing equation with a periodic forcing [4], the Hénon-Heiles system [5], or Newton's method to find complex roots [6].

The problem first arose as an investigation of regions in the plane: Can three or more open, disjoint, connected regions S_j in the plane have the same boundary? This question was answered in the affirmative by L.E.J. Brouwer in Ref. [7]. In Ref. [8], K. Yoneyama gave an example that he attributes to *Mr. Wada*, his Ph.D. supervisor, Takeo Wada. Hocking and Young [9] used the term *lakes of Wada*, a pun on water, so it was natural to extend the wordplay to dynamical systems by introducing the term *basins of Wada* [10]. The papers [11], [12] applied this concept to dynamical systems and devised a method to identify Wada basins. It is remarkable how improbable the original topological examples appeared, seeming unrelated to anything real, and yet surprisingly appear to be common in dynamical systems including physical systems like the forced damped pendulum.

The Nusse-Yorke (NY) method [11] observes that when the unstable manifold of a boundary saddle point q crosses three or more different basins, then the point q is a Wada point, as is every point in the stable manifold of q and in its closure. It can be difficult to show that the closure of that stable manifold is the entire boundary. The procedure for carrying that out is based on a concept called *basin cells*, which requires detailed knowledge of stable and unstable manifolds. The NY method is an adequate approach for basins in two dimensional phase spaces. However, the method is not suitable in many cases.

The Wada property appears in diverse situations such as the parameter space of the Hénon map [13] or the one-dimensional phase space of a competition model in ecology [14]. We can also find experimental and theoretical examples where the Wada property seems very likely to be present but the absence of a proper method

of characterization prevents its study [15], [16]. We present a special case where the basins of the dynamical system share their boundaries, but the different basins are not connected. These *disconnected* Wada basins can be illustrated as follows. Figure 4.1(a): divide a disk in six sectors and color three alternate sectors with different colors; Fig. 4.1(b): divide each empty sector into three sectors and color the central one with the color that is not at the left nor at the right; Fig. 4.1(c): repeat the second step indefinitely until filling the whole disk. The boundary of the different colors displays the Wada property by construction, but the basins are not connected; indeed the set of Wada points on the boundaries possesses a Cantor set structure. There is a rich literature documenting systems with disconnected Wada sets: the experiment of light scattered by reflecting balls [17], the Newton method to find complex roots [6], chaotic scattering in more than two dimensions [18], etc.

4.2 A grid approach

We propose a simple method, straightforward to implement, to test the Wada property in all kind of systems. Furthermore, our method/terminology allows us to classify intermediate situations where only some basins and some of the boundary present the Wada property, which receives the name of *partially* Wada basins [19], [20].

We first need some assumptions. We will discuss the notation for the case of a two dimensional space, though it is easily adapted to other cases.
1.- There is a bounded region Ω containing $N_A \geq 3$ disjoint regions S_j where $j = 1, \cdots, N_A$.
2.- There is a rectangular grid G covering Ω. We typically use a 1000×1000 grid. Hence Ω is covered by a set $P = \{box_1, ..., box_K\}$ of grid boxes (whose interiors do not intersect each other). Here K would be 10^6 for that usual grid.
3.- For each point x in Ω, it is possible to determine to which set S_j it belongs to. In other words, there is a function C with $C(x) = j$ if $x \in S_j$ and $C(x) = 0$ if x is in none of the sets S_j. If the sets are basins, the trajectory for each $x \in \Omega$ leads to an atractor labelled by $C(x)$. Notice that we do not impose different labels for each attractor. It is possible to merge several attractors into the same category. For any rectangular box denoted as box we define $C(box) = C(x)$ where x is the point at the center of box. If it does not go to an attractor in our collection of numbered attractors, then $C(box) = 0$, such events are reported at the end of the run. For convenience we will refer to this numerical value C as the *color* of the grid box. Of course other points in the same box might lead to different attractors.
4.- We define $b(box_j)$ to be the collection of grid boxes consisting of box_j and all the grid boxes that have at least one point in common with box_j, so in dimension two, $b(box_j)$ is a 3×3 collection of boxes with box_j being the central box.
5.- For each box_j, we determine the number of different (non-zero) colors in $b(box_j)$ and write $M(box_j)$ for that number.
6.- In each box_j with $M(box_j) \neq 1, N_A$, that is, which is not in the interior nor in the Wada boundary, we accomplish the following procedure. We select the two

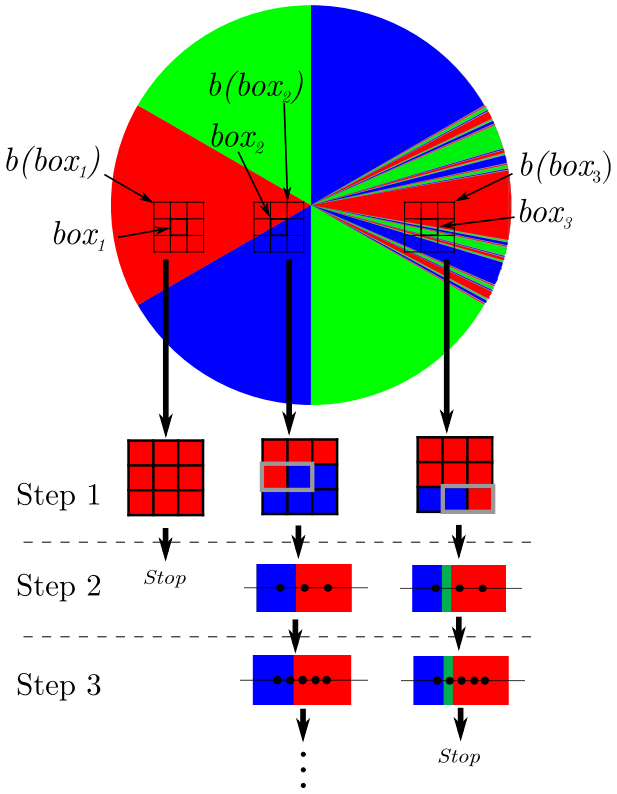

Figure 4.2. Sketch of the method. We set up a grid of boxes box_j covering the whole disk. The center point of each box defines its color. In the first step, we see that box_1 belongs to the interior because its surrounding 8 boxes have the same color. On the other hand, box_2 and box_3 are in the boundary of two attractors, i.e., they are adjacent to boxes whose color is different. In the next step the algorithm classifies box_2 still in G_2 (boundary of two), while box_3 is now classified in G_3 (boundary of three). Ideally the process would keep on forever redefining the sets G_1, G_2 and G_3 at each step, though in practice we can impose some stopping condition. This plot constitutes an example of *partially* Wada basins.

closest boxes in $b(box_j)$ with different colors and trace a line segment between them. We compute the color of the middle point of the segment. In case that the color newly computed completes all colors inside $b(box_j)$, then $M(box_j) = N_A$ and the algorithm stops. Otherwise, we compute two new points: one in the middle of the leftmost and central point, and another in the middle of the rightmost and central point. In the second step, four points interspersed with the previous five points would be calculated. In the third step, we would compute eight points interspersed with the previous nine. The procedure keeps on until $M(box_j) = N_A$ or the number of calculated points in that segment reaches some maximum value previously set up. A major computational advantage of this method is that the refinement is made in a one dimensional subspace (the segment linking the two points), no matter the dimension of Ω.

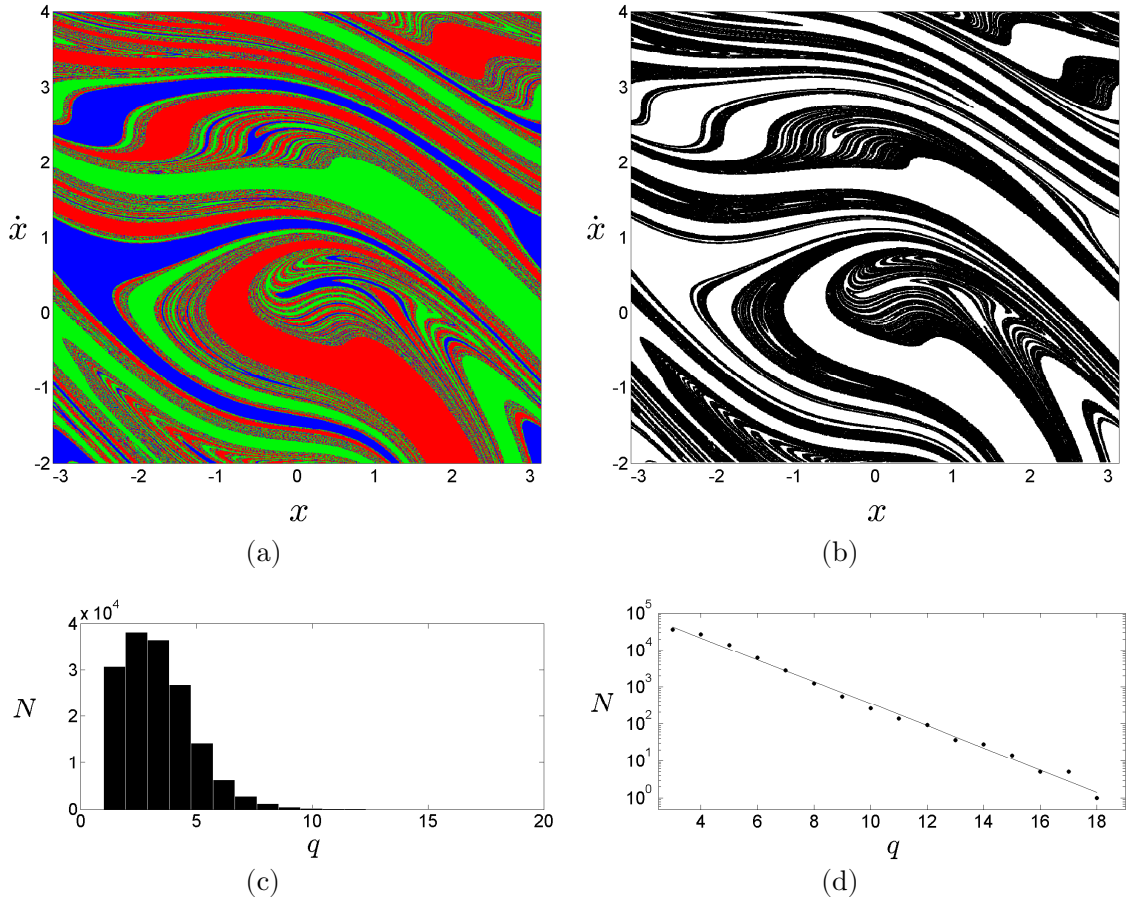

Figure 4.3. Forced damped pendulum. (a) Basins of attraction for the damped forced pendulum $\ddot{x}+0.2\dot{x}+\sin x = 1.66\cos t$. (b) All 1000×1000 boxes are labeled either in the interior (white) or in the boundary of the three basins (black). (c) Histogram showing the number of points N that take q steps to be classified as boundary of three. (d) After a maximum, there is an exponential decay of the computational effort related to the fractal structure of the basins. The log-plot reflects this tendency.

7.- Next we define G_m to be the set of all the original grid boxes box_j for which $M(box_j) = m$.

For $m = 1$, all the boxes inside the ball $b(box_j)$ have the same color as they all lead to the same attractor. In fact G_1 represents points that are in the interior of a basin. A grid box box_j is in the set G_2 (boundary of two) if there are two different colors inside the ball $b(box_j)$, a grid box is in the set G_3 (boundary of three) if there are three different colors inside the ball and so forth. To account for the evolution of these sets as the algorithm progresses, we call G_m^q the set G_m at step q.

Then, we will say that the system is Wada if $\lim_{q\to\infty} \sum_{m=2}^{N-1} \#G_m^q = 0$. This simply means that the grid boxes are either in the interior G_1 or in the Wada boundary

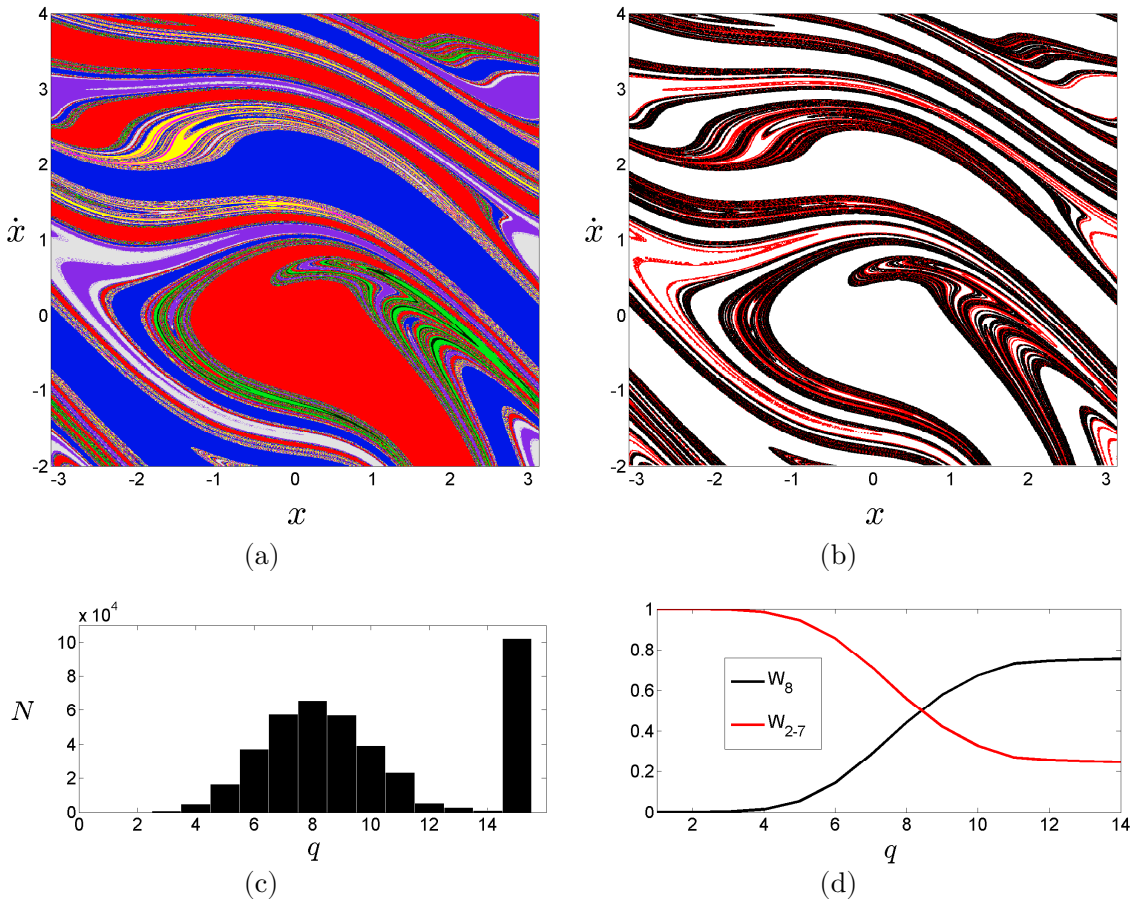

Figure 4.4. Forced damped pendulum with eight basins. (a) The damped forced pendulum with parameters $\ddot{x} + 0.2\dot{x} + \sin x = 1.73 \cos t$ shows eight basins of attraction mixed intricately. (b) Some boxes are classified to be in the boundary of eight basins (black dots), but not all of them (red dots), which is a clear example of *partial Wada*. (c) The computational effort presents the usual shape for the Wada boundary, but the points which are not Wada keep refining indefinitely (bar at rightmost). Our algorithm works best in systems with the Wada property. (d) Evolution of the proportion of boxes in the Wada boundary (W_8 in black) and proportion of boxes in a boundary which is not Wada (W_{2-7}) as a function of the q-step. The convergence of W_8 is used to determine the stopping rule.

G_{N_A} after a sufficient number of steps q.

The basic idea underlying the whole process is that if three basins are Wada, then it is always possible to find a third color between the other two colors (similar reasoning can be done for Wada basins with more than three colors). Notice also that if a boundary separates two basins we will only see those two basins at all resolutions.

To illustrate the iterative process we represent in Fig. 4.2 our example of a *partial Wada* set and compute the boundary set for three grid boxes box_1, box_2, and

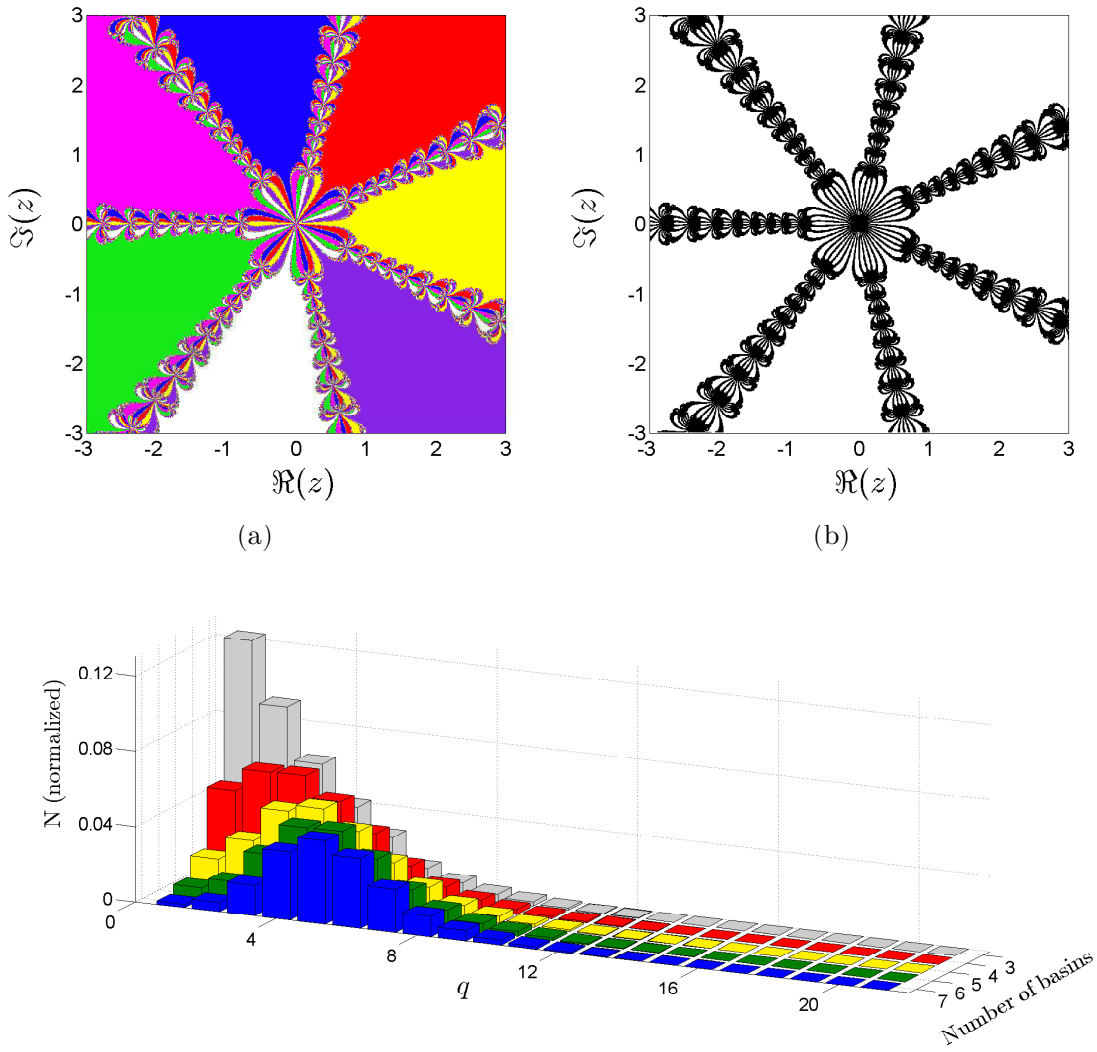

Figure 4.5. Newton method to find complex roots. (a) The map $z_{n+1} = z_n - (z^r - 1)/(rz^{r-1})$ with $r = 7$ has seven basins of attraction with the disconnected Wada property. (b) All the boxes lie in the boundary of the seven basins or in the interior. (c) Computational effort as we vary r from 3 to 7. As the number of basins increases the maximum of the histograms shift to the right, that is, the more basins the larger the computational effort. The maximum number of steps q needed for any of these basins to be considered Wada is 21.

box_3 on a regular rectangular grid forming a partition P^0 of the phase space. The first iteration for box_1 shows that it belongs to the interior region G_1^0, as the eight boxes surrounding it have the same color. At this point, we can consider box_1 in G_1^0 without refining the partition. The second, box_2, lies in the boundary of two sets because two different colors are found in its ball. The successive iterations of

the algorithm classify box_2 into G_2. A different situation arises for box_3. The first iteration classifies $box_3 \in G_2^0$ because only two colors are found in its ball. But as we increase the resolution, box_3 turns out to be in a boundary of three basins G_3^1.

In order to decide whether a system is Wada, not Wada, or presents an intermediate situation, we can count the number of boxes belonging to the boundary of m different basins. For that purpose we can define a useful parameter

$$W_m = \lim_{q\to\infty} \frac{\#G_m^q}{\sum_{j=2}^{N_A} \#G_j^q}, \tag{4.1}$$

where $m \in [2, N_A]$. This parameter $W_m \in [0, 1]$ takes a value zero if the system has no grid boxes that are in the boundary separating m basins and it takes a value one if all the boxes in the boundary separate m basins. Thus, if $W_{N_A} = 1$ the system is said to be Wada. Partial Wada occurs when $0 < W_m < 1$ with $m \geq 3$. As we will see, W_m is also useful to test the global numerical convergence.

4.3 Application of the method

In all the examples presented in this chapter, we use as initial partition a uniform grid of one million boxes, and the verification of the Wada property is made until that resolution. In order to illustrate the features of the described method, we will present an analysis of the results for the damped forced pendulum and the Newton method to find complex roots. They could be considered as paradigmatic examples of connected and disconnected Wada sets respectively. Nonetheless, we have also tested our method for the Duffing oscillator [4], the Hénon-Heiles system [5] and the magnetic pendulum [21]. In all of them, we have obtained values of $W_3 = 1$ which means they all posses the Wada property. For further details on these supplementary examples see Appendix B.

The first system we will analyze is the forced damped pendulum defined by $\ddot{x}+0.2\dot{x}+\sin x = 1.66\cos t$, which constitutes a paradigmatic system with connected Wada basins [4]. After applying our method to the basin of attraction of Fig. 4.3(a), we find that all the boxes lie either in the boundary of the three basins or in the interior within the resolution of the method (see Fig. 4.3(b)). The histogram of Fig. 4.3(c) reflects the computational effort needed to test the Wada property in this system. It shows that most of the points take less than five iterations to be labeled into the set boundary of three. Most importantly, the fractal structure of the boundary allows fast computation: as the number of steps q grows the number of remaining points N decreases exponentially (see Fig. 4.3(d)). At the end of the process, we find that $W_3 = 1$, which implies that the system is Wada.

A more challenging case arises when we increase the amplitude of the external forcing: $\ddot{x} + 0.2\dot{x} + \sin x = 1.73\cos t$. For these parameters the damped forced pendulum has at least eight attractors, and its basins are mixed complicatedly as shown in Fig. 4.4(a). When we apply our algorithm, we see that not all the boxes are classified as Wada (Fig. 4.4(b)). This is an example of *partial Wada* basins. The

points in the boundary which are not Wada (points in G_2 to G_7 in our example) increase the computational effort of the algorithm (Fig. 4.4(c)). The reason is due to nature of the process, the algorithm stops computing when $M(box_j) = N_A$ for each box or the maximum of allowed steps is reached.

In order to establish a stopping rule we can use the parameter W_m: the algorithm stops when $|W_m(step+1) - W_m(step)| < \varepsilon$, being ε a small positive number previously fixed (see Fig. 4.4(d)). Another option to deal with *partial Wada* is to merge some basins of attraction, considering two colors as only one single color for example. Making such a redefinition of the basins, we can say that the system is Wada if all the new basins share the same boundary (assuming we have at least three basins).

The second system under study is the Newton method to find complex roots, which provides examples of disconnected Wada sets. To find the roots of $z^r = 1$, $z \in \mathbb{C}$ and $r \in \mathbb{N}$, the Newton method iterates the map $z_{n+1} = z_n - (z^r - 1)/(rz^{r-1})$. This map has r different fractalized and disconnected Wada basins corresponding to the complex roots of unity. In Fig. 4.5(a) we depict the basin for $r = 7$ and in Fig. 4.5(b) we see that the algorithm yields to $W_7 = 1$, that is, all the boxes belong to the interior or to the boundary of the seven basins. Thus, our method can verify the Wada property for an arbitrary number of basins and for disconnected Wada sets too. An analysis of the computational effort for the Newton method varying r from 3 to 7 reflects that it grows with the number of basins (the maxima of the histograms in Fig. 4.5(c) shifts to the right as the number of basins increases).

4.4 Discussion

Fractal Wada boundaries seem common in nonlinear systems. However they can be overlooked or misinterpreted with a simple fractal boundary. We can also have an intermediate situation such as *partial Wada*. Our algorithm shows that in a computationally affordable time, the Wada basins can be detected for a given grid precision. Furthermore it is possible to apply the technique to disconnected Wada sets, high-dimensional problems, experimental settings, partially Wada systems and delayed systems, as it will be shown in the next chapter.

A simple key idea drives the search: on the line segment between two points of different basins there is always a point belonging to another basin if the boundary is Wada. The indicator W_m quantifies the Wada property and allows comparisons between basins. We can imagine for example a study of the measurement W_m as a function of a parameter of the system under study. Using this procedure, a Wada parameter set could be defined, in the same way that Lyapunov exponents allow the definition of the chaotic parameter set. We can also imagine an optimization algorithm to implement a heuristic search for Wada basins. We believe that this algorithm can constitute a powerful tool in the study of dynamical systems in general and of the Wada property in particular.

Bibliography

[1] H. E. Nusse, E. Ott, and J. A. Yorke, "Saddle-node bifurcations on fractal basin boundaries", *Phys. Rev. Lett.* **75**, 2482–2485 (1995).

[2] J. S. E. Portela, I. L. Caldas, R. L. Viana, and M. a. F. Sanjuán, "Fractal and wada exit basin boundaries in tokamaks", *Int. J. Bifurcation Chaos* **17**, 4067–4079 (2007).

[3] Z. Toroczkai, G. Károlyi, A. Péntek, T. Tél, C. Grebogi, and J. A. Yorke, "Wada dye boundaries in open hydrodynamical flows", *Physica A* **239**, 235–243 (1997).

[4] J. Aguirre and M. A. F. Sanjuán, "Unpredictable behavior in the Duffing oscillator: Wada basins", *Physica D* **171**, 41–51 (2002).

[5] J. Aguirre, J. C. Vallejo, and M. A. F. Sanjuán, "Wada basins and chaotic invariant sets in the Hénon-Heiles system", *Phys. Rev. E* **64**, 066208 (2001).

[6] B. Epureanu and H. Greenside, "Fractal basins of attraction associated with a damped Newton's method", *SIAM Rev.* **40**, 102–109 (1998).

[7] L. E. J. Brouwer, "Zur analysis situs", *Math. Ann.* **68**, 422–434 (1910).

[8] K. Yoneyama, "Theory of continuous sets of points", *Tokohu Math. J.* **11**, 43–158 (1917).

[9] J. G. Hocking and G. S. Young, *Topology*. Reading: Addison Wesley, 1961.

[10] J. Kennedy and J. A. Yorke, "Basins of Wada", *Physica D* **51**, 213–225 (1991).

[11] H. E. Nusse and J. A. Yorke, "Wada basin boundaries and basin cells", *Physica D* **90**, 242–261 (1996).

[12] H. E. Nusse and J. A. Yorke, "Fractal basin boundaries generated by basin cells and the geometry of mixing chaotic flows", *Phys. Rev. Lett.* **84**, 626–629 (2000).

[13] Y. Zhang and G. Luo, "Unpredictability of the Wada property in the parameter plane", *Phys. Lett. A* **376**, 3060–3066 (2012).

[14] J. Vandermeer, "Wada basins and qualitative unpredictability in ecological models: a graphical interpretation", *Ecol. Model.* **176**, 65–74 (2004).

[15] G. L. Gattobigio, A. Couvert, B. Georgeot, and D. Guéry-Odelin, "Exploring classically chaotic potentials with a matter wave quantum probe", *Phys. Rev. Lett.* **107**, 254104 (2011).

[16] G. L. Gattobigio, A. Couvert, G. Reinaudi, B. Georgeot, and D. Guéry-Odelin, "Optically guided beam splitter for propagating matter waves", *Phys. Rev. Lett.* **109**, 030403 (2012).

[17] D. Sweet, E. Ott, and J. A. Yorke, "Topology in chaotic scattering", *Nature* **399**, 315–316 (1999).

[18] Z. Kovács and L. Wiesenfeld, "Topological aspects of chaotic scattering in higher dimensions", *Phys. Rev. E* **63**, 056207 (2001).

[19] J. Aguirre, R. L. Viana, and M. A. F. Sanjuán, "Fractal structures in nonlinear dynamics", *Rev. Mod. Phys.* **81**, 333–386 (2009).

[20] Y. Zhang and G. Luo, "Wada bifurcations and partially Wada basin boundaries in a two-dimensional cubic map", *Phys. Lett. A* **377**, 1274–1281 (2013).

[21] A. E. Motter, M. Gruiz, G. Károlyi, and T. Tél, "Doubly transient chaos: generic form of chaos in autonomous dissipative systems", *Phys. Rev. Lett.* **111**, 194101 (2013).

Chapter 5
Wada property in systems with delay

"En général, on néglige la durée de la transmission et on regarde les deux événements comme simultanés. Mais, pour être rigoureux, il faudrait faire encore une petite correction par un calcul compliqué... "

-Henri Poincaré, *La valeur de la science*

In Chapter 2 and Chapter 3, we observed that the delay can induce instabilities in a system, increasing its unpredictability. Now we further inquire about this relation between delay and unpredictability, paying special attention to the appearance of the Wada property in systems with delay. The particularities of delayed systems prevented the application of the classical methods to study the Wada property, but thanks to the algorithm introduced in Chapter 4 we can test the Wada property in any kind of system, delayed systems included.

5.1 Introduction

The objective of this chapter is twofold: on the one hand, we study the effects of the delay in nonlinear dynamical systems, focusing on their associated uncertainty; on the other hand, we study the emergence of the Wada property when delays are involved.

Delay differential equations (DDEs) take into account the time taken by systems to sense and react to the information they receive, in other words, that the information transmission cannot be instantaneous, but delayed. For practical purposes, these lags can often be ignored when their timescales are very small compared to the dynamics of the system. However, there are situations where large delays cannot be overlooked: genetic oscillators [1], neuron networks [2], respiratory and hematopoietic diseases [3], electronic circuits [4], optical devices [5], engineering applications [6], etc. Delay differential equations provide a very useful tool for the modelling of the previous examples. Moreover, they are able to display such interesting kind of

dynamics as deterministic Brownian motion [7], hyperchaos [8] and many cooperative effects [9]–[11]. It is also important to mention that DDEs have the property of time-irreversibility [12], which introduces further difficulties in the analysis, but also gives a more realistic perspective of many processes.

As we have already mentioned in previous chapters, a crucial feature of DDEs is that they need an infinite set of initial conditions to be integrated. This set is usually called *history* and provides the state of the system before the action of the delayed terms. Sometimes history is set randomly, although given the sensitivity of some systems with delay and the difficulties arising when an infinite set of initial random points is needed, the choice of random histories is a delicate issue. A better option is to set the history as the solution of the system without the delayed terms. Another possibility are history functions[1] described by some parameters and properly chosen for each physical situation.

A convenient way to handle this infinite number of initial conditions is to define history functions characterized by a finite number of parameters. This supposes a huge difference with respect to nonlinear systems modelled with ordinary differential equations (ODEs), since the space of the history functions and the real phase space are not in correspondence. Therefore, basins of attraction, which are a very powerful tool to study sensitivity in dissipative systems, have a different nature in DDEs.

In dissipative dynamical systems defined by ODEs, the basins of attraction register in a plot the attractors reached by different initial conditions. In DDEs the same idea can be exploited: we can plot basins of attraction varying the parameters of the history functions. These basins are subspaces of the infinite dimensional space of history functions, but still can provide much information about the sensitivity of the system. Only a few authors have studied basins of attraction in DDEs [13]–[15]. In this chapter, we study how the delay can induce uncertainty in the system, and we pay special attention to the appearance of the Wada property in these basins of attraction made out of different history functions.

In Chapter 4, we saw that the Wada property is a topological property that can be stated as follows: given more than two open sets, they all share the same boundary. This situation is very counter-intuitive, since most boundaries are only between two sets. In some cases there might be some points or regions that separate more than two open sets, but the case where every point in the boundary is in the boundary of all the sets is unique.

The interest in the Wada property lies on the fact that their boundaries are the most entangled that we can imagine, since they separate all the basins at the same time. Therefore, small perturbations near the boundaries can lead to any of the different attractors of the system. This unique uncertainty of Wada basins is revisited from a different perspective in Chapter 6.

The Wada property also appears in systems with more than two degrees of freedom [16]–[18]. In these cases the basins have more than two dimensions and the subspaces generally show the disconnected Wada property: the different basins share

[1]For more details about history functions see Appendix C.

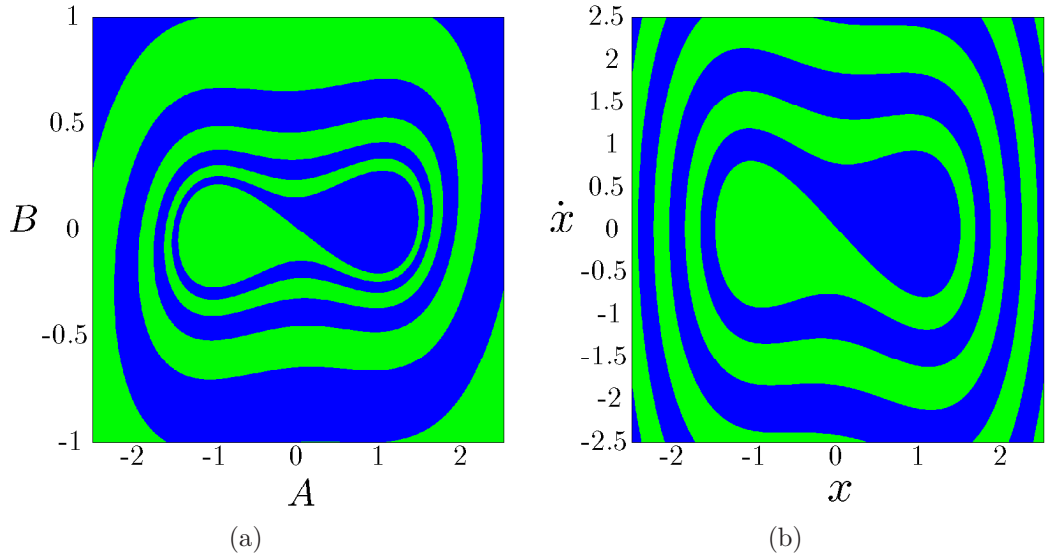

Figure 5.1. Comparison between the delayed action and Duffing oscillators. (a) Basin of attraction of the delayed action oscillator $\dot{x} + x((1+\alpha)x^2 - 1) - \alpha x_\tau = 0.$ with $\alpha = -0.95$ and $\tau = 1.065$. (b) Basin of attraction of the Duffing oscillator $\ddot{x} + \gamma\dot{x} + x(x^2 - 1) = 0.$ with $\gamma = 0.15$. Both figures show a similar topology, but Fig. 5.1 (b) represents only a slice of the infinite dimensional space of history functions, given by the family of history functions of Eq. 5.2.

the same boundary but they are disconnected. These disconnected Wada basins can be analyzed by means of the techniques developed in Chapter 4.

The aim of the present chapter is to investigate the connection between delay and unpredictability, looking also for the Wada property in systems with delay. We organize this search as follows. In Sections 5.2 and 5.3 we introduce two delayed systems that present different degrees of the Wada property. Finally, in Section 5.4 we briefly summarize and discuss our main results.

5.2 Forced delayed action oscillator

We start studying an apparently simple system sometimes called the delayed action oscillator (DAO). It is a single variable system with a double-well potential and a linear delayed feedback with constant time delay τ, that we will denote x_τ. It can be stated as follows,

$$\dot{x} + x((1+\alpha)x^2 - 1) - \alpha x_\tau = 0. \tag{5.1}$$

where $\alpha, \tau \in \mathbb{R}$. Boutle et al. [19] proposed this model in the context of the ENSO (El Niño Southern Oscillation) phenomenon, where the variable x represents the temperature anomaly of the ocean's surface. in Ref. [20], the authors analyze the stability and bifurcations of this system by a center manifold reduction. They

demonstrate that as the delay increases beyond a critical value τ_c, the steady state solution $x = 0$ can undergo a Hopf bifurcation giving rise to a limit cycle. Without the delayed term, this system would be a one-dimensional ODE and could not oscillate, but the linear delayed feedback makes the system infinite-dimensional allowing oscillatory dynamics. In the case that $\alpha > -1$ and $\tau > \tau_c$ the limit cycle coexists with two stable fixed points, so the system can be multistable. To visualize the situation in a plot, we choose the following family of history functions defined by two parameters A and B,

$$x(t) = A + Bt, \, \forall \, t \in [-\tau, t_0] \, . \tag{5.2}$$

Unless specified, this linear equation will be the family of history functions chosen by default along the present chapter. Now, we can compute a basin of attraction varying A and B. Figure 5.1(a) represents the basin for $\alpha = -0.95$ and $\tau = 1.065$, below the critical value τ_c. It is interesting to notice the analogy between the DAO and the well-known Duffing oscillator

$$\ddot{x} + \gamma \dot{x} + x(x^2 - 1) = 0. \tag{5.3}$$

The structure of its basin of attraction is very similar to the DAO model as shown in Fig. 5.1(b). However it is important to notice that the two basins have different nature: we have the real phase space for the Duffing oscillator and a slice of the infinite space of history functions in the case of the DAO.

At this point it is important to make a connection with Ref. [21]. In that work, Aguirre and Sanjuán studied the Duffing oscillator driven by a periodic forcing $F \sin \omega t$ on the right hand side of Eq. (5.3). They showed that if the parameters are carefully chosen ($\gamma = 0.15, \omega = 1, F \in (0.24, 0.26)$), the system can display the Wada property. Making a naive analogy, it is plausible that we will encounter the same effect by including the periodic forcing in the DAO such as

$$\dot{x} + x((1 + \alpha)x^2 - 1) - \alpha x_\tau = F \sin \omega t. \tag{5.4}$$

For $\alpha = -0.925$, $\tau = 1.065$, $F = 0.525$ and $\omega = 1$, this system presents three attractors (see Fig. 5.2(a)). Given the periodic forcing, we can make a stroboscopic map taking $t = (2\pi/\omega)n, n \in \mathbb{Z}$. In this map, two of these attractors are period-three orbits, suggesting the possibility of chaotic dynamics in the system [22]. In fact, a chaotic attractor exists for other parameters. For the chosen set of parameters, we can tell that it is the delay that makes possible the appearance of chaotic dynamics in the phase space. Otherwise for $\tau = 0$, the system would have a dimension equal to two, forbidding any chaotic motion.

A few authors have studied the relation between delay and chaos [23], [24], but the delay was always considered in a nonlinear term. We show here that a linear delayed feedback can also induce chaos in a continuous system. Some systems displaying chaos have been modified with a linear delayed feedback, preserving the chaotic motion [13]. But in this model, the linear delayed feedback is providing the

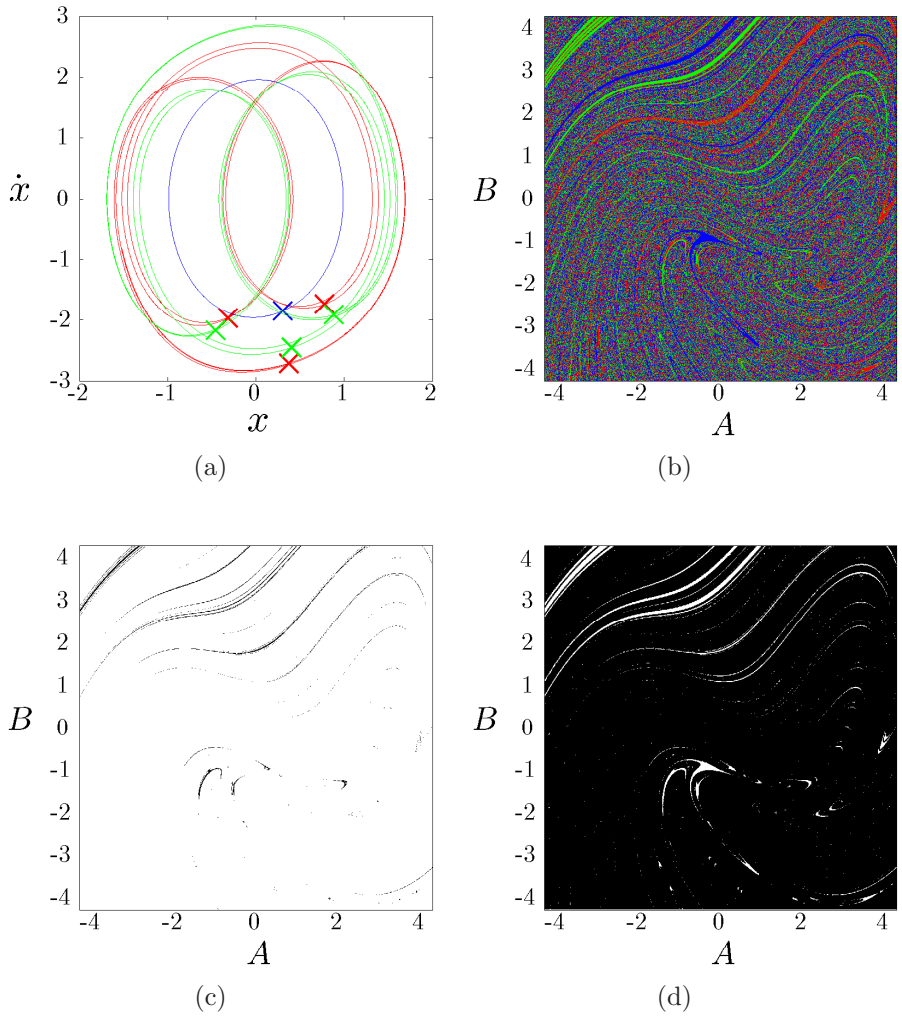

Figure 5.2. Transient chaos induced by linear delay. (a) Attractors of the forced DAO defined by $\dot{x}+x((1+\alpha)x^2-1)-\alpha x_\tau = F\sin\omega t$ for $\alpha=-0.925$, $\tau=1.065$, $F=0.525$, and $\omega=1$. There is a period-1 orbit (in the stroboscopic map) and two symmetric period-3 orbits. Trajectories intersect because this is a projection in $(x,\dot{x})$, but the system lives in infinite dimensions in principle. (b) The basins of attraction are highly mixed, increasing the unpredictability of the system. However, as panels (c) and (d) show the system is not completely Wada: some points separate only two basins, so the system is only partially Wada.

extra dimensions that the system needs to display chaos, in the same way that the delay allows sustained oscillations in a system of one variable.

The system of Eq. 5.4 presents transient chaos and possesses three attractors (depicted in Fig. 5.2(a)). If we plot the basin of attraction (Fig. 5.2(b)) we can see that the picture is highly fractalized and looks like Wada. As discussed before, the Nusse-Yorke method to verify if the basin is actually Wada is not applicable

here, since we do not have a correspondence between the phase space of the history functions and the actual phase space. However, we can apply the test presented in Chapter 4 in order to decide whether it is Wada or not.

In the previous chapter, we have explained how the algorithm sets a grid and searches for the points lying on the boundary of two or three atractors. The test for Wada is conclusive if all the points in the boundary belong to the boundary of three atractors. Applying our grid method, the 3-boundary has box-counting dimension equal to 1.602 (see Fig. 5.2(c)) and the 2-boundary 0.761 (see Fig. 5.2(d)). The indicator $W_3 = 0.990$ also reveals that the system is not fully Wada, but only partially Wada. In fact, if we zoom in, we can see that the red and green basins do not mix with the blue one, so there is a boundary between red and green that they do not share with the blue basin.

It is clear from the plot of the basin in Fig. 5.2(b) that the system is highly unpredictable, but it does not show the Wada property. We have scanned a wide range of parameters and we have not been able to find the Wada property for the forced DAO of Eq. 5.4. Perhaps there are small parameter ranges where the Wada property arises, but since the requirements that a system must fulfill to exhibit the Wada property are unclear, we cannot assure nor discard that the forced DAO can display the Wada property. Nonetheless, the delay can induce not only chaos, but also the Wada property, as we will see in the next section.

5.3 Forced DAO with nonlinear delayed feedback

After studying the forced DAO a question arises: what are the differences between the forced DAO and the forced Duffing oscillator? In principle, both of them have the same nonlinear potential, a periodic forcing and enough dimensions to show chaos, and possibly Wada. However, there is an important feature that makes them different.

In order to contrast the two systems, let us write on the one hand the forced Duffing oscillator equation as the following first order autonomous system,

$$\begin{aligned} \dot{x}_0 &= \omega \\ \dot{x}_1 &= \alpha x_N + x_1 - (1+\alpha)x_1^3 + F\sin x_0 \\ \dot{x}_i &= \frac{N}{\tau}(x_{i-1} - x_i), \text{ for } i \geq 2. \end{aligned} \tag{5.5}$$

On the other hand, following a usual technique for delay differential equations (see e.g. [7]), we can rewrite the forced DAO of Eq. (5.4) in form of an ODE with infinite dimensions:

$$\begin{aligned} \dot{x}_0 &= \omega \\ \dot{x}_1 &= -\gamma x_1 + x_2 + x_2^3 + F\sin x_0 \\ \dot{x}_2 &= x_1, \end{aligned} \tag{5.6}$$

Comparing the expressions (5.6) and (5.5) we see that they are very similar, but there is one important difference. In the case of the forced Duffing oscillator (Eq. 5.6),

the evolution of x_1 depends on the nonlinear term of the variable x_2. However, in the forced DAO (Eq. 5.5) the evolution of x_1 depends linearly on x_N, and the nonlinearity is in x_1 (see table 5.1 for an easy visualization of the two systems side by side).

Forced Duffing	Forced DAO extended
$\dot{x}_0 = \omega$ $\dot{x}_1 = -\gamma x_1 + x_2 + x_2^3 + F \sin x_0$ $\dot{x}_2 = x_1,$	$\dot{x}_0 = \omega$ $\dot{x}_1 = \alpha x_N + x_1 - (1+\alpha)x_1^3 + F \sin x_0$ $\dot{x}_i = \frac{N}{\tau}(x_{i-1} - x_i),$ for $i \geq 2.$

Table 5.1. Comparison between the forced Duffing and the forced DAO. The main difference between them is that the evolution of x_1 depends on the nonlinear term of x_2 in the forced Duffing, while it depends linearly on x_N for the forced DAO.

As we mentioned earlier, the conditions for the Wada property are unknown, but in our exploration of delayed systems we find pertinent to study the system with the delay in the nonlinear term, looking even more similar to the forced Duffing oscillator. This system can be written in the usual manner as

$$\dot{x} + \alpha(x_\tau^3 - x_\tau) + x = F \sin \omega t. \tag{5.7}$$

In the extended version of this equation, we can see that the evolution of x_1 depends on the nonlinear term x_N^3. A careful exploration of the parameter space reveals that for $\alpha = 2.5$, $\tau = 1$, $F = 1.15$, and $\omega = 1.2$ the system has three attractors: one attractor at infinity (solutions that diverge) and the two period-2 attractors of Fig. 5.3(a). Plotting the basin of attraction (Fig. 5.3(b)), we see that it looks like a disconnected Wada set. The grid method to verify the Wada property, described in the previous chapter, confirms our intuition after a few steps: every point in the boundary separates three basins (see Fig. 5.3(c)) giving a Wada parameter of $W_3 = 1$. The basins are disconnected because we are only looking at one slice of the infinite dimensional space of history functions, as it happens in the basins of the 3D scattering of Ref. [17]. For every history function we have tested, no matter how many parameters (dimensions) it had: the basin always shows the property of Wada. For example, Fig. 5.3(c) is the plot of the basins of attraction for the same system with another family of history functions, a different slice of the infinite dimensional history function space, also showing the Wada property. These are solid arguments to affirm that the delay induces chaos and gives rise to the Wada property in the infinite dimensional space of history functions, turning the system strongly unpredictable and very sensitive to small changes in the history function.

It is interesting to note that the rings that appear in the full Wada basin of Fig. 5.3-(b) can be easily reproduced by means of an iterative process to construct disconnected Wada sets, as the one we used in the previous chapter. The procedure

to develop a set of disconnected Wada rings can be summarized in the three steps sketched in Fig. 5.4: (a) draw a disk with two concentric rings around it, each one with a different color leaving some space between them; (b) divide each white space in three rings and color the central part with a different color from the closest colored rings; (c) repeat the previous step infinitely until filling the whole disk. Figure 5.4(d) is a zoom of the basin depicted in Fig. 5.3(b). The similarity between Fig. 5.4(c) and Fig. 5.4(d) is clear.

5.4 Discussion

In our exploration of the interplay between uncertainty and delay, we have investigated some simple delayed systems and their basins of attraction in the space of history functions. Given the apparent similarities between the delayed action and the Duffing oscillators, we have decided to add a periodic forcing to the delayed action oscillator and to look for the Wada property as it appeared in the basins of the Duffing oscillator. We have found the first example, to the best of our knowledge, where a linear delayed term induces transient chaos in a continuous system. Nonlinear delayed terms were known to induce chaotic dynamics [3], [23], [24], but in this case the linear delay provides the extra dimensions that the system needs to show chaos. Although this constitutes an interesting result by itself, our objective is also to study the properties of the basins of attraction. Despite our careful research, we were unable to find the Wada property in the forced delayed action oscillator. Perhaps it happens in a small region of the parameter space, or perhaps it does not happen. Although the phase space is *highly fractalized* and the system is very close to show the full Wada property, we must label it as partially Wada.

Finally, we introduced the delay in the cubic term. In this system we were able to find not only transient chaos, but also the full Wada property. The basins of attraction that we plot are subspaces of the infinite dimensional history function space, and all of them have the same properties. This means that this is probably the first report of the full Wada property in infinite dimensions. Infinite Wada basins can be obtained varying the family of history functions, and we can also modify the number of parameters obtaining Wada basins of arbitrary dimension. Without delay, this system would only show oscillatory dynamics, but here the delay induces both chaos and the Wada property. We expect that this study contributes to the investigation of delayed systems, especially concerning its sensitivity.

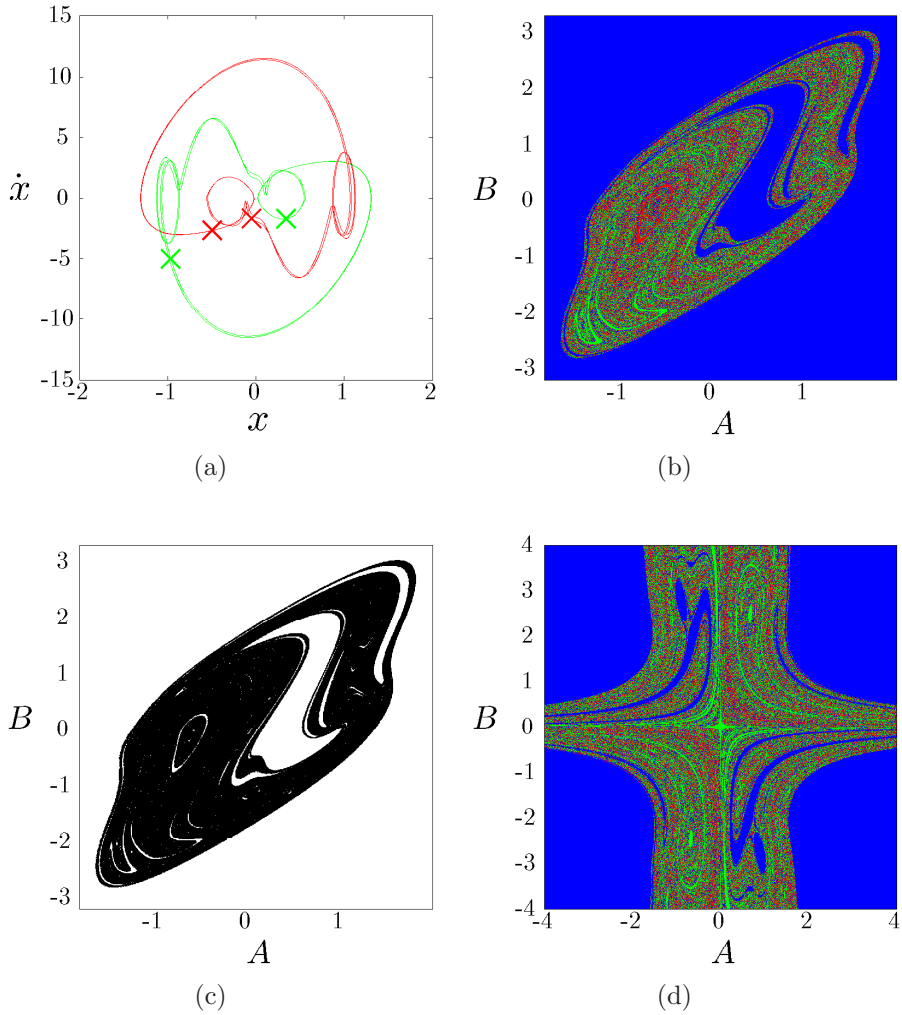

Figure 5.3. Wada property induced by delay in nonlinear feedback. (a) Attractors of the system $\dot{x} + \alpha(x_\tau^3 - x_\tau) + x = F \sin \omega t$ with $\alpha = 2.5$, $\tau = 1$, $F = 1.15$, and $\omega = 1.2$. The system has two period-2 orbits and also diverging trajectories. Trajectories intersect themselves because this is a projection in $(x, \dot{x})$, but in principle, the system lives in infinite dimensions. (b) Basin of attraction: history functions leading to infinity are colored in blue, and the red and green colors are for history functions leading to the two period-2 orbits. This is an example of disconnected Wada basin. (c) All the points in the boundary separate three basins, thus the system possess the Wada property. (d) Basin of attraction with an oscillating history function $x(t) = A \sin Bt$, $\forall\, t \in [-\tau, t_0]$. The Wada property is independent of the initial history function chosen ($W_3 = 1$). Different initial history functions are different subspaces of the same infinite dimensional space, they all have the Wada property.

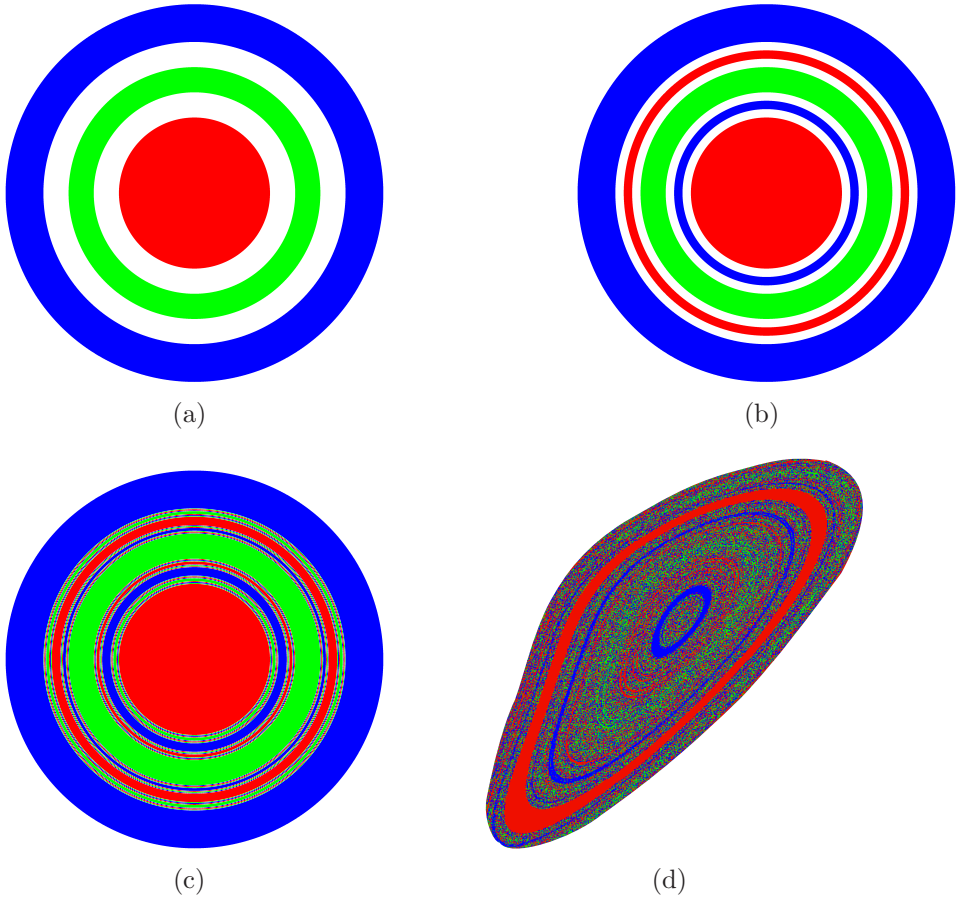

Figure 5.4. Disconnected Wada property in rings (a)-(b)-(c) Three different steps of the iterative toy example to build a disconnected Wada set. The white space between rings in panel (a) is filled in such a way that the basins (colors) share the same boundary, but they are disconnected sets. (d) Zoom from Fig. 5.3-(b), where we can see a structure topologically equivalent to our toy example.

Bibliography

[1] J. Lewis, "Autoinhibition with transcriptional delay: a simple mechanism for the zebrafish somitogenesis oscillator", *Curr. Biol.* **13**, 1398–1408 (2003).

[2] A. Nordenfelt, J. Used, and M. A. F. Sanjuán, "Bursting frequency versus phase synchronization in time-delayed neuron networks", *Phys. Rev. E* **87**, 052903 (2013).

[3] M. C. Mackey and L. Glass, "Oscillation and chaos in physiological control systems", *Science* **197**, 287–289 (1977).

[4] X. F. Wang, G.-Q. Zhong, K.-S. Tang, K. Man, and Z.-F. Liu, "Generating chaos in Chua's circuit via time-delay feedback", *IEEE T. Circuits-I* **48**, 1151–1156 (2001).

[5] K. Ikeda and K. Matsumoto, "High-dimensional chaotic behavior in systems with time-delayed feedback", *Physica D* **29**, 223–235 (1987).

[6] Y. N. Kyrychko and S. J. Hogan, "On the use of delay equations in engineering applications", *J. Vib. Control*, (2010).

[7] J. C. Sprott, "A simple chaotic delay differential equation", *Phys. Lett. A* **366**, 397–402 (2007).

[8] K. Ikeda and K. Matsumoto, "Study of a high-dimensional chaotic attractor", *J. Stat. Phys.* **44**, 955–983 (1986).

[9] D. V. Ramana Reddy, A. Sen, and G. L. Johnston, "Experimental evidence of time-delay-induced death in coupled limit-cycle oscillators", *Phys. Rev. Lett.* **85**, 3381–3384 (2000).

[10] A. Nordenfelt, A. Wagemakers, and M. A. F. Sanjuán, "Frequency dispersion in the time-delayed Kuramoto model", *Phys. Rev. E* **89**, 032905 (2014).

[11] M. Lakshmanan and D. V. Senthilkumar, *Dynamics of nonlinear time-delay systems*. Berlin: Springer, 2011.

[12] M. C. Mackey, "The dynamic origin of increasing entropy", *Rev. Mod. Phys.* **61**, 981–1015 (1989).

[13] J. M. Aguirregabiria and J. R. Etxebarria, "Fractal basin boundaries of a delay-differential equation", *Phys. Lett. A* **122**, 241–244 (1987).

[14] J. Losson, M. C. Mackey, and A. Longtin, "Solution multistability in first?order nonlinear differential delay equations", *Chaos* **3**, 167–176 (1993).

[15] S. R. Taylor and S. A. Campbell, "Approximating chaotic saddles for delay differential equations", *Phys. Rev. E* **75**, 046215 (2007).

[16] B. Epureanu and H. Greenside, "Fractal basins of attraction associated with a damped Newton's method", *SIAM Rev.* **40**, 102–109 (1998).

[17] Z. Kovács and L. Wiesenfeld, "Topological aspects of chaotic scattering in higher dimensions", *Phys. Rev. E* **63**, 056207 (2001).

[18] D. Sweet, E. Ott, and J. A. Yorke, "Topology in chaotic scattering", *Nature* **399**, 315–316 (1999).

[19] I. Boutle, R. H. S. Taylor, and R. A. Römer, "El Niño and the delayed action oscillator", *Am. J. Phys.* **75**, 15–24 (2007).

[20] B. F. Redmond, V. G. LeBlanc, and A. Longtin, "Bifurcation analysis of a class of first-order nonlinear delay-differential equations with reflectional symmetry", *Physica D* **166**, 131–146 (2002).

[21] J. Aguirre and M. A. F. Sanjuán, "Unpredictable behavior in the Duffing oscillator: Wada basins", *Physica D* **171**, 41–51 (2002).

[22] T.-Y. Li and J. A. Yorke, "Period three implies chaos", *Am. Math. Mon.* **82**, 985–992 (1975).

[23] U. a. d. Heiden and M. C. Mackey, "The dynamics of production and destruction: analytic insight into complex behavior", *J. Math. Biology* **16**, 75–101 (1982).

[24] J. K. Hale and N. Sternberg, "Onset of chaos in differential delay equations", *J. Comput. Phys.* **77**, 221–239 (1988).

Chapter 6
Basin entropy

"It's abundantly obvious that one doesn't know the world around us in detail. [...]. When you look at early stuff of Van Gogh there are zillions of details that are put into it, there's always an immense amount of information in his paintings. "

-Mitchell Feigenbaum in *Chaos: making a new science* by James Gleick

The notion of unpredictability in dynamical systems is the central topic of this thesis. In particular, we mostly focus in the difficulties that arise in the final state prediction when fractal structures arise in phase space. But what do we mean when we talk about unpredictability in this context? Is it something that we can measure? For instance, Chapter 4 and Chapter 5 are dedicated to the Wada property, and the interest of this topological property is commonly assumed to lie in its unique unpredictability, but how can we account for it?

The present chapter aims to answer all these questions by introducing the notion of *basin entropy*, a quantitative measure of unpredictability. In this respect, this chapter is fundamental for this thesis since it confers a quantitative basis for the interest of all the problems studied here. Additionally, some of the results derived from the concept of *basin entropy* have interesting applications in experimental settings, as we will see in the next chapter.

6.1 Introduction

This whole thesis deals with dynamical systems, that is, a set of deterministic rules that describe magnitudes evolving in time. These magnitudes evolve in time towards some asymptotic behavior depending on the initial conditions and on the specific choice of parameters. If a given dynamical system possesses only one attractor in a certain region of phase space, then for any initial condition its final destination is clearly determined, so that we may say that we have a complete certainty about its ultimate behavior: any orbit starting at any initial condition will tend to that

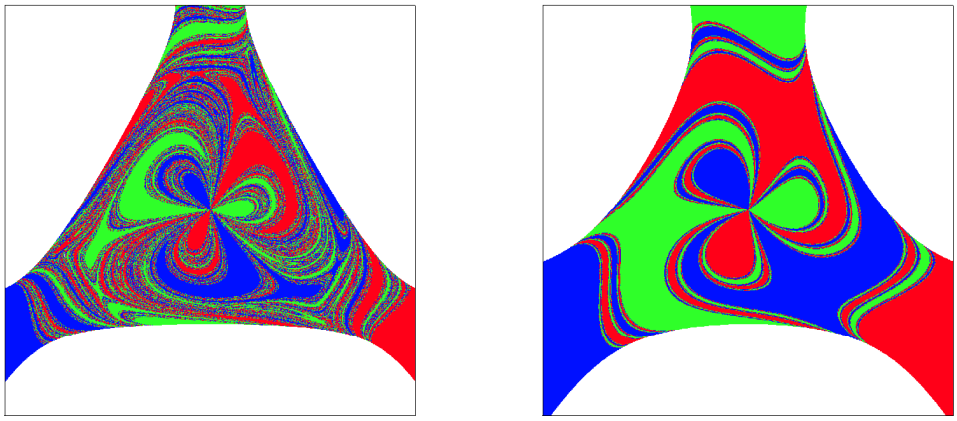

(a) (b)

Figure 6.1. Comparison between basins. Escape basins for the Hénon-Heiles system but different energies. They represent which exit will take each initial condition. It is clear that determining the final destination of the trajectories in the case (a) is harder than in the case (b).

attractor. However, as we have already seen in previous chapters, dynamical systems often present several attractors: the genetic toggle switch or the delayed action oscillator are examples of multistable dynamical systems. In these cases, elucidating which orbits tend to which attractor becomes a fundamental question.

The concept of basin of attraction [1] has already been introduced in previous chapters: it is defined as the set of points that, taken as initial conditions, lead the system to a specific attractor. When there are two different attractors in a certain region of phase space, two basins exist which are separated by a basin boundary. We have showed examples where the basin boundary can be a smooth curve or can be instead a fractal curve, and we have seen that the study of these basins can provide much information about the system. For example, the topology of the basins is deeply related to the dynamical nature of the system, so that systems with chaotic dynamics usually display basins of attraction with fractal structures [2].

The previous discussion applies typically to dissipative dynamical systems. Indeed, the concept of attractors or basins of attraction is meaningless for Hamiltonian systems. However, for open systems, we can define escape basins in an analogous way to the basins of attraction in a dissipative system. An escape basin, or exit basin, is the set of initial conditions that escape through a certain exit. The Hénon-Heiles Hamiltonian is a well-known model for an axisymmetrical galaxy and it has been used as a paradigm in Hamiltonian nonlinear dynamics. It is a two-dimensional time-independent dynamical system, where orbits having an energy above the critical one can escape through one of the three different exits. It is widely known that when two

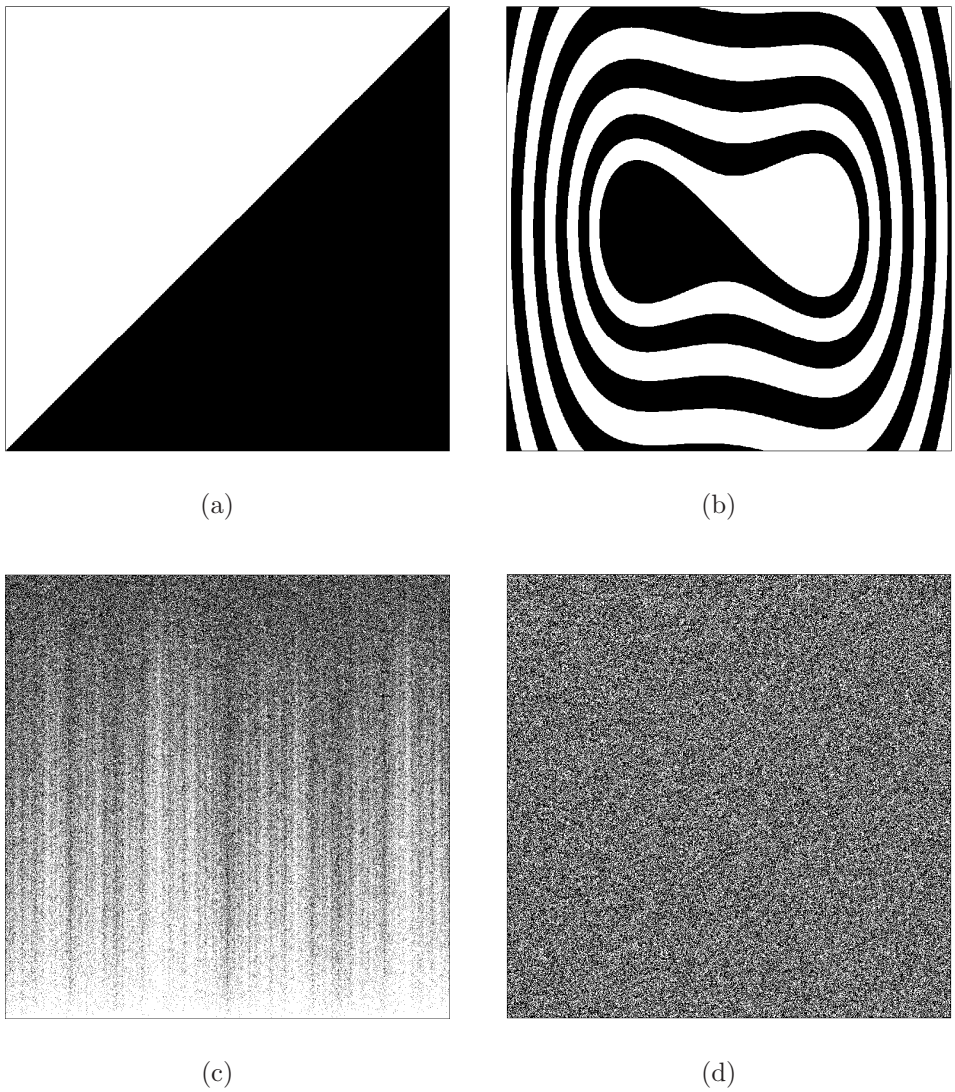

Figure 6.2. Comparison of the different techniques. The figure shows different basins obtained from well-known dynamical systems with two attractors. In panels (a) and (b), the uncertainty exponent is $\alpha = 1$ since both boundaries are smooth, while in (c) and (d) $\alpha = 0$ since both of them are riddled basins. The basin stability is equal to 1/2 for the four basins. However, the basin entropy is able to distinguish the four cases and provides a method to measure quantitatively the unpredictability in increasing order from (a) to (d).

or more escapes are possible in Hamiltonian systems, fractal boundaries typically appear [3]. Hence, the dynamics of the system is in some sense unpredictable, as the boundary that separates one basin from another one is complex.

In order to give an intuitive picture of the problem under study in the present chapter, we may look at Fig. 6.1(a) and Fig. 6.1(b). The figures show the escape

basins of the Hénon-Heiles Hamiltonian for two different values of the energy E above the critical energy that separates bounded motions from unbounded motions. Most initial conditions leave the region through one of the three different exits to infinity for any E above this critical energy. The colors represent points that taken as initial conditions leave the region through a specific exit. With this in mind, we may intuitively understand that it is harder to predict in advance which will be the final destination of an orbit in Fig. 6.1(a) than in Fig. 6.1(b).

The problem is that, even though we can have an intuitive notion that Fig. 6.1(a) is more uncertain than Fig. 6.1(b), there is no quantitative measure to affirm this. Moreover, this is not easy to assess when we compare two figures of basins corresponding to close values of the energy.

This is precisely the idea of uncertainty or unpredictability that we are considering here. This remark is important since we are aware that these terms are polysemic and consequently their use in the literature might be confusing. In this chapter, we refer to unpredictability or uncertainty as the difficulty in the determination of the final state of a system, that is, to which attractor the initial conditions will tend to. Note that we speak about attractors for simplicity, though the discussion is identical for open Hamiltonian systems, where there are no attractors. This notion of unpredictability strongly differs from others used in nonlinear dynamics, like the Kolmogorov-Sinai entropy [4], [5], the topological entropy [6], or the expansion entropy [7], which refer to the difficulty of predicting the evolution of the trajectories. All these quantities are related to the topology of the trajectories, whereas our aim here is to develop an entropy depending on the topology of the basins.

The question we are trying to solve here is not merely theoretical: the concept of basin of attraction is broadly used in all branches of science. Beyond the examples that we have already examined in previous chapters, the scientific literature is full of interesting applications of the idea of basin of attraction. The flow of water close to an obstacle can be described by means of basins of attraction, and their complicated structure explains the heterogeneity of phytoplankton and the information integration of the early macromolecules evolution [8]. Ideas traveling in a neuronal network can be expressed in terms of orbits moving among different basins of attraction [9]. The decisions of agents subjected to changes in the market information exhibit complex dynamics, and this is reflected in their intricate basins of attraction [10]. The prediction of the evolution of interacting populations can be difficult when fractal boundaries separate the possible outcomes [11]. These are just a few examples, but we want to highlight that the idea of basins of attraction appears in all sort of problems. Consequently, we can gain much insight in those questions by measuring and understanding its associated uncertainty, which is our present purpose.

Many authors describe fractal basin boundaries associated to unpredictability in either dissipative dynamical systems possessing basins of attraction or in open Hamiltonian systems which possess escape basins, and when discussing the unpredictability of the orbits many vague affirmations are found due to a lack of an appropriate indicator. In particular, this has been the case with the Wada basins which have received much attention in the past few years and also in the present

thesis. It is commonly said that Wada basins are even more unpredictable than fractal basins without the Wada property [3], [11]–[14], and though this affirmation can be intuitively accepted, there is actually no quantitative basis for it.

Our present work constitutes an attempt to give a quantitative answer to the question of the uncertainty of the basins and this is precisely the problem that we discuss here. We propose a natural way to characterize the uncertainty of the basins by defining a quantitative measure that we call *basin entropy*.

The main idea is to build a grid in a given region of phase space, so that through this discretization a partition of the phase space is obtained where each element can be considered as a random variable with the attractors as possible outcomes. Applying the Gibbs entropy definition to that set results in a quantitative measure of the unpredictability associated to the basins.

The discretization that we are considering arises naturally both in experiments and in numerical simulations. First, the experimental determination of initial conditions in phase space is physically impossible due to the intrinsic errors of the measurements. In the case of numerical experiments, the limitations of the computing resources constrain the resolution of the phase space under analysis. This unavoidable scaling error can induce wrong predictions even in deterministic models. Then, a natural question arises: how does the uncertainty in the initial conditions affect the final state prediction?

A first approach to study the final state uncertainty has been investigated by Grebogi et al. [15]. Given two attractors, they studied how the predictability of the system depends on the topology of their basins of attraction. They found a quantity α called uncertainty exponent, which is the dimension of the phase space D minus the capacity dimension d of the boundary that separates both basins

$$\alpha = D - d. \tag{6.1}$$

The uncertainty exponent takes the value $\alpha = 1$ for basins with smooth boundaries, and $\alpha < 1$ for basins with fractal boundaries. The closer α gets to zero, the more difficult it becomes to predict the system. If smooth and fractal basins are mixed, the uncertainty exponent can still be calculated for each boundary, although the procedure is cumbersome [16]. As we will discuss later on, while the concept of uncertainty exponent is truly useful, its application has several limitations.

Another approach to measure the unpredictability consists of evaluating the volume of each basin of attraction in a certain region of phase space. The ratio of the volume occupied by a single basin to the total volume defines the basin stability [17]. It aims at classifying the different basins according to their relative sizes: larger basins are considered more stable. This notion has proved to be useful for the study of large networks of coupled oscillators, nevertheless it does not take into account how the basins are mixed. For different sets of parameters, a basin with two attractors can show smooth or fractal boundaries while the volume of each basin remains constant. The basin stability would be the same in both cases but obviously fractal boundaries have a more complex structure. A clear example

is shown in Fig. 6.2, where all the basins[1] have the same basin stability. The uncertainty exponent also fails to capture the uncertainty associated to these basins. However, the basin entropy clearly distinguishes the four of them.

In the following we provide the mathematical foundation of the basin entropy and a method for its computation. Numerical simulations carried out for several examples of dynamical systems help illustrate the different ingredients that need to be taken into account to compute the basin entropy and the corresponding uncertainty associated to the basins.

The first source of uncertainty is related to the size of the boundary. By this we refer to the region of the phase space, in terms of the grid, occupied by the boundary. The second source of uncertainty is the uncertainty exponent, which is directly related to the dimension of the boundaries. The last source of uncertainty is the number of attractors: the more attractors the more unpredictable.

Finally, we propose some applications of the basin entropy to chaotic systems, such as the basin entropy parameter set and the $\log 2$ criterion.

6.2 Concept and definition of basin entropy

Suppose we have a dynamical system with N_A attractors for a choice of parameters in a certain region Ω of the phase space. We discretize Ω via a finite number of boxes covering it. Here we study two-dimensional phase spaces, so that we cover Ω with a grid of boxes of linear size ε. Now we build an application $C : \Omega \longrightarrow \mathbb{N}$ that relates each initial condition to its attractor, so that we will refer to that application as the *color*. Each box contains in principle infinitely many trajectories, each one leading to a color labeled from 1 to N_A. In practice we can only use a finite number of trajectories per box. Indeed, it would correspond to the number of times an experiment is repeated, or the number of trajectories computed in a numerical simulation. In this work, we use square boxes with twenty-five trajectories per box (if not otherwise stated) in our numerical simulations. We have seen that twenty-five trajectories per box allows fast computation and provides accurate values of the basin entropy in all the cases studied here.

Although ε is our limiting resolution, the information provided by the trajectories inside a box can be used to make hypotheses on the uncertainty associated to the box. We consider the colors into the box distributed at random according to some proportions. We can associate a probability to each color j inside a box i as $p_{i,j}$ which will be evaluated by computing statistics over the trajectories inside the box.

Taking into account that the trajectories inside a box are independent in a statistical sense, the Gibbs entropy of every box i is given by

$$S_i = \sum_{j=1}^{m_i} p_{i,j} \log\left(\frac{1}{p_{i,j}}\right), \tag{6.2}$$

[1]Panels (a) and (b) correspond to the toggle-switch analyzed in Chapter 2 and the Duffing oscillator described in this chapter. Details concerning the systems of panels (c) and (d) can be found in Ref. [18], [19] respectively.

where $m_i \in [1, N_A]$ is the number of colors inside the box i, and the probability $p_{i,j}$ of each color j is determined simply by the number of trajectories leading to that color divided by the total number of trajectories in the box.

We choose non-overlapping boxes covering Ω, so that the entropy of the whole grid is computed by the addition of the entropy associated to each one of the N boxes of the grid

$$S = \sum_{i=1}^{N} S_i = \sum_{i=1}^{N} \sum_{j=1}^{m_i} p_{i,j} \log\left(\frac{1}{p_{i,j}}\right). \tag{6.3}$$

This entropy can be easily computed for any given basin of attraction. We note here that the growth of the number of boxes N with the reduction of ε provokes a counterintuitive effect: as we reduce the scaling box size ε the entropy S grows. In order to avoid this effect, we consider the entropy S relative to the total number of boxes N and define the following variable

$$S_b = \frac{S}{N}, \tag{6.4}$$

which we call *basin entropy*. An interpretation of this quantity is associated to the degree of uncertainty of the basin, ranging from 0 (a sole attractor) to $\log N_A$ (completely randomized basins with N_A equiprobable attractors). This latter upper value is in practice seldom realized even for extremely chaotic systems. While the basin entropy does not depend on the precise shape of the boxes at a given resolution, it decreases in general with the scaling box size ε, as explained hereafter. We now have a tool to quantitatively compare different basins of attraction.

At this point, we can delve deeper into the consequences of this definition by considering a simple hypothesis, which is to assume that the colors inside a box are equiprobable, thus $p_{i,j} = 1/m_i, \forall j$. If we add the entropy of all the trajectories in a box, then we recover the Boltzmann expression for the entropy $S_i = \log(m_i)$, where m_i are the different colors inside a box (the accessible microstates of the Boltzmann entropy). Then the equiprobable total entropy becomes $S = \sum_{i=1}^{N} S_i = \sum_{i=1}^{N} \log(m_i)$. Furthermore, if we have a grid on a given region of phase space, many boxes will have an equal number of colors. That is, many boxes will be in the interior or lie near the boundary between two or more basins. Then we can say that there are N_k equal boxes (in the sense that they have the same number of colors), where $k \in [1, k_{max}]$ is the label for the different boundaries[2]. Boxes lying outside the basin boundaries do not contribute to the entropy as they only have one color. In other words, what matters is what happens at the basin boundaries. Then, the basin entropy reads

$$S_b = \sum_{k=1}^{k_{max}} \frac{N_k}{N} \log(m_k). \tag{6.5}$$

[2]Glossary of indices: i box, j color, k boundary.

By following the method of the box-counting dimension D_k [20], by which we compute fractal dimensions of basin boundaries, the number of boxes that contains a boundary grows like $N_k = n_k \varepsilon^{-D_k}$ where n_k is a positive constant. In the case of smooth boundaries, the equation $D_k = D - 1$ holds, D being the dimension of the phase space. For fractal boundaries D_k can be larger, but obviously we always have $D_k \leq D$. On the other hand, the number of boxes in the whole region of phase space, grows as $N = \tilde{n}\varepsilon^{-D}$, where $\tilde{n}$ is a positive constant. Substituting these expressions for N_k and N in Eq. 6.5, and recalling that $\alpha_k = D - D_k$ is the uncertainty exponent [15] for each boundary, we get

$$S_b = \sum_{k=1}^{k_{max}} \frac{n_k}{\tilde{n}} \varepsilon^{\alpha_k} \log(m_k). \tag{6.6}$$

This last expression reveals important information. The basin entropy has three components: the term $n_k/\tilde{n}$ is a normalization constant that accounts for the boundary size which is independent of ε; the term of the uncertainty exponent α_k, is related with the fractality of the boundaries and contains the variation of the basin entropy with the box size; finally there is a term that depends on the number of different colors m_k. All these terms depend on the dynamics of the system, while the scaling box size ε depends only on the geometry of the grid.

Equation 6.6 sheds light into some interesting questions. First, we can compare smooth boundaries ($\alpha_k = 1$) and fractal boundaries ($\alpha_k < 1$). For both of them, smooth and fractal basins, we get $S_b \to 0$ when $\varepsilon \to 0$, but it converges faster in the smooth case. That is, it is more difficult for the basin entropy to decrease its value in a system with fractal boundaries. Despite other important factors, fractal boundaries introduce a larger uncertainty than the smooth ones. Furthermore, if $\alpha_k = 0$ then $S_b > 0$ no matter the scaling box size (this might happen in riddled basins [19], [21], [22]).

These ideas can be successfully applied for Wada basins. As explained in previous chapters, basins exhibiting the Wada property have only one boundary that separates all the basins [12], [23]. In our basin entropy framework, we can argue that increasing the number of colors in the boundary boxes increases the uncertainty too. In particular, having all possible colors in every boundary box is a unique situation found only in Wada basins. Nevertheless, Eq. 6.6 also reveals that some non-Wada basins can show larger basin entropy than others exhibiting the Wada property. This can be the case when a system has the Wada property but there is one basin which occupies most of the phase space. Other factors like the number of attractors and the boundary size also play a role in the uncertainty according to the basin entropy formulation. Therefore the Wada property increases the uncertainty under the basin entropy perspective, but each case must be carefully studied.

The basin entropy formalism can also be used to develop new tools. In some cases, we may be interested only in the uncertainty of the boundaries, instead of the uncertainty of the whole picture of the basins. In particular, we often want to know if a boundary is fractal. For that purpose we can restrict the calculation of

the basin entropy to the boxes falling in the boundaries, that is, we can compute the entropy only for those boxes N_b which contain more than one color,

$$S_{bb} = \frac{S}{N_b}, \tag{6.7}$$

where S is calculated in the same way described before (see Eq. 6.3). We refer to this number S_{bb} as *boundary basin entropy*, because it quantifies the uncertainty referring only to the boundaries.

The nature of this quantity S_{bb} is different from the basin entropy S_b defined in Eq. 6.4. The S_b is sensitive to the size of the basins, so it can distinguish between different basins with smooth boundaries, whilst the S_{bb} cannot. However, it is worthwhile to introduce this new concept since it provides a sufficient condition to assess easily that some boundaries are fractal. Let us develop the reasoning. Suppose that we have several basins separated by smooth boundaries. Then, every box in the boundary will have only two colors, except a few countable number of boxes that may contain three colors or more. If we take a sufficient number of boxes in the boundaries, the effect of those boxes containing more than two colors will be negligible for the computation of the basin entropy in the boundaries S_{bb}[3]. Then, the maximum possible value of S_{bb} that a smooth boundary can show is $\log 2$, which would imply a pathological case where every box in the boundary contains equal proportions of two basins $p_i = 1/2, \forall i \in \mathbb{N}$. Therefore, considering a sufficient number of boxes in the boundaries, we can affirm that if the boundary basin entropy is larger than $\log 2$, then the boundary is fractal, which can be expressed as

$$S_{bb} > \log 2 \Rightarrow \alpha < 1. \tag{6.8}$$

This is a sufficient but not necessary condition: as we shall discuss in Section IV, there may be fractal boundaries with $S_{bb} < \log 2$. Nevertheless, this threshold can be very useful to assess quickly the fractality of some boundaries, avoiding to compute the boundaries for different scales (which is not always possible). In Section IV, we will show on an example that the criterion (6.8) enables reliably to find parameter regions exhibiting fractal boundaries.

6.3 What does the basin entropy measure?

Here we illustrate the main features of basin entropy with several examples of dynamical systems, showing how its dependence on the boundary size $n_k/\tilde{n}$, the uncertainty exponent α_k and the number of attractors N_A.

The term $n_k/\tilde{n}$ corresponds to an estimate of the size of the boundary, since it normalizes the number of boxes containing the boundaries divided by the total number of boxes covering Ω:

$$\frac{N_k}{N} = \frac{n_k}{\tilde{n}} \varepsilon^{\alpha_k}. \tag{6.9}$$

[3]See Appendix D for an exhaustive proof of the $\log 2$ criterion.

To study the contribution of this term, we consider the damped Duffing oscillator given by

$$\ddot{x} + \delta\dot{x} - x + x^3 = 0. \tag{6.10}$$

This equation describes the motion of a unit mass particle in a double well potential with dissipation. This system presents two attractive fixed points in $(\pm 1, 0)$ of the $(x, \dot{x})$ phase space, which correspond to the minima of the double well potential function. The higher the damping coefficient δ the faster the orbits tend to the fixed points and, as a consequence, the basin of attraction appears more deformed for smaller values of δ (Fig. 6.3(a)-(c)). The damped Duffing oscillator is bistable, $N_A = 2$, and has a smooth boundary with uncertainty exponent $\alpha = 1$.

Observing the basins of attraction corresponding to the three different values of δ, it is noticeable that the basin of Fig. 6.3(c) has a much simpler structure than the basin in Fig. 6.3(a). The outcome of an initial condition within an ε-box would be more difficult to predict in the second case. Nevertheless, both basins have the same uncertainty exponent $\alpha = 1$ since in both cases the boundary is smooth. The differences in the values of the basin entropy originates from the differences in the region of discretized phase space occupied by the boundary, that is, the boundary size, which is reflected by the term $n/\tilde{n}$ (indices have been dropped since now there is only one boundary).

In order to highlight this effect, we have computed the basin entropy S_b versus the scaling box size[4] ε for three different values of the damping coefficient δ. The results are shown in the log-log plot of Fig. 6.3(d), where each fit corresponds to a different value of δ. In order to interpret these results, we can take logarithms on both sides of Eq. 6.6 yielding to

$$\log(S_b) = \alpha \log(\varepsilon) + \log\left(\log(N_A)\frac{n}{\tilde{n}}\right). \tag{6.11}$$

Since in this case, we have $\alpha = 1$ and $N_A = 2$ for all our simulations, it is clear that the variation of the basin entropy with δ is entirely due to the term $n/\tilde{n}$. Most importantly, we have obtained values of the slope $\alpha = 1$ within the statistical error for all the fits. Therefore, although all these basins have the same uncertainty exponent, they have a different basin entropy for a given value of ε. The basin entropy is sensitive to their different structure and is able to quantify their associated unpredictability.

The fractal dimension of the boundaries also plays a crucial role in the formulation of the basin entropy. This is reflected in the uncertainty exponent α_k [15] of Eq. 6.6. In order to highlight the effects of the variations in the uncertainty exponent, we have chosen a model that can display the Wada property [3]. This means that there is only one fractal boundary separating all the basins. The model is the Hénon-Heiles Hamiltonian [24],

$$H = \frac{1}{2}(\dot{x}^2 + \dot{y}^2) + \frac{1}{2}(x^2 + y^2) + x^2 y - \frac{1}{3}y^3, \tag{6.12}$$

[4]In this work we have normalized the region of the phase space, so that the values of the scaling box size ε in the plots are the inverse of the number of pixels used as a grid.

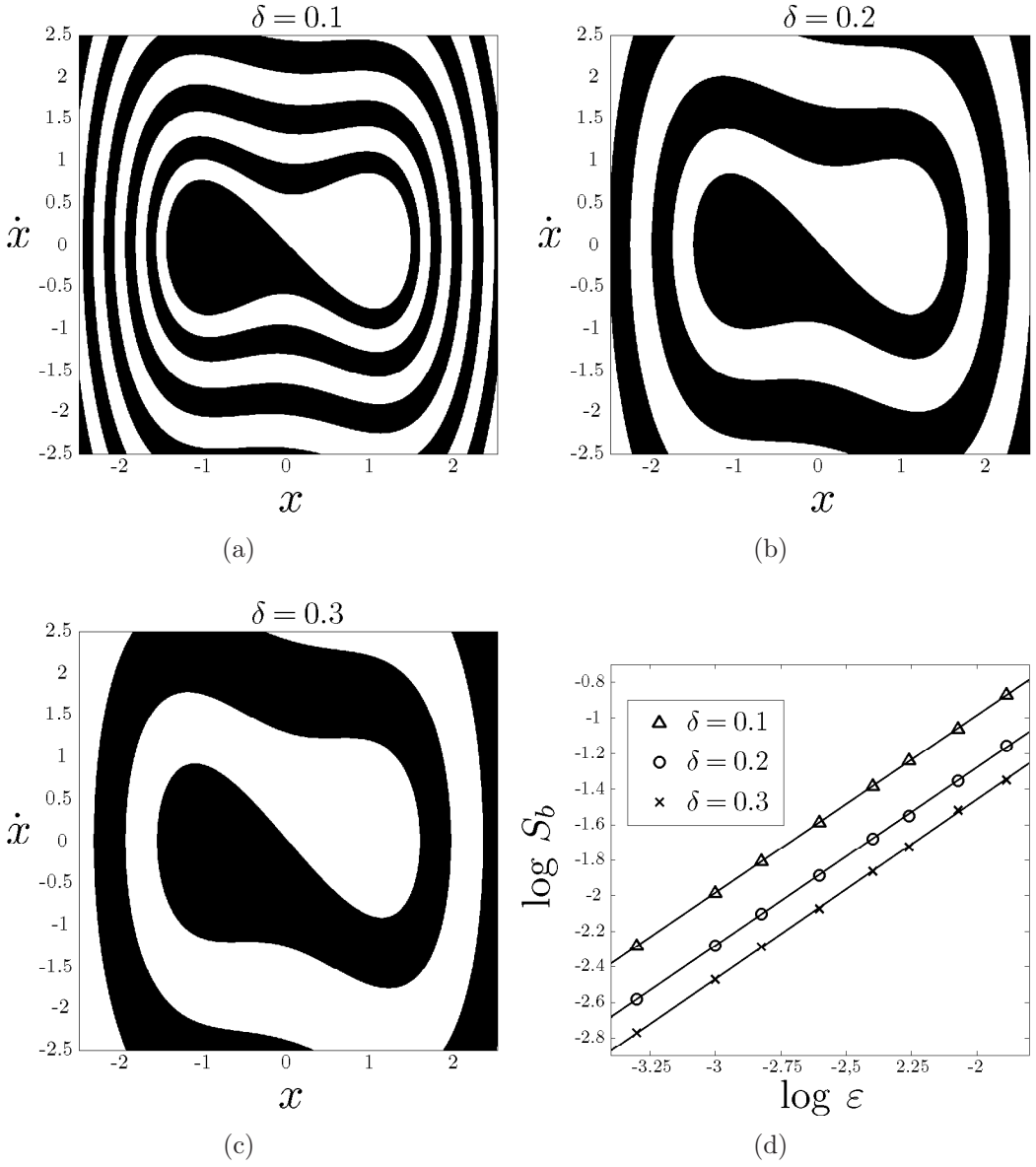

Figure 6.3. Basin entropy dependence on the boundary size. (a)-(c) Basins of attraction of $\ddot{x} + \delta\dot{x} - x + x^3 = 0$ for different values of the damping coefficient δ. As the damping increases the boundary occupies a smaller region of the phase space. Although the boundary is always smooth ($\alpha = 1$), the uncertainty in basin (a) is larger than in basin (c) no matter the scaling box size ε. (d) A log-log plot of the basin entropy versus the scaling box size for values of the damping coefficient $\delta = 0.1$ (triangles), $\delta = 0.2$ (circles) and $\delta = 0.3$ (crosses). The three fits have the same slope $\alpha = 1$ within statistical error. However, the basin entropy is different for each value of the parameter δ, reflecting the different uncertainty associated to each basin.

which describes the motion of a particle in an axisymmetrical potential well that for energy values above a critical one, the trajectories may escape from the bounded region inside the well and go on to infinity through three different exits. For this Hamiltonian system, we define escape basins in a similar way to the basins of attraction in dissipative systems, i.e., an escape basin is the set of initial conditions that lead to a certain exit. If we vary the energy from $E = 0.2$ to $E = 0.22$, the fractal dimension of the boundaries is modified with E, though the Wada property is preserved [25] (see Fig. 6.4(a)-(c)). The proportion of red, blue and green remains as a constant for these three basins, leading to constant values of the basin stability. However, the basin entropy accounts for their different structures.

As we compute the basin entropy for different scaling box sizes, we observe that the main effect of varying the parameter E is a change of the slope in the log-log plot of Fig. 6.4(d). Equation 6.11 relates these changes in the slope to the uncertainty exponent α of the boundary. Smaller energies lead to smaller uncertainty exponents, since the boundaries have a more complex structure and consequently the slopes in the log-log plot decrease too. Obviously the offset also varies for the different values of the energy. This is related to changes in the boundary size $n/\tilde{n}$ which in this case cannot be completely separated from the changes in α. This example shows that the scaling of the basin entropy with box size directly reflects the fractal dimension of the basin boundaries. For small box sizes this effect dominates and the largest fractal dimensions of the basins gives the largest basin entropies, even though the offsets are different (see Fig. 6.4).

The last factor that contributes to the basin entropy, according to Eq. 6.6, is the number of attractors N_A. In general, as the number of attractors increases, the uncertainty increases too, and so does the basin entropy. Furthermore, it is impossible to isolate the effect of the number of attractors from the contribution of the boundary size, since they are not independent: if a new attractor emerges while tuning a parameter, a new boundary is also created. We illustrate these effects using a simple map where the number of attractors can be tuned. This map comes from the Newton method to find the complex roots of unity $z^r = 1$ [26], and can be written as

$$z_{n+1} = z_n - \frac{z^r - 1}{r z^{r-1}}, \tag{6.13}$$

where $z \in \mathbb{C}$ and $r, n \in \mathbb{N}$. The attractors of this map are the solutions of $z^r = 1$, so the parameter r determines the number of attractors, $r = N_A$ (see Fig. 6.5(a)-(c) for $r = 4, 5, 6$). The basins of attraction of this system have disconnected Wada boundaries, that is, all the basins share the same boundaries and are disconnected [23].

From Eq. 6.11 we can predict that increasing the number of attractors increases the offset in the log-log plot of the basin entropy versus the box size. This can be observed in Fig. 6.5(d), where an increasing number of attractors leads to an increasing value of the basin entropy for all the ε considered.

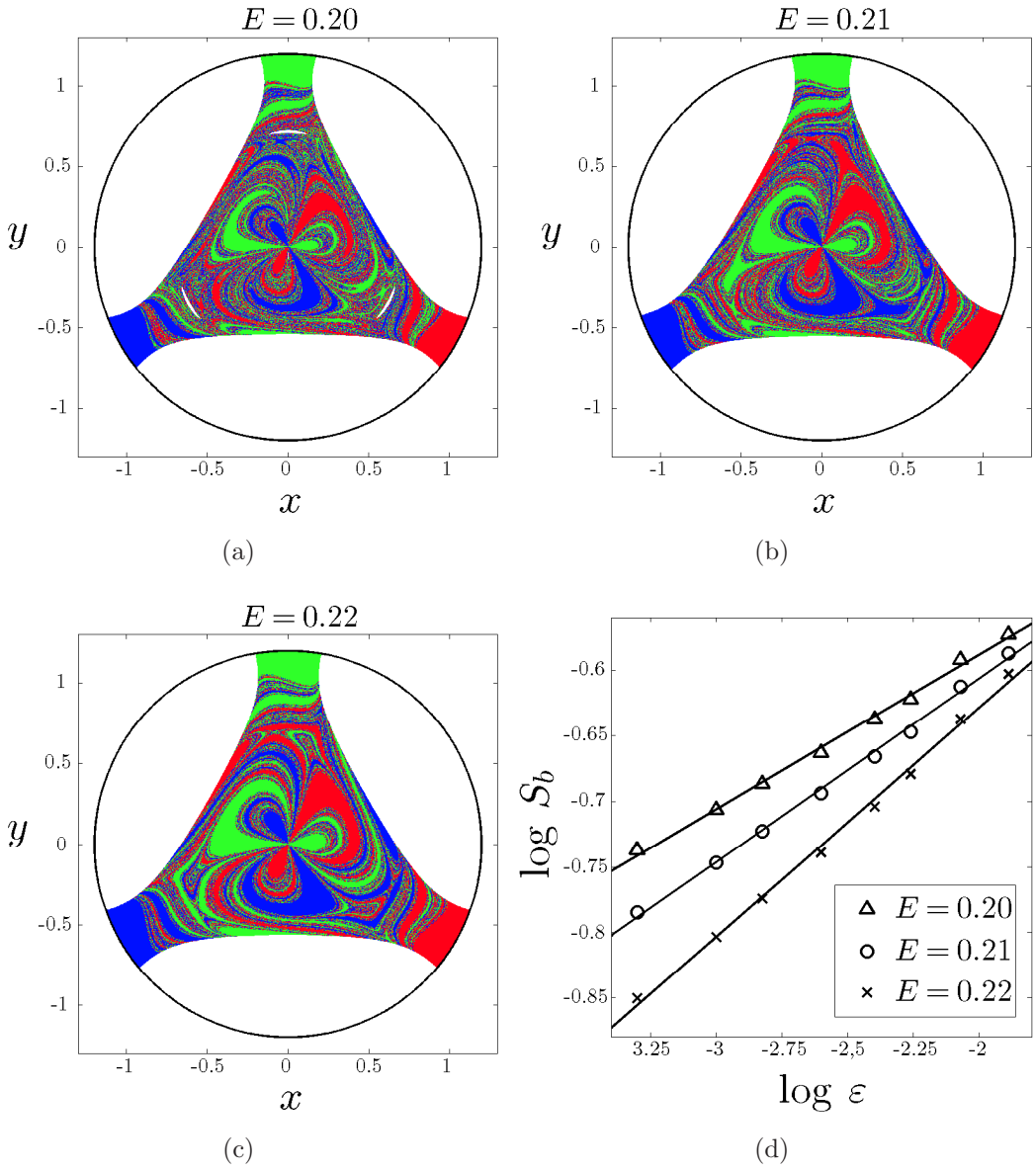

Figure 6.4. Basin entropy dependence on the uncertainty exponent. (a)-(c) Escape basins of the Hénon-Heiles Hamiltonian $H = \frac{1}{2}(\dot{x}^2 + \dot{y}^2) + \frac{1}{2}(x^2 + y^2) + x^2 y - \frac{1}{3}y^3$ for different values of the energy E. Inside the circles the proportion of red, blue and green boxes is always equal to 1/3. However, as E increases the boundary becomes less uncertain, so that we can intuitively see that basin (a) is more unpredictable than basin (c). This intuition is confirmed quantitatively by the computation of the basin entropy in the log-log plot of panel (d). The most remarkable effect observed in the fits is that the slopes change because of the different dimensions of the boundaries, as expected. This effect cannot be isolated since the offsets also vary. Finally, for coarse-grained basins the basin entropy is almost equivalent.

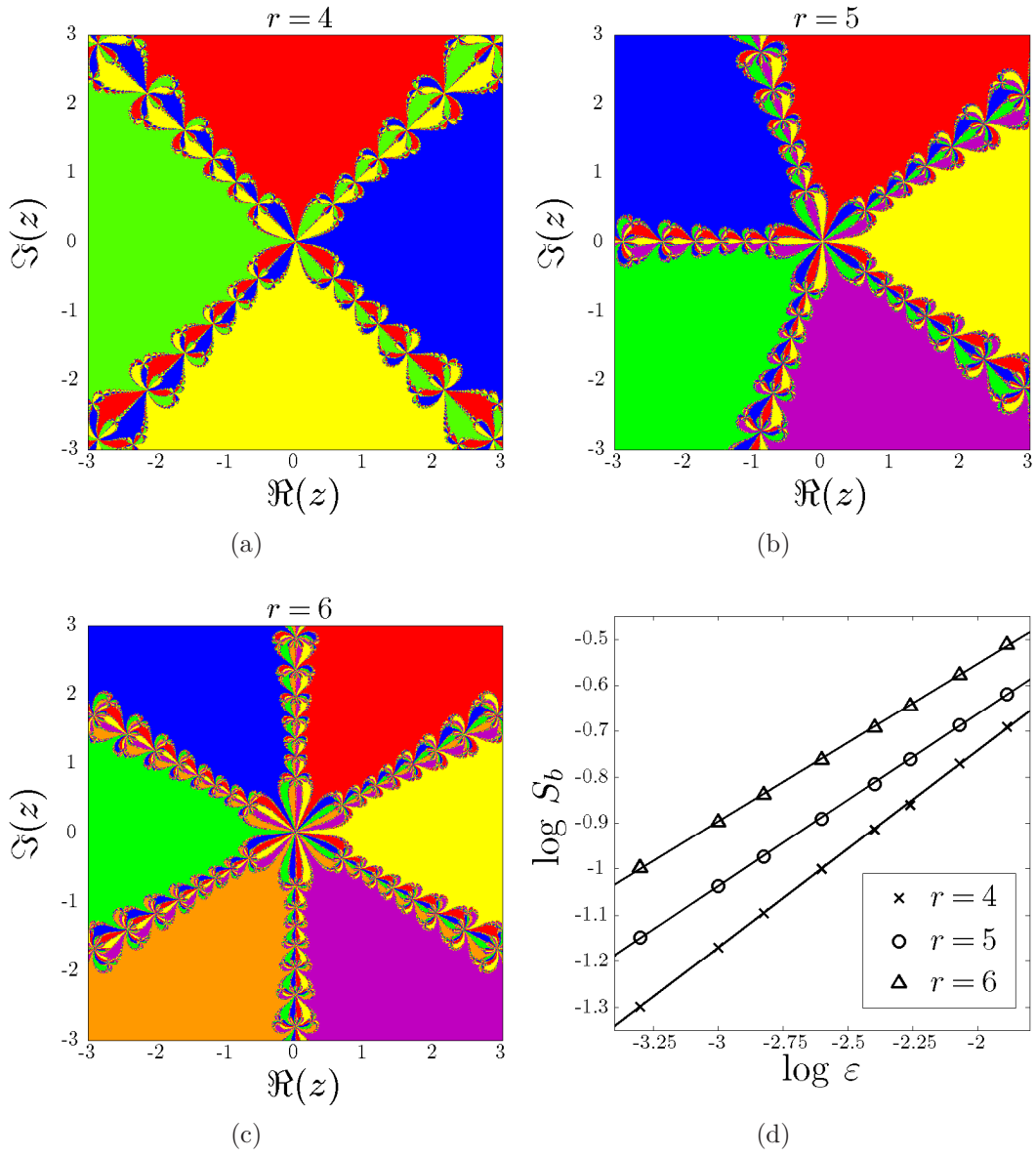

Figure 6.5. Basin entropy dependence on the number of attractors. (a)-(c) The basins of attraction indicate the initial conditions that lead to the complex roots of unity using the Newton method described by $z_{n+1} = z_n - \dfrac{z^r - 1}{r z^{r-1}}$. Here we plot the cases $r = 4, 5, 6$. The log-log plot of panel (d) shows that the basin entropy increases when the number of attractors increases, leading to larger values in the intercepts of the fits as predicted. Nevertheless, the effect of the increasing number of attractors is impossible to separate from the other contributions to the basin entropy, since the boundaries change with the number of attractors.

6.4 Characterizing chaotic systems

In this section, we present some applications of the basin entropy and related methodology that can be useful for chaotic systems.

6.4.1 Basin Entropy Parameter Set

One of the most interesting applications of the basin entropy is to use it as a quantitative measure to compare different basins of attraction. We propose an analogy with the concept of *chaotic parameter set* [27], which is a plot that visually illustrates in a parameter plane when a dynamical system is chaotic or periodic by simply plotting the Lyapunov exponents for different pairs of parameters. Here, first we choose a given scaling box size ε, and then we evaluate the basin entropy associated to the corresponding basins of attraction for different parameter settings. We call the plot of the basin entropy in a two-dimensional parameter space *basin entropy parameter set*. To illustrate the possibilities of this technique, we study the periodically driven Duffing oscillator

$$\ddot{x} + \delta\dot{x} - x + x^3 = F \sin \omega t, \tag{6.14}$$

whose dynamics can be very different depending on the parameters. We vary the forcing amplitude F and the frequency ω of the driving, and for each basin we compute its corresponding basin entropy. We have used a resolution of 200×200 boxes ($\varepsilon = 0.005$) with 25 trajectories per box (a million trajectories per basin) to compute the basins of attraction and the same region of the phase space $\Omega = [-2.5, 2.5] \times [-2.5, 2.5]$ for all the pairs (F, ω).

The result is presented in Fig. 6.6(a), which is a color-code representation of the basin entropy in the parameter plane (F, ω) for different values of the forcing amplitude and frequency. The *hot* colors indicate higher values of the basin entropy, while the white pixels are for zero basin entropy. The set of parameters with zero basin entropy indicates that the basin of attraction has only one attractor. Although there is no uncertainty about the final attractor of any initial condition, trajectories may still be very complicated if the attractor is chaotic. This is actually the case for Fig. 6.6(b), where there is only one chaotic attractor.

The *hottest* point of the basin entropy parameter set corresponds to the basin of attraction shown in Fig. 6.6(c) with eight different attractors whose basins are highly mixed. The reason for having this high value of the basin entropy lies at a combination of a high number of attractors and the uncertainty exponent associated to the boundaries that makes basins of attraction more unpredictable. In Fig. 6.6(d), we can see a basin of attraction with extremely mixed basins, but it has only three attractors so its basin entropy is lower than for Fig. 6.6(c). The converse situation arises in Fig. 6.6(e), where there are sixteen different attractors but the boundaries are not very intricate.

Remarkably, it is also possible to explore the parameter space using only a few boxes instead of computing the high resolution basin for each parameter set. To

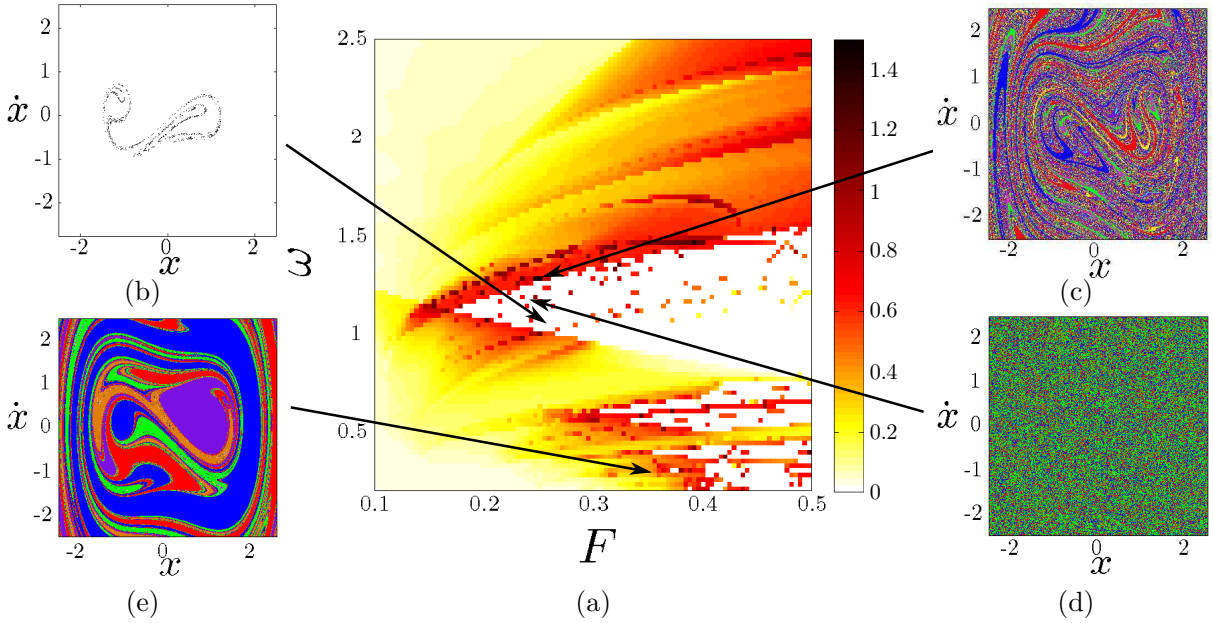

Figure 6.6. Basin entropy parameter set. (a) Basin entropy parameter set for the periodically driven Duffing oscillator given by $\ddot{x} + \delta\dot{x} - x + x^3 = F\sin\omega t$. It is a color-code map of the basin entropy for different values (F, ω) of the forcing amplitude and frequency, where we have fixed the scaling box size $\varepsilon = 0.005$ and the damping coefficient $\delta = 0.15$. We have used a color code where the *hot* colors represent larger values of the basin entropy. (b) Example of a basin of attraction with zero basin entropy because there is only one attractor, actually a chaotic attractor (whose Poincaré section is plotted in black), for the parameters $F = 0.2575$ and $\omega = 1.075$. (c) Basins of attraction corresponding to the highest value of the basin entropy in this parameter plane, for $F = 0.2495$ and $\omega = 1.2687$. (d) Basins of attraction with three attractors and a very low uncertainty exponent happening for $F = 0.2455$ and $\omega = 1.1758$. (e) Basins of attraction with sixteen different attractors for the parameters $F = 0.3384$ and $\omega = 0.2929$.

infer a good approximation of the basin entropy, we applied a Monte Carlo sampling method. We used 2000 boxes for each point in the parameter set, *i.e.*, 50000 trajectories for each value of (F, ω), instead of the million trajectories needed for the usual procedure (we mean by usual procedure computing the whole basin of attraction and then calculate the basin entropy). Thus, we speed up the computation by a factor 20. The resulting basin entropy parameter set obtained by random sampling is visually indistinguishable from the one in Fig. 6.6(a). To show the discrepancies between the usual procedure and the random sampling we calculated the relative error $\varepsilon_{rel} = \frac{|S_b - S_b(RS)|}{\langle Sb \rangle} \times 100$. The results are displayed in Fig. 6.7, where we can see that on this example the differences are very small (less than 5%) for most choices of the parameters. If higher precision is desired one can always increase the number of boxes N, since the error decreases as $\frac{1}{\sqrt{N}}$ in the Monte Carlo method as shown in Fig. 6.7(b). Therefore, one can calculate the basin entropy using a small number of

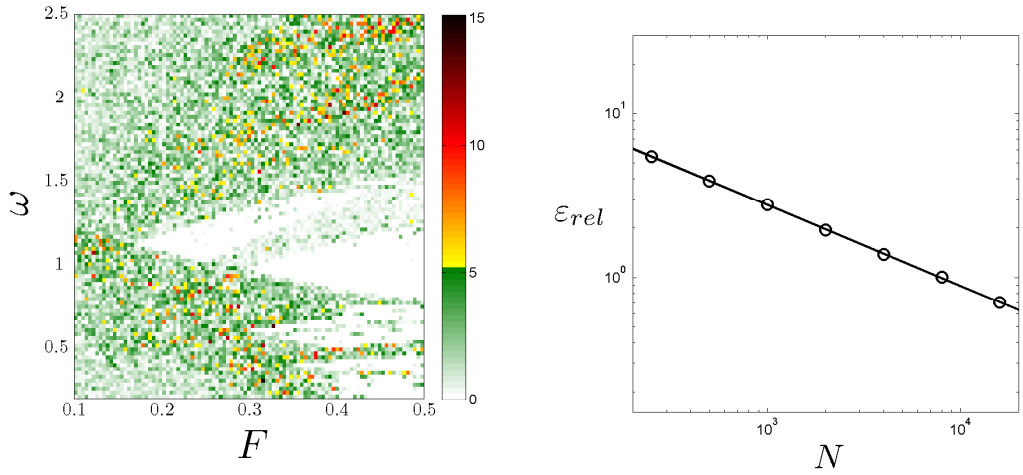

Figure 6.7. Random sampling error. (a) This plot presents the relative error of the basin entropy estimation, that is $\frac{|S_b - S_b(RS)|}{\langle Sb \rangle} \times 100$, using 2000 boxes for the random sampling. For most of the parameters the relative error is below 5%. (b) If a more precise value is needed the error decreases as $\frac{1}{\sqrt{N}}$, as shown in the figure.

boxes and afterwards, one can compute with a finer grid the most interesting basins, which are indicated by larger values of the basin entropy. It is also possible to define gradients in the basin entropy parameter set. This allows to learn in which directions the variations of the parameters lead to larger values of the basin entropy, and thus, to larger uncertainty in the final state determination. The random sampling procedure is especially appealing to compute the basin entropy in high dimensional systems or for high dimensional parameter sets.

6.4.2 Log 2 criterion

Using the same data, we can also study the boundary basin entropy S_{bb} in the parameter plane. This quantity reflects the uncertainty associated to the boundaries, and we have seen in Section 6.2 that if $S_{bb} > \log 2$ then the boundary is fractal. Of course, for a given resolution, that is, a fixed scaling box size ε, this process cannot distinguish a true fractal boundary from a smooth boundary which at this scale separates more than two basins inside one box. We have checked numerically that this is the case, but for small resolution this requires pathological systems which are not usually found in nature. The results for the periodically driven Duffing oscillator are depicted in the colormap of Fig. 6.8(a), where white color is assigned to the pairs (F, ω) displaying only one attractor. By means of this plot we can detect parameter regimes where boundaries are fractal, depicted with hot colors. We can also detect the regimes where it is more likely that boundaries are smooth, that is, those showing smaller values of S_{bb}. Fig. 6.8(b) shows in hot colors the parameters

leading to fractal boundaries and in cold those with smooth boundaries. We can see that not all the fractal boundaries pass the $\log 2$ criterion, but only some regions. We depict in Fig. 6.8(c) the parameters leading to smooth boundaries colored in blue, fractal boundaries with $S_{bb} < \log 2$ colored in orange, and fractal boundaries with $S_{bb} > \log 2$ colored in green. It is visible that only basins with more than three attractors pass the $\log 2$ criterion (see Fig. 6.8). These pictures confirm that the $\log 2$ criterion is a *sufficient but not necessary condition* for fractal boundaries. Indeed, when boundaries are fractal but there is a dominant basin that occupies a large portion of the phase space, then the $\log 2$ criterion is not fulfilled. Nevertheless the $\log 2$ criterion is a very good criterion of fractality for basins of comparable size, and is much faster to compute than the direct determination of fractal dimension since it does not require the use of different scales. This makes it especially appealing for experimental settings where the resolution cannot be tuned at will.

6.5 Discussion

In nonlinear dynamics, different tools are commonly used to gain knowledge of a system. For instance, Lyapunov exponents are used to characterize its dynamics. On its behalf, basins of attraction contain much information about the asymptotic behavior of the system. Some efforts had already been made in the past to characterize the complex structure of basins of attraction, such as the uncertainty exponent [15] and the notion of basin stability [17]. The uncertainty exponent takes into account the nature of the boundary between two basins, and the basin stability informs about the percentage of phase space occupied by each basin. However, in many situations these concepts are insufficient to describe the complex structure of the basins of attraction [25].

The basin entropy integrates these concepts from the theoretical perspective of information entropy. It provides a quantitative measure of the uncertainty associated to the basins of attraction for a given scaling box size. This should become a very useful tool with a wide range of applications, as exemplified by the different systems that we have used to illustrate this concept. For instance, escape basins are widely used in astronomy, as shown in recent studies on the Pluto-Charon system [28]. In these investigations it is commonly argued that basins close to the escape energy present a *higher degree of fractalization* [29], [30]. Here we have shown an example of an open Hamiltonian system used in galactic dynamics, namely the Hénon-Heiles potential, and we have been able to quantify its uncertainty for different values of the energy.

Another kind of problems where basins of attraction are very common is in iterative algorithms. Such algorithms abound in all sort of research fields, where basins of attraction are used to visualize the sensitivity of different methods [31], [32]. In this work we have applied the basin entropy idea to a prototypical iterative algorithm: the Newton method to find complex roots. We have quantified the uncertainty associated to this algorithm for different numbers of roots. The basin entropy technique can be used to compare the performances of different algorithms

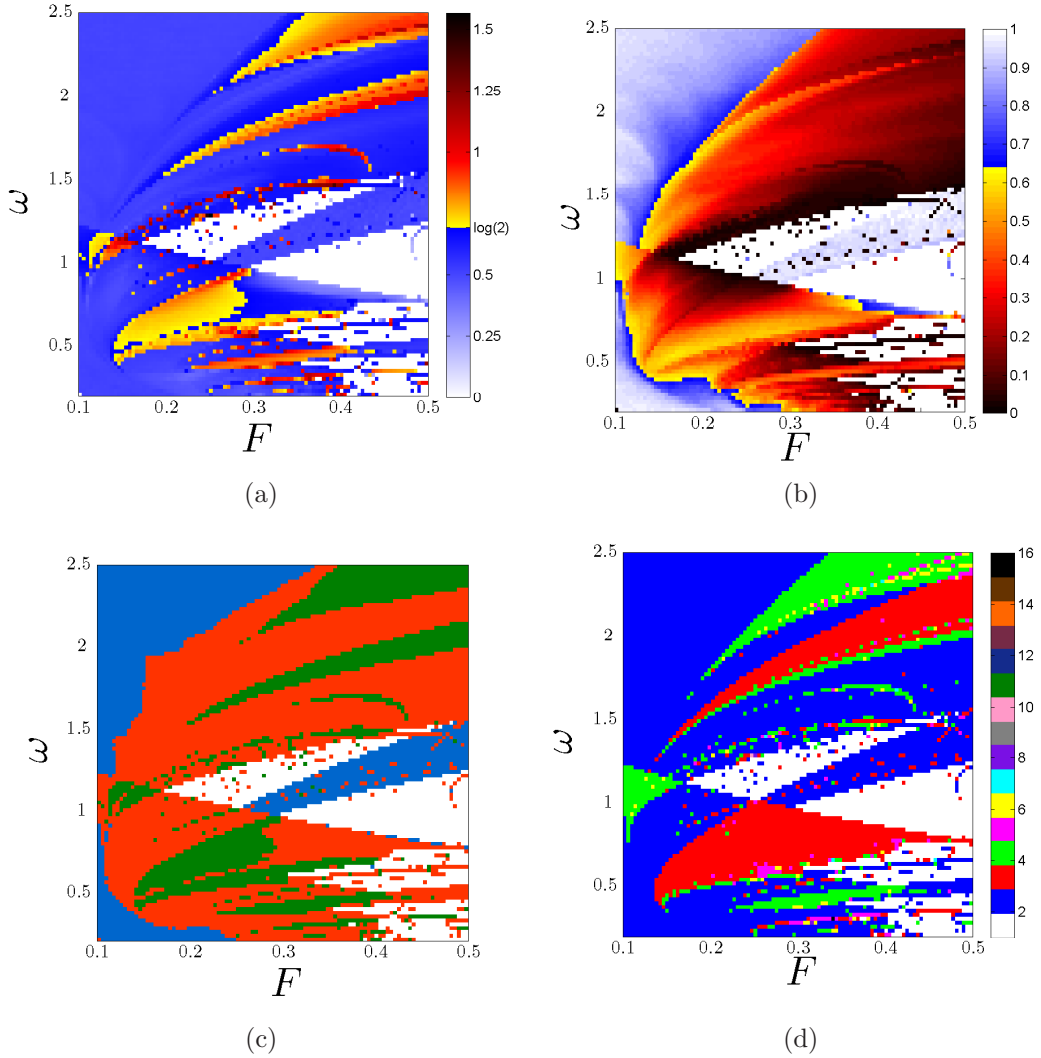

Figure 6.8. Boundary basin entropy S_{bb} parameter set. (a) A color map of the boundary basin entropy S_{bb} for different parameters (F, ω) for the periodically driven Duffing oscillator $\ddot{x} + \delta\dot{x} - x + x^3 = F\sin\omega t$ for $\delta = 0.15$ and $\varepsilon = 0.005$. (b) Uncertainty exponent in the parameter plane. (c) The white color indicates basins with one attractor, blue is for smooth boundaries, orange for fractal boundaries and green for fractal boundaries with $S_{bb} > \log 2$.(d) Number of attractors in the parameter plane.

or to see how modifications in some parameters like the damping may alter the uncertainty of the iterative processes.

Thanks to the framework given by the basin entropy, we have been able to specify and quantify the uncertainty of the Wada property, a recurring issue in the literature [3], [11]–[14]. Moreover, using the idea of boundary basin entropy, we provide a sufficient condition to demonstrate fractality. In contrast with other methods like box-counting dimension that require computation at different resolutions, the $\log 2$

criterion can be used with a fixed resolution. We believe that this opens a new window for experimental demonstrations of fractal boundaries, as we will show in the next chapter.

We have also proposed a new technique called basin entropy parameter set, that can flesh out the information given by bifurcation diagrams and chaotic parameter sets. Combined with Monte Carlo sampling, the basin entropy parameter set can also be used as a quick guide to find parameters leading to simple or more complicated basins of attraction.

The basin entropy and the related methodology will be used in the next chapter to investigate the dynamics of propagating matter waves.

Bibliography

[1] H. E. Nusse and J. A. Yorke, "Basins of attraction", *Science* **271**, 1376–1380 (1996).

[2] J. Aguirre, R. L. Viana, and M. A. F. Sanjuán, "Fractal structures in nonlinear dynamics", *Rev. Mod. Phys.* **81**, 333–386 (2009).

[3] J. Aguirre, J. C. Vallejo, and M. A. F. Sanjuán, "Wada basins and chaotic invariant sets in the Hénon-Heiles system", *Phys. Rev. E* **64**, 066208 (2001).

[4] A. N. Kolmogorov, "New metric invariant of transitive dynamical systems and endomorphisms of Lebesgue spaces", *Dokl. Akad. Nauk. SSSR* **119**, 861–864 (1959).

[5] Y. G. Sinai, "On the notion of entropy of a dynamical system", *Dokl. Akad. Nauk. SSSR* **124**, 768–771 (1959).

[6] R. L. Adler, A. G. Konheim, and M. H. McAndrew, "Topological entropy", *Trans. Amer. Math. Soc.* **114**, 309–319 (1965).

[7] B. R. Hunt and E. Ott, "Defining chaos", *Chaos* **25**, 097618 (2015).

[8] G. Károlyi, A. Péntek, I. Scheuring, T. Tél, and Z. Toroczkai, "Chaotic flow: the physics of species coexistence", *P. Natl. Acad. Sci. USA* **97**, 13661–13665 (2000).

[9] M. Rabinovich, R. Huerta, and G. Laurent, "Transient dynamics for neural processing", *Science* **321**, 48–50 (2008).

[10] W. Brock and C. Hommes, "A rational route to randomness", *Econometrica* **65**, 1059–1096 (1997).

[11] J. Vandermeer, "Wada basins and qualitative unpredictability in ecological models: a graphical interpretation", *Ecol. Model.* **176**, 65–74 (2004).

[12] J. Kennedy and J. A. Yorke, "Basins of Wada", *Physica D* **51**, 213–225 (1991).

[13] H. E. Nusse and J. A. Yorke, "Characterizing the basins with the most entangled boundaries", *Ergod. Theor. Dyn. Syst.* **23**, 895–906 (2003).

[14] J. Aguirre and M. A. F. Sanjuán, "Unpredictable behavior in the Duffing oscillator: Wada basins", *Physica D* **171**, 41–51 (2002).

[15] C. Grebogi, S. W. McDonald, E. Ott, and J. A. Yorke, "Final state sensitivity: an obstruction to predictability", *Phys. Lett. A* **99**, 415–418 (1983).

[16] C. Grebogi, E. Kostelich, E. Ott, and J. A. Yorke, "Multi-dimensioned intertwined basin boundaries and the kicked double rotor", *Phys. Lett. A* **118**, 448–452 (1986).

[17] P. J. Menck, J. Heitzig, N. Marwan, and J. Kurths, "How basin stability complements the linear-stability paradigm", *Nat. Phys.* **9**, 89–92 (2013).

[18] R. F. Pereira, S. Camargo, S. E. de S. Pinto, S. R. Lopes, and R. L. Viana, "Periodic-orbit analysis and scaling laws of intermingled basins of attraction in an ecological dynamical system", *Phys. Rev. E* **78**, 056214 (2008).

[19] Y.-C. Lai and R. L. Winslow, "Geometric properties of the chaotic saddle responsible for supertransients in spatiotemporal chaotic systems", *Phys. Rev. Lett.* **74**, 5208–5211 (1995).

[20] K. T. Alligood, T. D. Sauer, and J. A. Yorke, *Chaos: an introduction to dynamical systems*. New York: Springer, 1996.

[21] J. Alexander, J. A. Yorke, Z. You, and I. Kan, "Riddled basins", *Int. J. Bifurcat. Chaos* **02**, 795–813 (1992).

[22] E. Ott, J. C. Sommerer, J. C. Alexander, I. Kan, and J. A. Yorke, "Scaling behavior of chaotic systems with riddled basins", *Phys. Rev. Lett.* **71**, 4134–4137 (1993).

[23] A. Daza, A. Wagemakers, M. A. F. Sanjuán, and J. A. Yorke, "Testing for basins of Wada", *Sci. Rep.* **5**, 16579 (2015).

[24] M. Hénon and C. Heiles, "The applicability of the third integral of motion: Some numerical experiments", *Astron. J.* **69**, 73 (1964).

[25] F. Blesa, J. M. Seoane, R. Barrio, and M. A. F. Sanjuán, "To escape or not to escape, that is the question - perturbing the Hénon-Heiles Hamiltonian", *Int. J. Bifurcat. Chaos* **22**, 1230010 (2012).

[26] B. Epureanu and H. Greenside, "Fractal basins of attraction associated with a damped Newton's method", *SIAM Rev.* **40**, 102–109 (1998).

[27] M. A. F. Sanjuán, "Using nonharmonic forcing to switch the periodicity in nonlinear systems", *Phys. Rev. E* **58**, 4377–4382 (1998).

[28] E. E. Zotos, "Orbit classification in the planar circular Pluto-Charon system", *Astrophys. Space Sci.* **360**, 1–14 (2015).

[29] E. E. Zotos, "Escape dynamics and fractal basin boundaries in Seyfert galaxies", *Nonlinear Dyn.* **80**, 1109–1131 (2015).

[30] A. Ernst and T. Peters, "Fractal basins of escape and the formation of spiral arms in a galactic potential with a bar", *Mon. Not. R. Astron. Soc.* **443**, 2579–2589 (2014).

[31] D. Asenjo, J. D. Stevenson, D. J. Wales, and D. Frenkel, "Visualizing basins of attraction for different minimization algorithms", *J. Phys. Chem. B* **117**, 12717–12723 (2013).

[32] M. van Turnhout and F. Bociort, "Instabilities and fractal basins of attraction in optical system optimization", *Opt. Express* **17**, 314 (2009).

Chapter 7
Chaotic dynamics of propagating matter waves

"Todas las teorías son legítimas y ninguna tiene importancia. Lo que importa es lo que se hace con ellas."

-Jorge Luis Borges

We have seen that one of the major benefits of nonlinear dynamics is that it can be used in a wide variety of scientifically relevant situations. In this last chapter, we apply techniques from nonlinear dynamics to the study of propagating quantum matter waves. To this aim, we extend and adapt the concept of basin entropy to chaotic scattering situations and show how it enables to extract important information from the experimental data. In particular, we specify how to implement experimentally the equivalent of a Monte Carlo calculation of such quantities.

We show how these techniques can be used to characterize the chaotic dynamics of the system and to demonstrate the presence of fractal structures in phase space. We also discuss how other methods like the basin stability allow to predict the efficiency of the switch and splitter regimes in a cross beam configuration. The escape time distribution can also be obtained and gives access to the dynamical evolution of the system. These proposals can be implemented with current experimental techniques.

7.1 Introduction

In the early 2000's, splitters for guided propagating matter-wave were thoroughly investigated in the thermal regime [1]–[5]. In the following decade, the Bose-Einstein condensate regime was explored using optical waveguides [6], [7], and the splitting of the matter-waves was related with its underlying chaotic dynamics. Despite the quantum nature of these systems, some results could be understood using classical mechanics. For instance, a classical approximation was employed to unveil fractal structures in phase space using numerical simulations. An estimation for positive Lyapunov exponents was also found, highlighting the chaotic nature of the system. The recent development of new techniques of nonlinear dynamics allows to extract much more information from the same kind of experiments and, more importantly, to

indicate how we can infer these signatures of chaos not only by numerical simulations, but from direct measurements.

One of these powerful tools is the basin entropy introduced in the previous chapter. The framework of the basin entropy theory allows to quantify the unpredictability associated to the different outcomes in a dynamical system. Here, we extend the basin entropy formalism to scattering problems, where we can get the maximal information using minimal data. By using only the data that could be measured in real experiments such as the crossed guide setting of Ref. [7], we show that we can detect reliably the presence of fractal structures in phase space, to a given resolution. Furthermore, we are also able to test the Wada property [8], [9], a more restrictive property than fractality.

In the crossed guide configuration, two different propagating behaviors were observed: the switch and splitter regimes. In the first case, the beam is totally deflected in a given guide. In the second one, the beam splits into the different available guides, a feature that could be used to design a guided matter wave interferometer. The efficiency and robustness of the switch and splitter regimes can be studied by means of the so-called basin stability [10]. The survival probability of the atoms in the waveguides can also be measured, leading to some information concerning the chaotic saddle of the system.

The qualitative difference of the results presented here with respect to previous works is that we do not simply use numerical simulations of the classical model to show the presence of chaos, but we use the theoretical tools of nonlinear dynamics to explain how we can directly measure quantities related to chaos in real experiments with cold atoms at the expense of a slightly modified experimental protocol.

In Sec. 7.2, we introduce the experimental setup made of two crossing guides and its modelization. Section 7.3 is devoted to the generalization of the concept of basin entropy to scattering situations. The application of this technique to the considered experimental cold atom system is detailed in Sec. 7.4. In Sec. 7.5, we explain how this approach enables one to experimentally characterize the fractal structure of the phase space. In Sec. 7.6, we investigate quantitatively the splitter and switch regimes. We discuss the survival probability at the crossing in Sec. 7.7.

7.2 The crossed-beam system

In this section, we present the system studied along this chapter. It corresponds to the motion of atoms in two crossed laser beams acting as wave-guides. This has been experimentally implemented in Ref. [7]. The potential experienced by the atoms in the presence of two Gaussian dipole beams crossing at an angle θ is

$$U(x,y,z) = -U_1 \frac{w_{10}^2}{w_1^2(x)} e^{-2(y^2+z^2)/w_1^2(x)} - U_2 \frac{w_{20}^2}{w_2^2(x')} e^{-2((y')^2+z^2)/w_2(x')^2)}. \tag{7.1}$$

with $x' = x\cos\theta - y\sin\theta$, $y' = x\sin\theta + y\cos\theta$, $U_i = \eta P_i/w_{i0}^2$ and $w_i^2(x) = w_{i0}^2(1 + x^2/x_{Ri}^2)$ for $i = 1, 2$. Subindexes 1 and 2 account for the two lasers, while θ is the

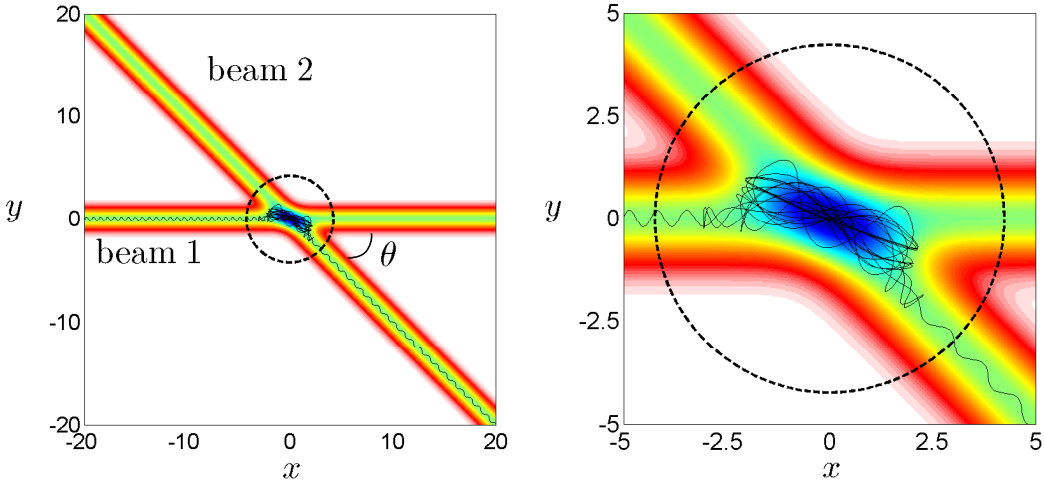

(a) (b)

Figure 7.1. Example of a trajectory in the crossed-beam configuration. The color code accounts for the depth of the potential. The parameters of the potential are $\alpha_1 = \alpha_2 = \beta_1 = \beta_2 = 1, \theta = 45°$. The dashed circle represents the scattering region $\sqrt{x^2+y^2} < 3\sigma$, with $\sigma = \sqrt{\frac{2}{\beta_i}}$. (a) Classical trajectory. (b) Close up of (a).

angle between them. The parameter w_{i0} refers to the waist of the Gaussian dipole laser i, λ_i to its wave length, and $x_{Ri} = \pi w_{i0}^2/\lambda_i$ to its Rayleigh length. The η parameter has a value that depends both on the atom and on the wave length of the dipole laser ($\eta = 1.3 \times 10^{-36}\mathrm{J}\cdot\mathrm{W}^{-1}\cdot\mathrm{m}^2$ for rubidium-87 with $\lambda = 1064$ nm) [11].

For the sake of simplicity, we shall use a two-dimensional model that captures the main features of the real system [7], [12]. For this purpose, we assume that the propagation is performed on a distance small with respect to the Rayleigh length so that $w_i^2(x) \simeq w_{i0}^2$ and we consider one transverse direction y (x is the direction of propagation). Thus, following a dimensionless procedure we can describe the motion of the atoms by means of the following Hamiltonian:

$$H = \frac{1}{2}\left(\dot{x}^2 + \dot{y}^2\right) - \alpha_1 e^{-\beta_1 y^2} - \alpha_2 e^{-\beta_2 (x\sin\theta + y\cos\theta)^2}. \tag{7.2}$$

The dimensionless procedure consists in introducing a length ℓ and a time τ scales. We get $\alpha_i = mU_i\tau^2/\ell^2$ and $\beta_i = 2\ell^2/w_{i0}^2$. For instance, for $\alpha_i = \beta_i = 1$, we have $w_{i0} = w_0$, $U_i = U_0$ and therefore $\ell = w_0\sqrt{2}$ and $\tau = w_0(2/mU_0)^{1/2}$. Then, the features of each laser enter two characteristic parameters: α related to the depth of the potential and β to the laser waist width.

Figures 7.1(a)-(b) show an example of a classical trajectory of this Hamiltonian. The coupling of the longitudinal and the transverse degrees of freedom that occurs at the crossing region is responsible for the complex dynamics. In Ref. [7], it was

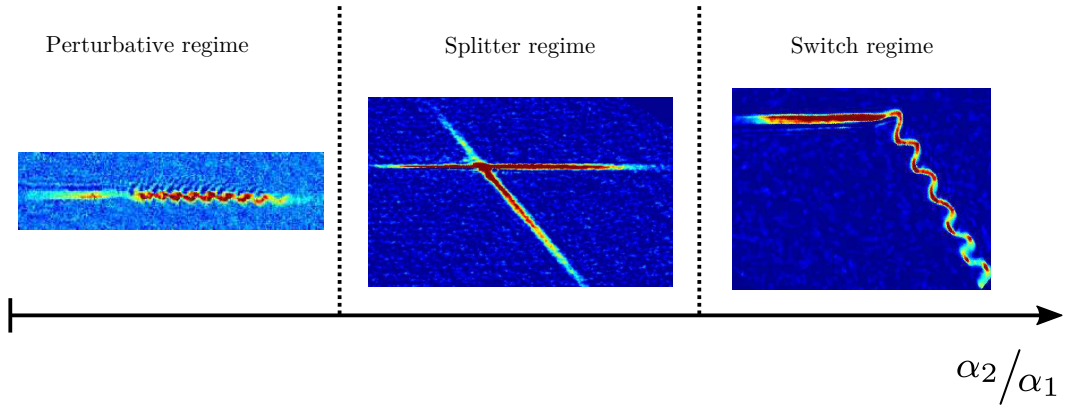

Figure 7.2. Qualitative presentation of the different experimental regimes. Depending on the power ratio α_2/α_1, we represent the three experimental regimes observed in the X-shape configuration of atom lasers from Ref. [7]. The position of the boundaries separating these different regimes also depends on the initial horizontal speed v_x. In the present work, we keep $\alpha_2/\alpha_1 = 1$ and modify v_x, which is also feasible in real experiments.

shown that due to the relatively short time spent in the scattering region by the wave packet and the 3D dynamics, interference effects were marginal in most cases and the classical description could account for most of the experimental results. In that work, the parameters governing the potential, i.e., the parameters of the wave guides $\alpha_1, \alpha_2, \beta_1, \beta_2$, were changed in order to produce different kind of dynamics. In particular, for low values of the ratio α_2/α_1 the waves were only slightly perturbed, whereas for similar intensities of both lasers the splitter regime was found and for large values of α_2/α_1 the switch regime was dominant (see Fig. 7.2). In the present chapter, we adopt a different perspective keeping the potential unchanged ($\alpha_1 = \alpha_2 = \beta_1 = \beta_2 = 1$) and varying the initial horizontal speed $v_x(t = 0)$, which is more in the spirit of the scattering problems. This is feasible in experiments by setting different gradients to accelerate the atoms [13], [14]. The initial horizontal speed $v_x(t = 0) > 0$ can be considered as a parameter of the system: depending on its value the dynamics can be largely different. Namely, when particles are shot with a low speed v_x trajectories have more time to explore the scattering region and to display chaotic dynamics. For high speed v_x, particles are barely affected by the nonlinear potential.

Therefore, keeping v_x and θ as parameters and considering sufficiently long shooting distances $x(t = 0)$ from the crossing region, we can analyze the dynamics in terms of (y, v_y). The set of initial conditions (y, v_y) that yields an escape through a given exit is referred to as an escape basin. Graphical representations of escape basins are provided in Fig. 7.3(a)-(c), where each color represents an exit according to the color code of Fig. 7.3-(d). Given the Gaussian profile of the potentials, we define unbounded trajectories as those going further than $3\sigma_i$ of each laser beam $i = 1, 2$, with $\sigma_i = \sqrt{\frac{2}{\beta_i}}$. White pixels are for such unbounded trajectories that provide atom

losses and also for what we call sticky trajectories, i.e., that spend more than $2 \cdot 10^6$ time steps without exiting (we have checked that they have a negligible influence). These two kinds of trajectories will not be considered for the calculations of basin entropy. The basin corresponding to them is however interwoven with the other basins, as shown in Fig. 7.3-(b), but it is only important for extremely low values of v_y and large initial transverse position. In the following, we will restrict our study for $v_y \in [-1.5, 1.5]$, $y \in [-1.5, 1.5]$.

The presence of fractal structures is evident for low speed basins (see Fig. 7.3-(a)), but harder to appreciate in the case of high speed e.g. Fig. 7.3-(c). A quantification of the different *degrees of fractality* can be accomplished with the help of the *basin entropy*.

7.3 The concept of basin entropy for scattering experiments

In the previous chapter, we introduced the idea of basin entropy in order to answer a simple question: how is it possible to affirm that one basin is more unpredictable than another? We have already shown how the basin entropy quantifies this final state unpredictability associating to each basin a number that ranges between 0 and $\log N_A$, being N_A the number of possible outcomes of the system. In the system under study here, the two guides give rise to four possible exits, that is $N_A = 4$.

The basin entropy computation in scattering problems presents some particularities that must be treated carefully. First, in the basin entropy calculation we usually work with flat distributions, in the sense that initial conditions are uniformly distributed in (x, v_x, y, v_y). When particles advance through the horizontal wave guide, before the scattering region, these distributions evolve in time. Indeed, the transverse Hamiltonian is close to integrability and possesses invariant curves which do not correspond to the original distribution. Trajectories follow these invariant lines towards a quasi stationary regime where they are uniformly distributed on these curves. This happens for sufficiently long times, i.e., for sufficiently long launching distances. If the particles do not have enough time to evolve to these asymptotic distributions the values of the basin entropy can be largely modified (see Fig. 7.4), thus, we must take large enough values of x_0.

Another different issue is the number of trajectories per box n_B. In order to get a reliable value of the basin entropy, it is necessary to have reliable values of the probabilities of each box. However, in numerical simulations we must reach a compromise between computational cost and statistical convergence. Figure 7.5 reflects the basin entropy calculation for different angles and different number of trajectories per box in the four-dimensional space. Results remain unaltered for values of the trajectory per box larger than 5^4, which will be the standard value used along the present chapter.

Finally, another fundamental parameter for the basin entropy calculation is the number of boxes N. Obviously, the larger the number of boxes N, the more precise will be the description. However, both in experiments and in numerical simulations we must take into account practical considerations concerning the number of exper-

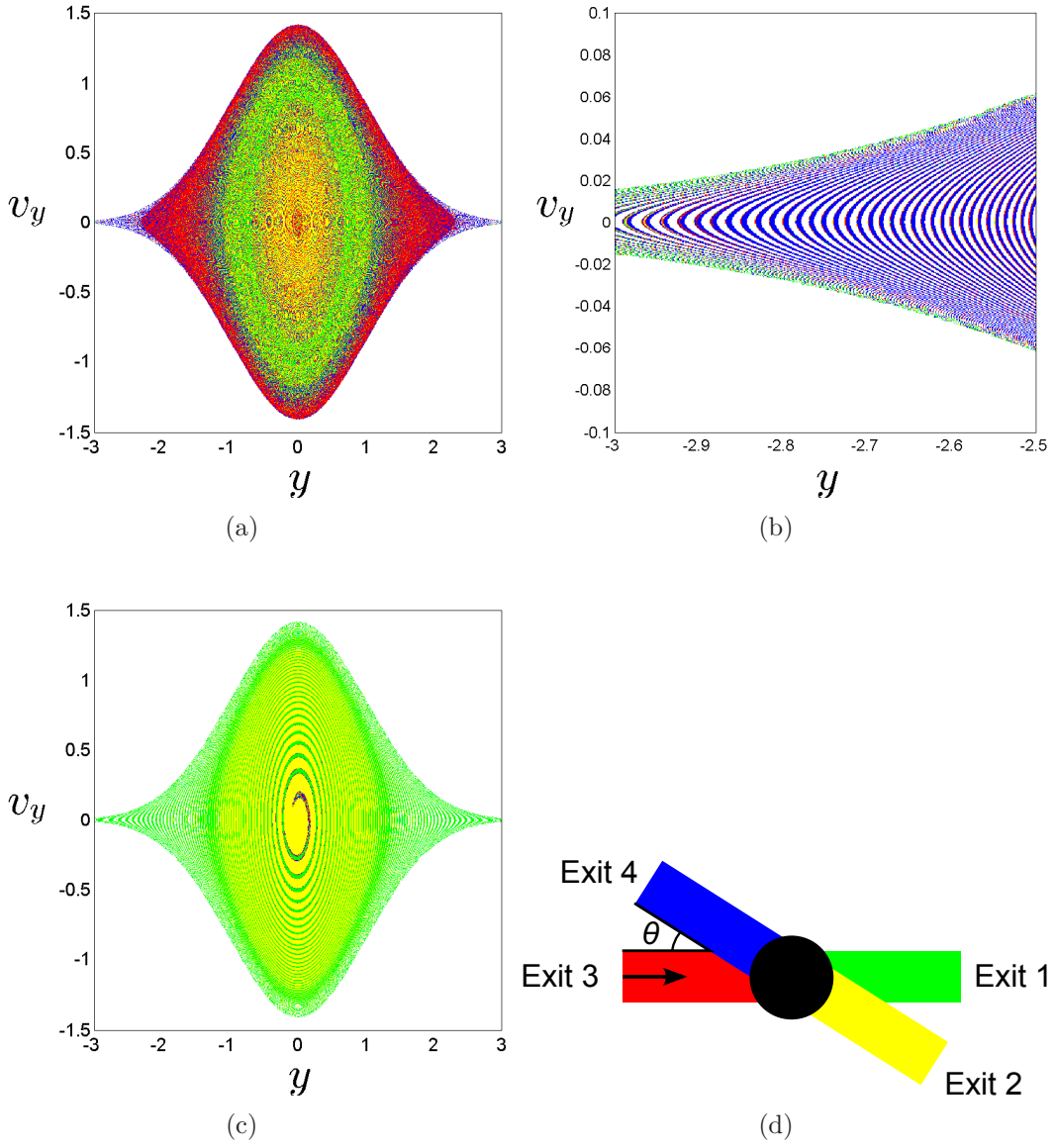

Figure 7.3. Escape basins. The parameters for these basins are $\theta = 45°, x_0 = -250$. (a) Escape basin for low shooting speed $v_x = 0.1$. (b) Zoom of the basin depicted in (a). (c) Escape basin for high shooting speed $v_x = 1$. (d) Color code used in the previous basins.

iments and the computational effort. In this respect, we have already demonstrated in Chapter 6 that a Monte Carlo procedure for the choice of the boxes in phase space leads to accurate values of the basin entropy minimizing the efforts.

7.4 Basin entropy from experimental cold atom data

The procedure to calculate the basin entropy with Monte Carlo technique and the scattering experiments with cold atoms share some important similarities. In both cases we consider ensembles of trajectories instead of single trajectories. In these experiments we have clouds of atoms with different values of velocity and position, and for the basin entropy calculation we must compute many trajectories with different initial conditions inside every box. Scattering experiments essentially study the output of the trajectories in order to gain knowledge about the system, just as the basin entropy does. We propose to use as the equivalent of boxes in the basin entropy scheme, wave packets of atoms which are launched in the scattering region. Indeed, these wave packets correspond to a group of atoms distributed around a mean value of velocity and position following a Gaussian distribution. The experimental measurement through absorption pictures provides access to the population of different branches, and thus to the probabilities inside every box.

In experiments, the problem of the stationarity of the distributions before arriving to the scattering region can be solved by varying the launching distance appropriately. The number of trajectories per box is related to the number of atoms in a wave packet, which is in the thousands. In fact, it can be further increased by repeating the experiment for a wave packet with same initial mean values.

Remarkably, the Monte Carlo sampling of phase space can be done experimentally by selecting different sets of initial conditions with different mean velocity v_y and mean position y. In practice, small clouds of atoms shall be successively delivered from a trap that accommodates a reservoir of atoms such as Bose-Einstein condensate placed upstream. The transverse position for outcoupling the atoms can be tuned by modifying by optical means the reservoir trap geometry and the mean transverse velocity can be transferred to the packet of atoms by applying a well-calibrated transverse magnetic gradient pulse. By repeating successively such an outcoupling procedures so to empty the reservoir, it is possible to reduce drastically the number of experimental runs. As shown in Fig. 7.6, for an achievable number of experiments (~ 50) the relative error in the basin entropy computation is below 10%.

An important point is therefore the minimal resolution that can be reached in this experimental procedure. This corresponds to the size of the wave packet compared to the size of the range of phase space that we want to explore. To access the achievable resolution, we focus on the velocity space. A similar argument is valid in position space. Typically, the range of variation of velocity is of the order of $\Delta v = \sqrt{U_0/m}$, associated to the depth U_0 of the guide. For a quantum packet in the transverse ground state, the velocity dispersion of the wave packet $\delta v_0 = \omega_0 a_0$, where $a_0 = (\hbar/m\omega_0)^{1/2}$, is the oscillator length and $\omega_0 = (4U_0/mw_y^2)^{1/2}$ is the transverse angular frequency obtained by expansion of (7.1). The realization of monomode atom laser has proved the experimental feasibility of the production of such packets [15]–[20]. With the parameters of [7], we find $\Delta v/\delta v_0 = (U_0 m w_y^2/4\hbar^2)^{1/4} \simeq 65$ ($w_y = 100$ μm and $U_0/k_B = 10$ μK). In practice, a linear resolution of several tens

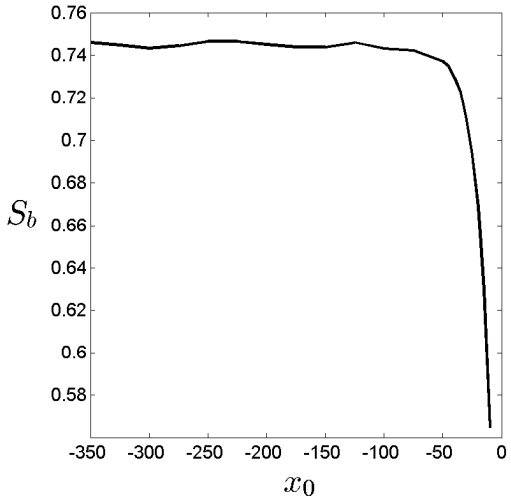

Figure 7.4. Basin entropy for different launching distances. The horizontal speed is $v_x(t=0) = 0.1$, the angle is $\theta = 45°$, $v_y \in [-1.5, 1.5]$ and $y \in [-1.5, 1.5]$. The basin entropy S_b saturates for long enough launching distances x_0 from the scattering center.

can therefore be obtained up to a maximum of one hundred.

In short, to compute the basin entropy S_b in the crossed beam configuration, one should make a sufficient number of experiments. Each of these experiments consists in sending a wave packet with some mean transversal velocity and position. The experiments must be carried out for sufficiently long launching distances. Then, the population exiting through each channel should be measured (by absorption images for instance). Each experiment provides a value of the basin entropy in a box S_{bi}. With an appropriate sampling of the region of phase space considered, the total basin entropy can be computed adding the basin entropy associated to each box.

7.5 Chaos and fractal structures

In this section, we investigate transient chaos and fractal structures appearing for low values of the horizontal speed v_x. Low speed implies that particles spend more time in the scattering region, i.e., the guide crossing region. Therefore, the exponential divergence of trajectories induced by the nonlinear potential makes the system difficult to predict. The phase space is *highly fractalized*, and the basin entropy accounts for that. As a first approach, we have sampled the basin entropy in the 2D space (y, v_y) using a Monte Carlo procedure. The basin entropy S_b for different angles θ and for different shooting speeds v_x is represented in Fig. 7.7-(a). We can see that the basin entropy is higher for lower speeds. Thus, the basin entropy quantifies our intuition: it is more difficult to predict the final destination of particles with low speed v_x.

Using these data, we can prove the presence of fractal structures in phase space

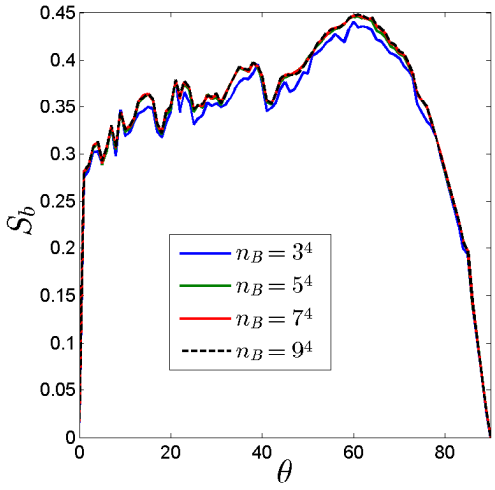

Figure 7.5. Basin entropy for different number of trajectories per box. As we increase the number of trajectories per box n_B the values of S_b converge. The region of the four dimensional space explored is $v_x \in [0.09, 0.11]$, $x \in [-250, -200]$, $v_y \in [-1.5, 1.5]$, $y \in [-1.5, 1.5]$.

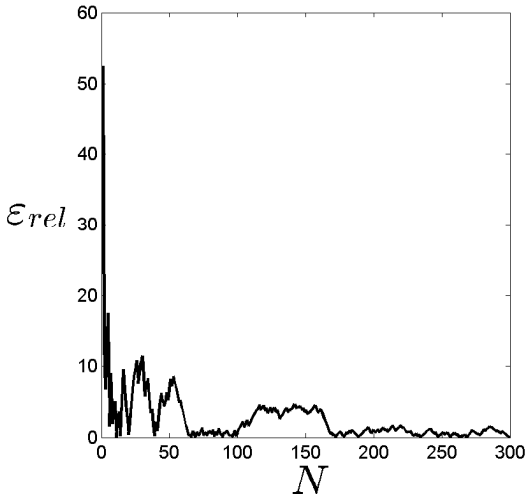

Figure 7.6. Convergence with the number of the Monte Carlo scheme. The relative error $\varepsilon_{rel} = \frac{|S_b - S_b(RS)|}{\langle Sb \rangle} \times 100$ as a function of the number of sampled boxes N is represented. For achievable number of experiments (50-100) the relative error is below 10%. The computations were done in the four dimensional space (x, v_x, y, v_y) for $\theta = 45°$ and $v_x \in [0.09, 0.11]$, $x \in [-250, -200]$, $v_y \in [-1.5, 1.5]$, $y \in [-1.5, 1.5]$.

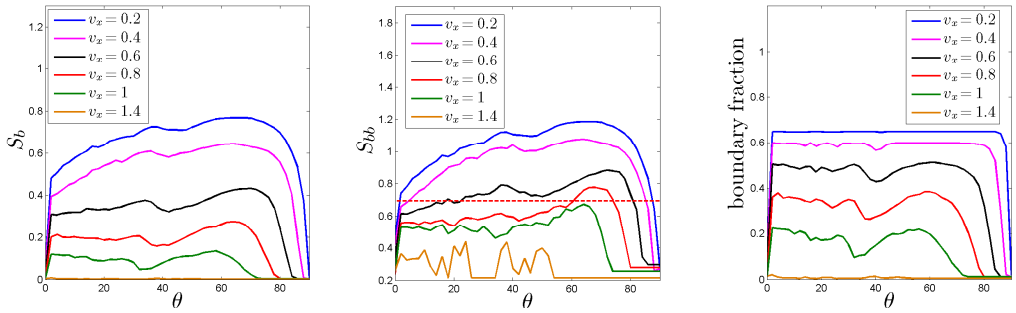

(a) (b) (c)

Figure 7.7. Random sampling computation in 2D using different values of the launching speed. For fixed values of v_x and θ indicated in the figures, $x_0 = -250$, we choose boxes randomly in the (y, v_y) space ($v_y \in [-1.5, 1.5]$, $y \in [-1.5, 1.5]$) and compute the basin entropy S_b. (a) As we increase the horizontal speed v_x (from top to bottom) the lower the basin entropy. (b) The basin boundary entropy S_{bb} is above the $\log 2$ threshold (red dashed line) for low speeds v_x, and is below for high speeds. (c) The fraction of boxes lying in the boundary decreases as we increase v_x from top to bottom. This can be helpful to determine experimentally the scale of the system with respect to simulations.

by means of the $\log 2$. As explained in the previous chapter, if we compute the boundary basin entropy S_{bb}, that is the basin entropy only in the boundary boxes, we can affirm that a boundary is fractal if $S_{bb} > \log 2$. The $\log 2$ criterion is a sufficient but not necessary condition for fractality: some fractal basins do not pass this criterion, for instance those having only two outcomes. In our case, the system presents four possible exits, and for low speeds the values of S_{bb} largely exceed the $\log 2$ threshold, as shown in Fig. 7.9. If such a curve was reproduced in experiments, it would directly imply that the phase space is fractal.

Nevertheless, it is important to recall that the $\log 2$ criterion detects fractals *at a given resolution*. Indeed, given a finite resolution it is impossible to distinguish a real fractal from something which is not a fractal, but that looks like it at that resolution. The $\log 2$ criterion presents a major advantage compared to other techniques like the box-counting dimension: it avoids the use of different scales of speed and position, which in the context of experiments with cold atoms is fundamental. The $\log 2$ criterion is a strong argument to test fractal structures using minimal requirements. Of course, we will detect fractal structures at the resolution that could be achieved with the experiments, which depend on the size of the wave packet compared to the size of the region of phase space considered. To illustrate this point, we show in Fig. 7.8 basins with different resolution, showing that experimentally achievable resolutions are enough to display fractal basins.

Some escape basins are not only fractal, but also possess the more restrictive property of Wada [8], [9]. This means that all the basins have a common boundary separating them. The experimental evidence of the Wada property would be that

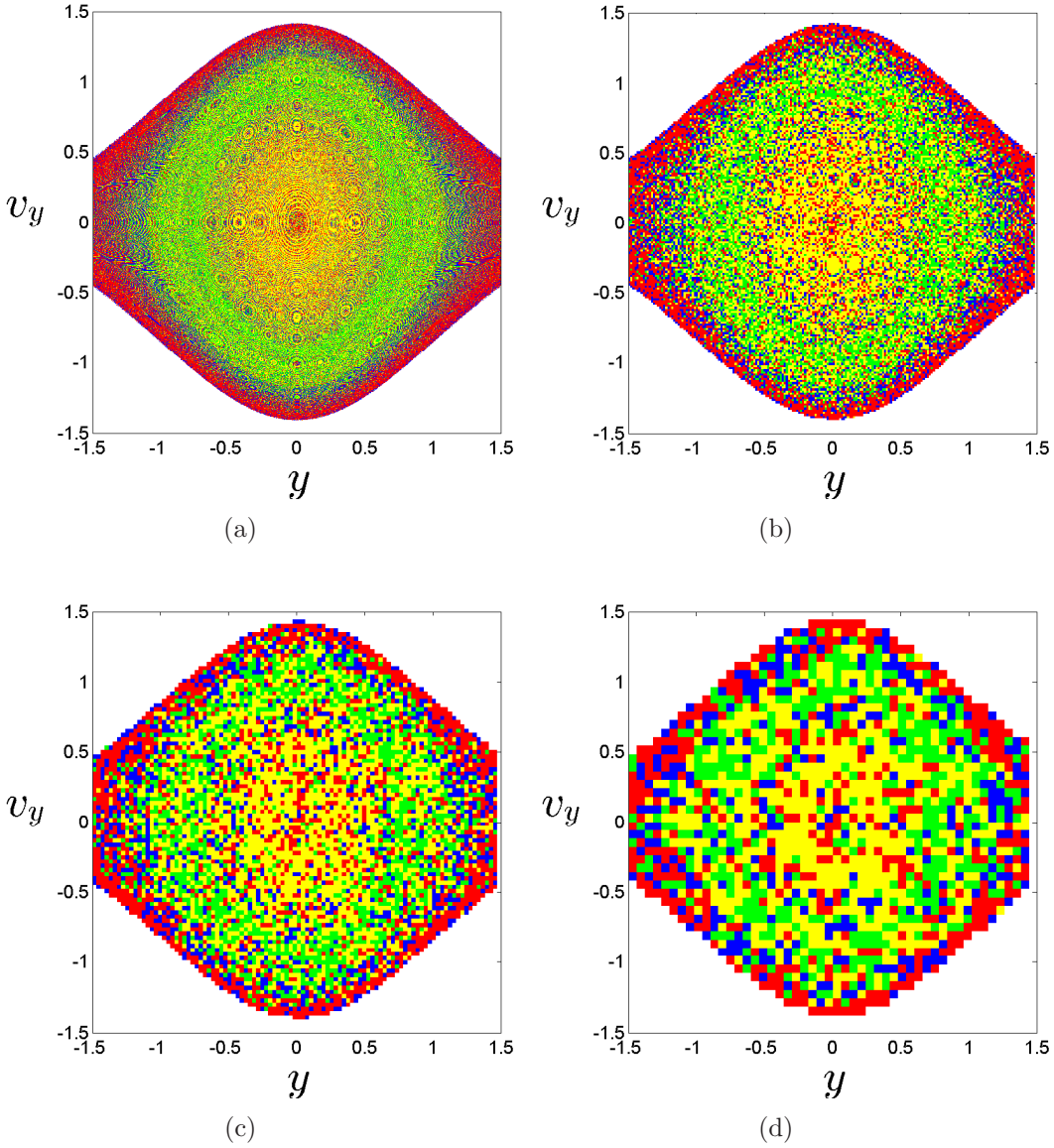

Figure 7.8. Fractal resolution. Escape basins in the (y, v_y) subspace for $\theta = 45°, x_0 = -250, v_x = 0.1$. The resolution are (a) 1000×1000, (b) 200×200, (c) 100×100 and (d) 50×50. The experimental resolution is probably close to (d), but still fractal structures are visible.

in this regime every time that more than one branch is populated, all the branches are populated. If the experiment is in the Wada regime, it will be seen through the impossibility to detect atoms only in two or three branches.

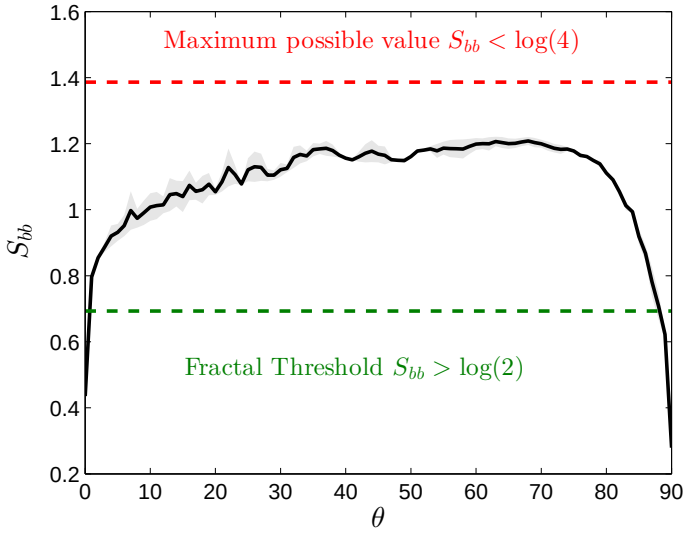

Figure 7.9. Log 2 criterion. The basin entropy in the boundaries S_{bb} for different angles θ. The region of initial conditions sampled is $v_x \in [0.09, 0.11]$, $x \in [-250, -200]$, $v_y \in [-1.5, 1.5]$, $y \in [-1.5, 1.5]$. The black line is for a computation made with 100 boxes composed of 5^4 trajectories each one, and the shaded region is the absolute error with respect to an asymptotic value taken at 800 boxes.

7.6 Splitter and switch regimes

Incident particles with high initial horizontal speed spend less time in the scattering region and most of them tend to escape through exits in the positive x direction. As a consequence, their asymptotic behavior is easier to predict, implying a decrease of the basin entropy for high $v_x(t = 0)$ (see Fig. 7.7-(a)). Despite the fact that the phase space is still fractal, the $\log 2$ criterion is no longer fulfilled, as shown in Fig. 7.7-(b). This happens because there are dominant basins occupying most of the phase space, and the number of boxes lying in the boundaries decreases (see Fig. 7.7-(c)).

Nevertheless, the appearance of a dominant basin is crucial for the efficiency of the switch regime, since this regime is characterized by a large portion of the incident particles escaping through exit 2. The basin entropy can give us a clue to find the parameters for this switch regime: if most particles escape through an exit, then the basin entropy must be low. Then, we can also apply the basin stability [10] to fully characterize the efficiency of the switch. The basin stability is simply the portion of phase space occupied by each basin, so $B_{Si} \in [0, 1]$ for $i = 1, ..., 4$ and $\sum_{i=1}^{4} B_{Si} = 1$. Therefore, computing the basin stability for the exit basin 2 is equivalent to calculate its efficiency. In cold atom experiments the basin stability can be computed using the Monte Carlo sampling described above.

Some angles like $\theta = 33°$ display a large switch efficiency for high speeds, as

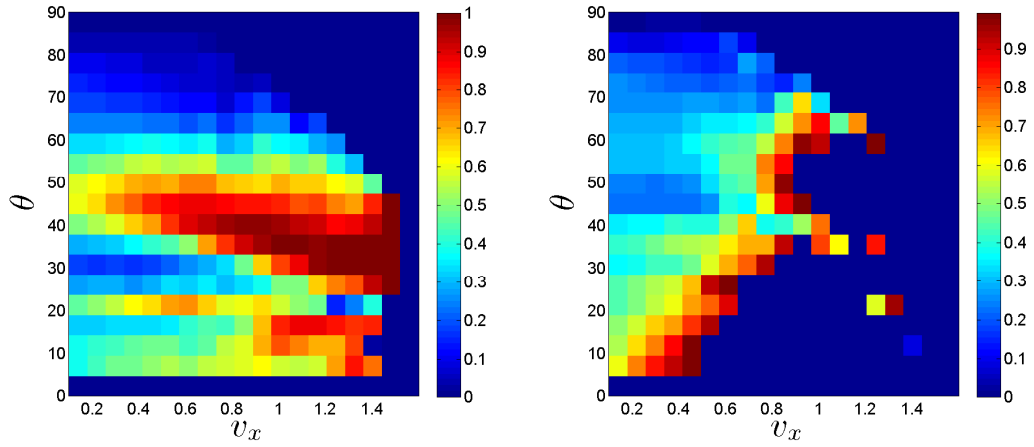

Figure 7.10. Efficiency of the switch and splitter regimes. (a) Color map representing the fraction of trajectories escaping through exit 2, that is, the efficiency of the switch regime. For these computations we have used initial conditions in the region $v_y \in [-0.5, 0.5]$, $y \in [-0.5, 0.5]$ and $x_0 = -250$. (b) Color map for the correlation of the basin stability of exits 1 and 2, defined as the normalized product of their basin stability $c = B_{S1}B_{S2}/4$. For values close to 1 the system is close to a perfect 50-50 splitter regime. This takes place for larger angles as the speed increases.

shown in Fig. 7.10-(a). This prediction could be checked in real experiments. We have also tested the robustness of these results against small perturbations of the laser parameters $(\alpha_1, \alpha_2, \beta_1, \beta_2)$. Sometimes in chaotic dynamics small perturbations of the system parameters may lead to different dynamical behaviors [21]. However this is not the case here, and the switch regime turns out to be robust against perturbations of the wave guide parameters.

In the splitter regime approximately half of the atoms escape through exit 1 and the other half through exit 2. Using the basin stability, we can define the efficiency of the switch regime as the correlation between basin stability of exits 1 and 2, which can be calculated as their normalized product $c = 4B_{S1}B_{S2}$, where the factor 4 is to normalize at the maximum correlation value of $B_{S1} = B_{S2} = 0.5$. This efficiency of the splitter c is calculated for different v_x and θ and represented in Fig. 7.10-(b). We can see that as the horizontal speed v_x is increased, the splitter regime happens for larger angles. The splitter is more sensitive to perturbations of the parameters than the switch regime, as can be inferred from the non-trivial structure of Fig. 7.10-(b).

7.7 Survival probability

The experimental setup described in Ref. [7] allows to measure not only the atom population of the branches, but also the population that lies in the crossing region for some time. Therefore, we can define the escape time as the time spent by atoms

in a region of radius 3σ centered in $(0, 0)$, which we call the scattering region. We also define the survival probability as the probability P of finding an atom at a time t in the scattering region, which exactly corresponds with the measurements made in experiments.

Depending on the hyperbolic or non-hyperbolic nature of the system, the survival probability is expected to present exponential or algebraic decay for long times. In numerical simulations, we normalize time dividing by $t_0 = x/v_{x0}$, which is the time that a particle would take to cross the scattering region if there were only one laser, and we find curves of probability versus time like the ones depicted in Fig. 7.11. The first plateau of this curve reflects that all the particles take at least $t = t_0$ to escape the scattering region. After the plateau, we can see an exponential decay for short times (see insets of Fig. 7.11). For very long times the decay is algebraic, a typical behavior of non-hyperbolic systems [22]. However, in real experiments we expect to see only the exponential decay for two reasons. The first one is that non-hyperbolic systems are structurally unstable [23], [24]. This means that the slightest perturbation provokes the change from algebraic to exponential decay for long times. The second reason is that in real experiments, the long time behavior is hard to follow because small atom populations are difficult to detect. Moreover, when a non-hyperbolic system is weakly perturbed the curve of probability versus time behaves as the first part of the non-perturbed system, that is, it shows an exponential decay characterized by the same mean-life τ [25].

7.8 Discussion

In this final chapter of the thesis, we apply ideas developed along the thesis to the hot research area of propagating matter waves. So far, nonlinear dynamics had only been used as an approximation to explain *a posteriori* some results concerning the chaotic dynamics of the atoms. But here we propose to go far beyond. We have explained in detail how it is possible to use new techniques from nonlinear dynamics to characterize the chaotic dynamics of the atoms directly from experiments.

We have focused on a double guide configuration, where the atoms can escape through four different exits. In real experiments, we can measure the atom population in each branch, and the time spent by the atoms in the scattering region. Using these data we can measure the basin entropy, the basin stability and the mean escape time. The number of atoms escaping through each branch allows us to determine the fractal nature of the phase space and the efficiency of the switch and splitter regimes. The escape times provides information about the hyperbolicity of the system. Moreover, an experimental approximation of the Lyapunov exponents is proposed in Ref. [6], which could be used to get a lower bound of the dimension of the chaotic saddle following a similar procedure to [26], [27]. Therefore, we can characterize the chaotic properties of the system.

An interesting modification of the experimental setting would be the inclusion of more guides. Indeed, with more exits, the $\log 2$ criterion would be more likely fulfilled, and the testing of fractality of the system shall be easier. Similarly, the

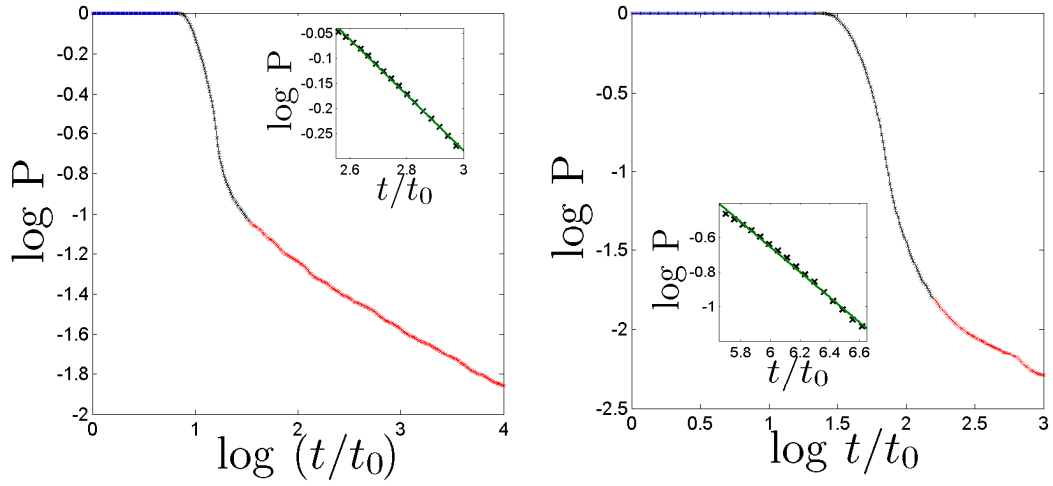

(a) (b)

Figure 7.11. Survival probability as a function of time. The survival probability P of the atoms in the scattering region as a function of time. After the initial plateau (in blue), there is an exponential decay (see inset) and for very long times an algebraic decay (in red). (a) $v_x = 0.3$. (b) $v_x = 0.9$. The rest of parameters are $\theta = 45°$, $v_y \in [-0.5, 0.5]$, $y \in [-0.5, 0.5]$ and $x_0 = -250$.

direct observation of the intriguing Wada regime could be made possible for the first time in an experiment with cold atoms.

This work lays the foundations for future research where experiments with cold atoms will be enriched by their dynamics characterization. Our study motivated by an experimental work provides a new approach to investigate nonlinear effects such as fractal structures or the Wada property in a way perfectly accessible with state of the art experimental techniques.

Bibliography

[1] D. Cassettari, B. Hessmo, R. Folman, T. Maier, and J. Schmiedmayer, "Beam splitter for guided atoms", *Phys. Rev. Lett.* **85**, 5483–5487 (2000).

[2] M. J. Renn, D. Montgomery, O. Vdovin, D. Z. Anderson, C. E. Wieman, and E. A. Cornell, "Laser-guided atoms in hollow-core optical fibers", *Phys. Rev. Lett.* **75**, 3253–3256 (1995).

[3] D. Müller, E. A. Cornell, M. Prevedelli, P. D. D. Schwindt, Y.-J. Wang, and D. Z. Anderson, "Magnetic switch for integrated atom optics", *Phys. Rev. A* **63**, 041602 (Mar. 15, 2001).

[4] O. Houde, D. Kadio, and L. Pruvost, "Cold atom beam splitter realized with two crossing dipole guides", *Phys. Rev. Lett.* **85**, 5543–5546 (2000).

[5] R. Dumke, M. Volk, T. Müther, F. B. J. Buchkremer, G. Birkl, and W. Ertmer, "Micro-optical realization of arrays of selectively addressable dipole traps: a scalable configuration for quantum computation with atomic qubits", *Phys. Rev. Lett.* **89**, 097903 (2002).

[6] G. L. Gattobigio, A. Couvert, B. Georgeot, and D. Guéry-Odelin, "Exploring classically chaotic potentials with a matter wave quantum probe", *Phys. Rev. Lett.* **107**, 254104 (2011).

[7] G. L. Gattobigio, A. Couvert, G. Reinaudi, B. Georgeot, and D. Guéry-Odelin, "Optically guided beam splitter for propagating matter waves", *Phys. Rev. Lett.* **109**, 030403 (2012).

[8] J. Kennedy and J. A. Yorke, "Basins of Wada", *Physica D* **51**, 213–225 (1991).

[9] A. Daza, A. Wagemakers, M. A. F. Sanjuán, and J. A. Yorke, "Testing for basins of Wada", *Sci. Rep.* **5**, 16579 (2015).

[10] P. J. Menck, J. Heitzig, N. Marwan, and J. Kurths, "How basin stability complements the linear-stability paradigm", *Nat. Phys.* **9**, 89–92 (2013).

[11] R. Grimm, M. Weidemüller, and Y. B. Ovchinnikov, "Optical dipole traps for neutral atoms", *Adv. At. Mol. Opt. Phys.* **42**, B. B. H̃. Walther, (Ed.), 95–170 (2000).

[12] E. Torrontegui, J. Echanobe, A. Ruschhaupt, D. Guéry-Odelin, and J. G. Muga, "Cold-atom dynamics in crossed-laser-beam waveguides", *Phys. Rev. A* **82**, 043420 (2010).

[13] F. Vermersch, C. M. Fabre, P. Cheiney, G. L. Gattobigio, R. Mathevet, and D. Guéry-Odelin, "Guided-atom laser: Transverse mode quality and longitudinal momentum distribution", *Phys. Rev. A* **84**, 043618 (2011).

[14] F. Damon, F. Vermersch, J. G. Muga, and D. Guéry-Odelin, "Reduction of local velocity spreads by linear potentials", *Phys. Rev. A* **89**, 053626 (2014).

[15] W. Guerin, J.-F. Riou, J. P. Gaebler, V. Josse, P. Bouyer, and A. Aspect, "Guided quasicontinuous atom laser", *Phys. Rev. Lett.* **97**, 200402 (Nov. 13, 2006).

[16] A. Couvert, M. Jeppesen, T. Kawalec, G. Reinaudi, R. Mathevet, and D. Guéry-Odelin, "A quasi-monomode guided atom laser from an all-optical Bose-Einstein condensate", *Europhys. Lett.* **83**, 50001 (2008).

[17] G. L. Gattobigio, A. Couvert, M. Jeppesen, R. Mathevet, and D. Guéry-Odelin, "Multimode-to-monomode guided-atom lasers: an entropic analysis", *Phys. Rev. A* **80**, 041605 (2009).

[18] G. Kleine Büning, J. Will, W. Ertmer, C. Klempt, and J. Arlt, "A slow gravity compensated atom laser", *Appl. Phys. B* **100**, 117–123 (May 29, 2010).

[19] R. G. Dall, S. S. Hodgman, A. G. Manning, and A. G. Truscott, "Observation of the first excited transverse mode in guided matter waves", *Opt. Lett.* **36**, 1131 (2011).

[20] N. P. Robins, P. A. Altin, J. E. Debs, and J. D. Close, "Atom lasers: production, properties and prospects for precision inertial measurement", *Physics Reports*, Atom lasers: production, properties and prospects for precision inertial measurement**, 529**, 265–296 (2013).

[21] M. A. F. Sanjuán, "Using nonharmonic forcing to switch the periodicity in nonlinear systems", *Phys. Rev. E* **58**, 4377–4382 (1998).

[22] Y.-C. Lai and T. Tél, *Transient chaos*. New York: Springer, 2011.

[23] J. M. Seoane, M. A. F. Sanjuán, and Y.-C. Lai, "Fractal dimension in dissipative chaotic scattering", *Phys. Rev. E* **76**, 016208 (2007).

[24] J. M. Seoane, L. Huang, M. A. F. Sanjuán, and Y.-C. Lai, "Effect of noise on chaotic scattering", *Phys. Rev. E* **79**, 047202 (2009).

[25] A. E. Motter and Y.-C. Lai, "Dissipative chaotic scattering", *Phys. Rev. E* **65**, 015205 (2001).

[26] S. Bleher, C. Grebogi, and E. Ott, "Bifurcation to chaotic scattering", *Physica D* **46**, 87–121 (1990).

[27] E. Ott and T. Tél, "Chaotic scattering: an introduction", *Chaos* **3**, 417–426 (1993).

Chapter 8
Conclusions

"Call it the satisfaction of curiosity. I understand a little of it today, perhaps a little more tomorrow. That's a victory in a way."

-Isaac Asimov, *Profession*

Here we schematically summarize the main results of the present thesis:

1. Physics of the 20th century shows that every step forward in Science also constitutes a new limit to scientific knowledge. This thesis is devoted to study the unpredictability in nonlinear dynamics.

2. Vibrational resonance is found in a time-delayed genetic toggle switch. We have shown the optimal enhancement of a low-frequency periodic signal by means of a high-frequency periodic perturbation in a dynamical system of the highest relevance in systems biology.

3. Vibrational resonance often happens for large perturbations. However, systems with fractal basins of attraction are able to show a new kind of vibrational resonance that occurs for small periodic perturbations. We call this new phenomenon *ultrasensitive vibrational resonance*.

4. Wada basins of attraction possess the most intricate boundaries that can be conceived. So far, the only method to prove the existence of Wada basins was restricted to two-dimensional phase spaces. We present a grid method able to test quantitatively the Wada property in any situation.

5. Delay differential equations are a powerful tool in situations where the delay in the transmission of the information cannot be overlooked. The inclusion of delays in dynamical systems may turn the system unpredictable. In particular, we show how the delay can induce transient chaos and the Wada property in the space of history functions.

6. Oftentimes, some basins of attraction are said to be *more fractal* or more unpredictable than others. We propose a quantitative measure of the uncertainty associated to the basins based in the Gibbs definition of entropy. This quantity, that we call *basin entropy*, allows us to identify the main ingredients that contribute to final state unpredictability and it also provides a sufficient criterion to prove the presence of fractal boundaries.

7. We apply concepts from nonlinear dynamics like the basin entropy, the basin stability and the survival probability to a crossed laser configuration used in matter waves propagation. In particular, we detail how to prove the presence of fractal and Wada boundaries using experimental data, we provide an estimation of the efficiency of the different regimes and we study the survival probability of the atoms in the optical guides.

Appendices

Appendix A: Linear stability analysis of the time-delayed toggle switch

Here we analyze the stability of the time-delayed toggle switch, given by the following equations

$$\begin{aligned}\frac{\mathrm{d}u}{\mathrm{d}t} &= \frac{\alpha}{1+v(t-\tau_r)^2} - u(t-\tau_d)\\ \frac{\mathrm{d}v}{\mathrm{d}t} &= \frac{\alpha}{1+u(t-\tau_r)^2} - v(t-\tau_d).\end{aligned} \tag{A.1}$$

We will show that the delay in the degradation term τ_d can induce sustained oscillations via a Hopf bifurcation, whereas the delay in the repressional term τ_r cannot.

First, let us study the system without delay, that is, the previous equations with $\tau_r = \tau_d = 0$. Setting $\dot{u} = 0$ and $\dot{v} = 0$, we can see that the fixed points must obey the following equations

$$\begin{aligned}u_0 &= \frac{\alpha}{1+v_0^2}\\ v_0 &= \frac{\alpha}{1+u_0^2}.\end{aligned} \tag{A.2}$$

Solving these equations we find three different equilibria e_1, e_2, e_3. The equilibria e_1 and e_3 satisfy $u_0 v_0 = 1$ and $u_0 + v_0 = \alpha$. This means that $u_0 = 1/2(\alpha \pm \sqrt{\alpha^2 - 4})$, and therefore $\alpha > 2$ sets the condition for bistability. On its behalf, e_2 satisfies $u_0 = v_0$. To analyze the stability of these equilibria, we must study the Jacobian matrix of A.1 for $\tau_r = \tau_d = 0$

$$J_0 = \begin{pmatrix} -1 & \frac{-2\alpha v_0}{(1+v_0^2)^2} \\ \frac{-2\alpha u_0}{(1+u_0^2)^2} & -1 \end{pmatrix}, \tag{A.3}$$

which leads to the following characteristic "polynomial"

$$(\lambda+1)^2 - \frac{4\alpha^2 u_0 v_0}{(1+u_0^2)^2(1+v_0^2)^2} = 0. \tag{A.4}$$

Simplifying for e_1 and e_3 we can see that the eigenvalues at the equilibrium are $\lambda_{1,2} = -1 \pm 2/\alpha$, so if $\alpha > 2$ the system without delay is bistable. Thus we have e_1 and e_3 as two symmetric equilibrium points and e_2 is the unstable separatrix $u_0 = v_0$ dividing the phase space.

The usual procedure to analyze the stability in systems with delay is to perturb the linearized system around its equilibria during a time equal to the maximum delay of the system,

$$\delta\dot{x} = J_0 \delta x + \dot{x} = J_\tau \delta x_\tau, \tag{A.5}$$

where $x = (u, v)$, J_0 is the Jacobian matrix with respect to the non-delayed variables evaluated at the equilibria and J_τ is the Jacobian matrix with respect to the delayed variables. If we assume the solutions of $\dot{x}$ to be exponential $x = Ae^{\lambda t}$, being λ the eigenvalues of the corresponding Jacobian and A a column vector, then we have that

$$\lambda A = (J_0 + e^{-\lambda\tau} J_\tau)A. \tag{A.6}$$

This equation will have a solution for amplitudes different from zero when

$$|(J_0 + e^{-\lambda\tau} J_\tau) - \lambda I| = 0, \tag{A.7}$$

where I is the identity matrix. Now, let us analyze separately the effects of the degradation delay τ_d and the repressional delay τ_r.

- *Case 1:* $\tau_r = 0, \tau_d > 0$

The Jacobian matrices with respect to the non-delayed and delayed variables are

$$J_0 = \begin{pmatrix} 0 & \frac{-2\alpha v_0}{(1+v_0^2)^2} \\ \frac{-2\alpha u_0}{(1+u_0^2)^2} & 0 \end{pmatrix}, \tag{A.8}$$

and

$$J_\tau = \begin{pmatrix} -1 & 0 \\ 0 & -1 \end{pmatrix}. \tag{A.9}$$

The equilibria e_1, e_2 verify $u_0 v_0 = 1$, so the characteristic "polynomial" derived from Eq. A.7 is

$$(\lambda + e^{-\lambda\tau_d})^2 - 4/\alpha^2 = 0. \tag{A.10}$$

The stability of the system is governed by the roots of this equation. Let us suppose there is a value of the delay $\tau > \tau_c$ where stability is lost and $\lambda = \pm j\omega_c$ just at the transition. Substituting this condition in Eq. A.10 and simplifying we have

$$\cos(\omega_c \tau_c) = \pm 2/\alpha \tag{A.11}$$

$$\omega_c = \sin(\omega_c \tau_c). \tag{A.12}$$

To verify that the eigenvalues cross to the right side of the complex plane, we implicitly derive Eq. A.10, yielding

$$\frac{\mathrm{d}\lambda}{\mathrm{d}\tau} = \frac{\lambda e^{-\lambda\tau_d}}{1 - \tau e^{-\lambda\tau_d}}. \tag{A.13}$$

For $\tau_d = \tau_c$ and $\omega = \omega_c$ we have

$$\mathfrak{Re}\left\{\frac{\mathrm{d}\lambda}{\mathrm{d}\tau}\right\}\Bigg|_{\tau_c,\omega_c} = \frac{\omega_c^2}{\tau_c^2 + 1 - 2\tau_c \cos(\omega_c \tau c).} \tag{A.14}$$

Since there are values of τ that make the previous expression positive, we can assure that the eigenvalues cross the imaginary axis, leading to a Hopf bifurcation and therefore to sustained oscillations.

- *Case 2:* $\tau_r > 0, \tau_d = 0$

Now we consider that the delay affects only the repressional terms. Linearization around e_1, e_2, leads to the following Jacobian matrices

$$J_0 = \begin{pmatrix} -1 & 0 \\ 0 & -1 \end{pmatrix} \tag{A.15}$$

and

$$J_\tau = \begin{pmatrix} 0 & \frac{-2\alpha v_0}{(1+v_0^2)^2} \\ \frac{-2\alpha u_0}{(1+u_0^2)^2} & 0 \end{pmatrix}. \tag{A.16}$$

Thus, the characteristic polynomial is

$$(\lambda+1)^2 - \frac{4\alpha^2 u_0 v_0 e^{-2\lambda\tau_r}}{(1+u_0^2)^2(1+v_0^2)^2} = 0. \tag{A.17}$$

Introducing the conditions for e_1 and e_3 we get

$$0 = (\lambda+1)^2 - \frac{4e^{-2\lambda\tau_r}}{\alpha^2}. \tag{A.18}$$

The solutions of this equation are given by

$$\lambda + 1 = \pm\frac{2e^{-\lambda\tau_r}}{\alpha}. \tag{A.19}$$

We are going to show that the solutions of this equations always are in the left hand side of the complex plane. First, let us suppose that this equation admits a pair of complex conjugate roots $\lambda = a \pm jb$, being $a > 0$. Substituting that solution into Eq. A.19 we get

$$1 + a + jb = \pm(2/\alpha)e^{-a\tau_r}e^{-jb\tau_r}, \tag{A.20}$$

if we take absolute value at both sides we find that

$$1 + a^2 + b^2 = \frac{4e^{-2a\tau_r}}{\alpha^2}. \tag{A.21}$$

This expression cannot hold for $\tau_r > 0$ and $\alpha > 2$, so the solutions $\lambda = a \pm jb$, being $a > 0$ are forbidden. The same can be extended to real solutions. Therefore we have shown that the delay in the repressional term τ_r cannot turn the equilibria e_1, e_3 unstable.

Finally, we have seen that the delay in the degradation term can induce sustained oscillations via a subcritical Hopf bifurcation, whilst the delay in the repressional term cannot. Thus, from the dynamical point of view, studying the delay in the degradation term is enough to understand the dynamics of the system.

Appendix B: Further examples on the testing for Wada basins

Here we provide further evidence of the performance of our method to verify the Wada property. We use our algorithm in several models known to show the Wada property.

- *Forced Duffing oscillator*

This beautiful example of Wada basins (Fig. B.1(a-b)) is found for the double-well Duffing potential, with dissipation and periodic forcing, expressed as

$$\ddot{x} + \delta\dot{x} - x + x = F\cos t. \tag{B.1}$$

The parameters chosen here are $\delta = 0.15, F = 0.245$ (see [1] for further details). The computational performance of the algorithm is prototypical for systems with the Wada property: a maximum for followed by an exponential decay (Fig. B.1(c-d)). We needed to compute 1719902 new points to check the Wada property in this system, that is the equivalent to less than the number of points in two basins of attraction.

- *Hénon-Heiles hamiltonian*

The Hamiltonian of Hénon-Heiles, used in galactic dynamics, has three symmetric exits in the x-y plane. It can be written as follows,

$$H = \frac{1}{2}(\dot{x}^2 + \dot{y}^2) + \frac{1}{2}(x^2 + y^2) + x^2 y - \frac{1}{3}y^3. \tag{B.2}$$

In this case, escape basins are defined as the initial conditions leading to the three different exits (Fig. B.2(a)). In Ref. [2], the authors make a slight modification of the NY condition and it is the unstable manifold of the Lyapunov orbit that crosses the three different basins. Here we simply use our algorithm with the basin corresponding to the $y - \dot{y}$ plane, for $E = 0.25$ and $x = 0$ (Fig. B.2(b)). Once again, the fractal structure of the Wada basins is responsible of the exponential decay in the computational effort (Fig. B.2(c-d)). The total number of points that we need to compute to check the Wada property is 1259510, that is approximately like computing a new basin and a quarter.

- *Magnetic pendulum*

The problem of a pendulum with an iron bob, under the influence of gravity, air friction, and three magnets forming an equilateral triangle with side equal to one, can be approximated [3] for small-angles as,

$$\ddot{q}_j + R\dot{q}_j - \sum_{i=1}^{3} \frac{q_{j,i} - q_j}{\left(\sum_{j=1}^{2}(q_j - q_{j,i}) + d^2\right)^{3/2}} + Cq_j = 0, \tag{B.3}$$

$$q_{j,i} = \left(\cos\left(\frac{2\pi j}{3}\right), \sin\left(\frac{2\pi j}{3}\right)\right), j = 1, 2. \tag{B.4}$$

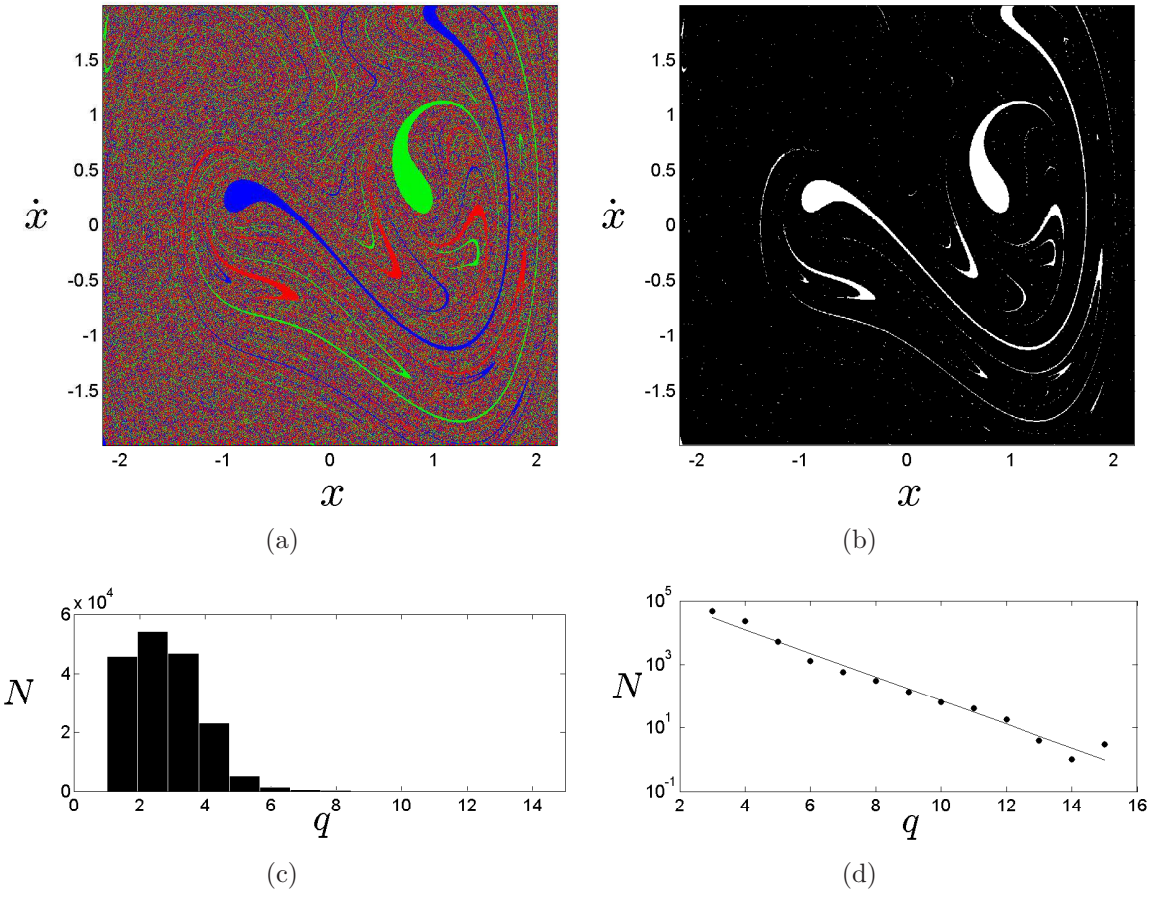

Figure B.1. Forced Duffing oscillator (a) Basins of attraction for the Duffing oscillator with dissipation and periodic forcing. (b) All the boxes in the boundary are classified into the boundary of the three basins category. (c) Most of the boxes need between one and five steps to test that they are in the boundary of three basins. After a maximum, there is an exponential decay related to the fractal structure of the basins, that allows fast computation. A fit of the exponential decay is shown in (d).

The parameters to obtain figures B.3 (a-b) are $R = 0.1, d = 0.01, C = 0.01$. This model is more delicate to analyze than the previous ones, since fractal basins get diluted upon magnification. From a mathematical point of view, this system is not Wada because fractality is lost at infinity. Nevertheless, from a physical point of view, i.e., with finite resolution, this system is Wada. The result of our algorithm, given its finite precision, is that the system is completely Wada. Our algorithm needed to compute 11330172 points to classify the initial million grid boxes either in the interior or in the boundary of three basins. The increase of computational effort in relation with other cases is likely to be caused by this lost of Wada property at infinity.

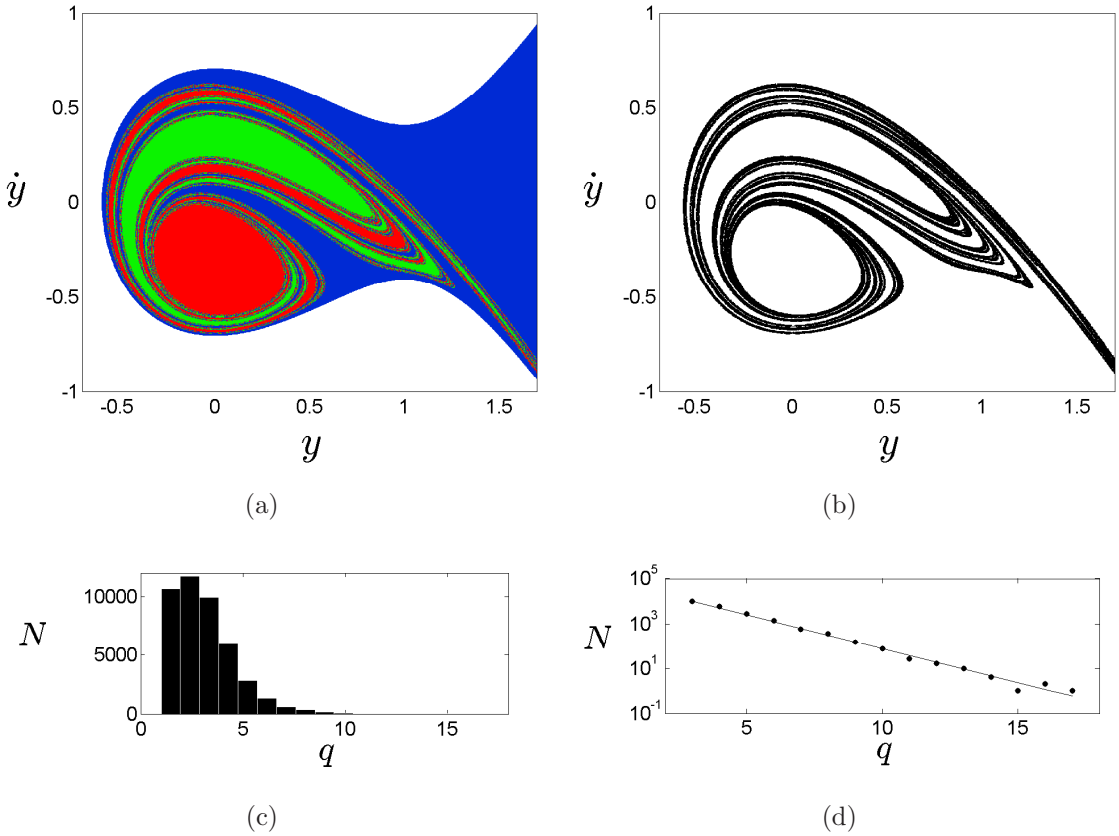

Figure B.2. Hénon-Heiles hamiltonian. (a) Escape basins for the Hénon-Heiles hamiltonian. (b) The initial million grid boxes are classified to be in the interior or in the Wada boundary. (c) Prototypical computational performance: after the maximum there is an exponential decay of the number of steps needed to check the Wada property. The fit of the exponential decay shown in (d) reflects the fractal nature of the basins.

- *Bisection method for Wada basins*

In case that the Wada property is tested in a system with three basins, there is a shortcut of the method that speeds up computation dramatically. Once the algorithm has chosen two points in a box and is ready to look for the third color between them, one can use an oriented version of the method making a small modification. Imagine we have a blue point at left and a red point at right. We compute the central point and we find it is red. Then, instead of computing two more points in the next step, we only compute one more point, which is the middle point of the blue and the most recent red (that is in the middle of our two leftmost points). In the following step we would use the same procedure, computing only one point at each step. Using this modification, the computational effort grows linearly with the number of steps q instead of exponentially. Although this method makes the computation incredibly fast, a proper generalization for more than three basins is still missing.

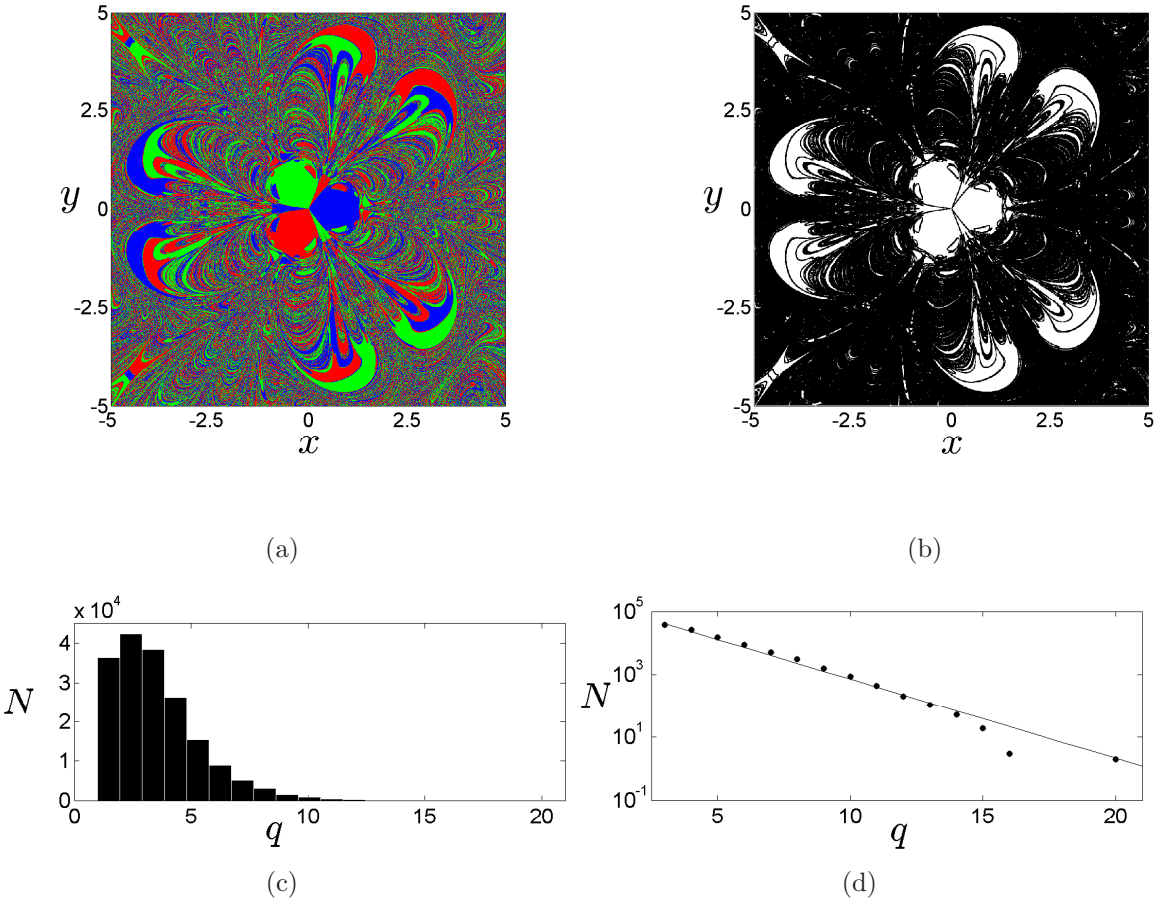

Figure B.3. Magnetic pendulum. (a) Basins of attraction for a simplified model of a magnetic pendulum with three magnets. (b) Our method classifies all the boxes either in the interior or in the boundary of three basins. (c) In this case the computational effort is larger due to the lost of fractality at infinity. (d) The last points do not follow the tendency because of the lost of the Wada property upon infinite magnification.

[1] J. Aguirre and M. A. F. Sanjuán, "Unpredictable behavior in the Duffing oscillator: Wada basins", *Physica D* **171**, 41–51 (2002).

[2] J. Aguirre, J. C. Vallejo, and M. A. F. Sanjuán, "Wada basins and chaotic invariant sets in the Hénon-Heiles system", *Phys. Rev. E* **64**, 066208 (2001).

[3] A. E. Motter, M. Gruiz, G. Károlyi, and T. Tél, "Doubly transient chaos: generic form of chaos in autonomous dissipative systems", *Phys. Rev. Lett.* **111**, 194101 (2013).

Appendix C: On history functions

Delay differential equations need an infinite set of initial conditions to determine its state before the action of the delayed terms. In other words, they need an initial history function defined in the interval $[-\tau, t_0]$. In most of the present literature, little or even no attention at all is paid to these initial history functions. Most of the times, the history is chosen to be constant or random for simplicity, but there is no deeper discussion about this delicate issue. Nevertheless, systems with delay can display multistability, transient chaos, chaos and hyperchaos. Therefore, the choice of different history functions determines the fate of delayed systems, so they play a central role in the dynamics of DDEs and must be examined carefully. To illustrate our arguments along this appendix, we will use the delayed action oscillator for simplicity

$$\dot{x} + x(x^2 - 1) - \alpha x_\tau = 0. \tag{C.1}$$

The first problem that one has to face to integrate a DDE is the choice of the history. In principle, the general properties of a system do not depend on the histories, in the same way that the properties of a usual system do not depend on the initial conditions. Thus, a very common choice is to set histories randomly. This choice presents practical and conceptual problems. The first one is that an infinite number of random points is needed. If the integration scheme uses interpolation, then a random value at the interpolated points must be provided, making the history a pathological fractal function made out of random values, which is hard to assume conceptually. The second problem is that in case that the system is sensitive to initial conditions, the choice of the history must be made carefully: one could interpret as a general result what actually happens only for some histories, and if these histories are random the results would be impossible to reproduce.

Therefore, we find much easier from a practical and conceptual point of view to choose deterministic history functions. The simplest option is to choose a constant history function:

$$x(t) = A, \, \forall \, t \in [-\tau, t_0] \, , \tag{C.2}$$

where $A \in \mathbb{R}$. Fixing the initial history function to a constant value is equivalent to suppose that the system has remained at some constant value for a time equal to the delay τ. If the constant value is not a fixed point the situation described is most of the times physically impossible (imagine a pendulum frozen for a while out of its equilibrium state), and if the history has a constant value equal to a fixed point then it will not evolve. Thus, other options should be considered.

A natural solution is to integrate the system without delay and consider that the delayed term starts acting at some time t_0. If we want the system to evolve naturally in the interval $[-\tau, t_0]$, we can integrate the equation without delay for that interval and then include the delayed term. The simplicity of the delayed action oscillator (Eq. C.1) allows us to make this integration analytically, although the same procedure can be applied numerically for any other system.

For instance, we can think that the term αx_τ is simply αx in the interval $[-\tau, t_0]$. In that case, the history function is given as the solution of the following ODE

$$\dot{x} + x(x^2 - 1) - \alpha x = 0. \tag{C.3}$$

After simple integration we get that our natural history function for every $t \in [-\tau, t_0]$ is

$$x(t) = \pm x_0 e^{(1+\alpha)(t+\tau)} \sqrt{\frac{1+\alpha}{1+\alpha - x_0^2(1 - e^{2(1+\alpha)(t+\tau))}}}. \tag{C.4}$$

We can see in this equation that when $t = -\tau$ the system is in $x = x_0$, that is, we let the system evolve naturally from the initial condition x_0. Also, we can make the limit $t \to \infty$ and see that if there was no delayed term and $\alpha > -1$, the system would finally end in one of the equilibria $x = \pm\sqrt{1+\alpha}$.

Let us continue deepening into the physical interpretation of the history. For instance, another physically reasonable situation would be to consider that the delayed term starts acting at $t = t_0$. This is simply a particular case of the preceding case where $\alpha = 0$ in the history function. A last attempt to include a *natural* history could be to get a piece of the solution of the DDE and use it as initial history function. But the problem is how to get that first solution of the DDE, we enter into a recursive problem that forces us to choose one history function the sooner or the later, attending to the criteria we consider more appropriate in each case.

Another approach is to play with various history functions in order to contrast the differences between DDEs and ODEs, sometimes leading to striking results. For instance, it is possible to construct a history such that in $t = 0$ the trajectory *passes through* one equilibrium. For instance choosing for every $t \in [-\tau, t_0]$

$$x(t) = e^{-At}\sqrt{1+\alpha}. \tag{C.5}$$

implies an exponential decay to the positive fixed point as the system goes from $t = -\tau$ to $t = 0$. Actually, with this history the system does not strictly pass through one of the equilibria, since that would mean that all the derivatives were equal to zero. However, if we only look at the time series, we see that $x = x_{eq}$ at $t = t_0 = 0$, and thereafter the system evolves differently depending on the history. It can even end in the other equilibrium point or display autonomous oscillations, as depicted in Fig. C.1(a). This happens because the system remembers a past state away from the equilibrium, making possible a switch to a different attractor without the action of any external forcing, but only its own memory.

Up to this point, we have restricted our analysis to history functions with only one parameter. Nonetheless, we can choose history functions with as many parameters as we want. We could even try to set an orthogonal basis for the history functions, but we always have to restrict ourselves to finite representations [1]. The phase space of a DDE is infinite dimensional, so the basins of attraction for different parameters are simply different subspaces of the infinite dimensional space of history functions. Therefore, choosing two parameters history functions is as fair as choosing

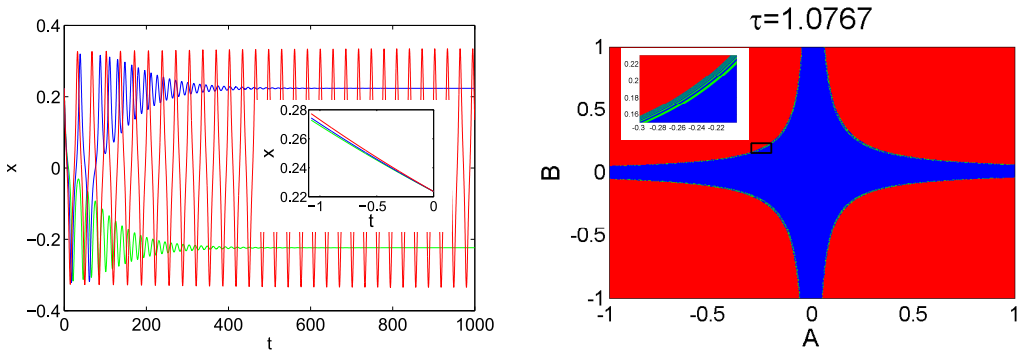

(a) (b)

Figure C.1. (a) Comparison of three time series for Eq. C.1 with $\alpha = -0.95, \tau = 1.0767$. The history function is $x(t) = e^{-At}\sqrt{1+\alpha}$. The three time series have been integrated with slightly different values for A: the blue line is for $A = 0.185$, $A = 0.19$ corresponds to green and $A = 0.2$ is in red. In the inset we can see the three different histories and how all of them "pass through" the equilibrium $x = \sqrt{1+\alpha}$ at $t = 0$, but the behavior in each case is completely different. (b) Basin of attraction of the delayed action oscillator (Eq. C.1) for $\alpha = -19/20$ and histories of the form $x(t) = A\sin(Bt) + \sqrt{1+\alpha}$. This kind of histories reflects oscillations around the fixed point.

one parameter history functions and can give more information. For instance, we can choose histories of the form

$$x(t) = A + Bt \tag{C.6}$$

for every $t \in [-\tau, t_0]$. This the chosen option along Chapter 3, where we illustrate the sensitivity of delayed systems.

Although the properties of the system do not depend on the choice of these history functions[1], they can have different physical meanings and produce rather different basins of attraction. For instance, we can think in a history consisting of oscillations around a fixed point,

$$x(t) = A\sin(Bt) + \sqrt{1+\alpha} \tag{C.7}$$

for every $t \in [-\tau, t_0]$. This kind of histories also passes through a fixed point, as the histories given by Eq. C.5, but instead of decaying exponentially to the fixed point, they represent oscillations around $\sqrt{1+\alpha}$. The basins produced by these histories share the dynamical properties of the previous ones, but they look completely different because we are looking to a different subspace (see. Fig. C.1(b)). It is also important to notice that the only way to give an infinite set of initial conditions is by means of a function, so these basins of attraction depending on different parameters are the only basins of attraction that can be constructed.

[1]The only requirement for these history functions is to be continuous.

[1] S. Leng, W. Lin, and J. Kurths, "Basin stability in delayed dynamics", *Sci. Rep.* **6**, 21449 (2016).

Appendix D: Proof of the log 2 criterion

The log 2 criterion is a sufficient condition to prove the fractality of the basin boundaries. It is based on the concept of *boundary basin entropy*, defined in Chapter 6 as

$$S_{bb} = \frac{S}{N_b}, \tag{D.1}$$

where N_b is the number of boxes containing more than one color, that is, the number of boxes in the boundaries, and

$$S = \sum_{i=1}^{N} S_i = \sum_{i=1}^{N} \sum_{j=1}^{m_i} p_{i,j} \log \left(\frac{1}{p_{i,j}} \right). \tag{D.2}$$

Let us now suppose that the boundaries separating the basins are smooth. In that case, the number of boxes lying in the boundary separating two basins grows as

$$N_2 = n_2 \varepsilon^{-(D-1)}, \tag{D.3}$$

being D the dimension of the phase space. For $D = 2$, the boundary would be a line, for $D = 3$, it would be a surface and so forth. However, there might be some boxes N_k lying in the boundaries of $k > 2$ different basins. These boxes are in the intersection of at least two subspaces of dimension $D - 1$, that is, they are in the intersection of two smooth boundaries. For instance, in $D = 2$ this simply means that two or more smooth curves intersect in a point or collection of points, and in $D = 3$ two or more smooth surfaces intersect forming smooth curves. Thus, the dimension of the subspace separating more than two basins must be $D - 2$, and the boxes N_k belonging to this subspace must grow like

$$N_k = n_k \varepsilon^{-(D-2)}. \tag{D.4}$$

Taking into account that the total number of boxes grows like $N = \tilde{n} \varepsilon^{-D}$, we can express N_2 in terms of N as

$$N_2 = n_2 \left(\frac{N}{\tilde{n}} \right)^{\frac{D-1}{D}}, \tag{D.5}$$

and for the boundary boxes separating more than two basins N_k, we have

$$N_k = n_k \left(\frac{N}{\tilde{n}} \right)^{\frac{D-2}{D}}. \tag{D.6}$$

At this point, we recall that the maximum possible value of S in a box with m different colors is $S = \log m$, which is the Boltzmann expression for the entropy of m equiprobable microstates. Then, we can find that all the boxes in the boundary of two basins have $S \leqslant \log 2$, while for boxes in the boundary of $k > 2$ different basins, $S \leqslant \log k$ holds. Notice that the equality of the previous equations would

be possible only in a pathological case where all the boxes in the boundaries have equal proportions of the different colors.

Then, the basin entropy S_{bb} for this hypothetical system with smooth boundaries is

$$S_{bb} \leq \frac{N_2 \log 2 + N_k \log k}{N_2 + N_k}. \tag{D.7}$$

By substituting N_2 and N_k by Eqs. D.5-D.6, we obtain the following expression

$$S_{bb} \leq \frac{n_2 \left(\frac{N}{\tilde{n}}\right)^{\frac{D-1}{D}} \log 2 + n_k \left(\frac{N}{\tilde{n}}\right)^{\frac{D-2}{D}} \log k}{n_2 \left(\frac{N}{\tilde{n}}\right)^{\frac{D-1}{D}} + n_k \left(\frac{N}{\tilde{n}}\right)^{\frac{D-2}{D}}}, \tag{D.8}$$

which can be simplified as

$$S_{bb} \leq \frac{n_2 N \log 2 + n_k \tilde{n} \log k}{n_2 N + n_k \tilde{n}}, \tag{D.9}$$

where $\tilde{n}, n_2, n_k$ are constants. Finally, we can take the limit of the previous inequality for a large number of boxes, that is $N \to \infty$, leading to

$$\lim_{N \to \infty} S_{bb} \leq \log 2. \tag{D.10}$$

Therefore, we have proven that if the boundaries are smooth, then $S_{bb} \leq \log 2$, which is the same as to say that if $S_{bb} > \log 2$, then the boundaries are not smooth, i.e., they are fractal. This is what we call the $\log 2$ criterion.

As shown in Chapter 7, this criterion is especially useful for experimental situations where the resolution cannot be arbitrarily chosen. In these cases we have a fixed value $\varepsilon > 0$. Nevertheless, if we take a sufficient large number of boxes N, then the $\log 2$ criterion holds. Moreover, the equality of Eq. D.10 never takes place, so that there is some room for the possible deviations caused by the impossibility of making an infinite number of simulations or experiments.

Curriculum Vitae

Publicaciones

- A. Daza, A. Wagemakers, B. Georgeot, D. Guéry-Odelin and, M. A. F. Sanjuán. "Chaotic dynamics of propagating matter waves", in progress.

- A. Daza, A. Wagemakers, B. Georgeot, D. Guéry-Odelin and, M. A. F. Sanjuán. "Basin Entropy", submitted (2016).

- A. Daza, A. Wagemakers and, M.A.F. Sanjuán, "Wada property in systems with delay", submitted (2016).

- A. Daza, A. Wagemakers, M.A.F. Sanjuán and, J. A. Yorke, "Testing for Wada basins", *Scientific Reports* **5**, 16579 (2015).

- A. Wagemakers, A. Daza and, M.A.F. Sanjuán, "Electronic modeling of synthetic genetic networks" in Handbook of Bioelectronics. Directly interfacing electronics and biological systems, eds. S. Carrara and K. Iniewski, Cambridge University Press, 266-274 (2015).

- A. Daza, A. Wagemakers and, M.A.F. Sanjuán, "Strong sensitivity of the vibrational resonance induced by fractal structures", *International Journal of Bifurcation and Chaos* **23**, 1350129 (2013).

- A. Daza, A. Wagemakers, S. Rajasekar and, M.A.F. Sanjuán, "Vibrational resonance in a time-delayed genetic toggle switch", *Communications in Nonlinear Science and Numerical Simulation* **18**, 411-416 (2013).

Presentaciones en congresos y seminarios

- **Conferencia**: Third International Workshop-School on Chaos, Complexity and Dynamics in Biological Networks
  Póster: Vibrational resonance in a time-delayed genetic toggle switch
  Autores: Álvar Daza, Alexandre Wagemakers, Shanmuganathan Rajasekar, Miguel A. F. Sanjuán
  Lugar y Fecha: Cargèse, Córcega, Francia, del 28 de mayo al 2 de junio de 2012

- **Conferencia**: Conference in honour of Michael Mackey's 70th birthday. Mathematical biology
  Presentación oral: Vibrational resonance phenomena in a time-delayed genetic toggle switch
  Autores: Álvar Daza, Alexandre Wagemakers, Miguel A. F. Sanjuán
  Lugar y Fecha: Univ. Lyon, Lyon, Francia, del 3 de junio al 6 de junio de 2013

- **Seminario**: Seminars at the IRSAMC 2016
  Presentación oral: Cold atoms and basin entropy
  Autores: Álvar Daza, Alexandre Wagemakers, Bertrand Georgeot, David Guéry-Odelin, Miguel A. F. Sanjuán
  Lugar y Fecha: Univ. Paul Sabatier, Toulouse, Francia, 24 de marzo de 2016

- **Seminario**: Seminars Prof. Yorke's Doctor Honoris Causa
  Presentación oral: Unpredictability induced by delay
  Autores: Álvar Daza, Alexandre Wagemakers, Miguel A. F. Sanjuán
  Lugar y Fecha: Univ. Rey Juan Carlos, Móstoles, Madrid, Spain, 30 January 2014

- **Seminario**: Seminars on the visit of Prof. Macau to the URJC
  Presentación oral: Vibrational resonance phenomena in a time-delayed genetic toggle switch
  Autores: Álvar Daza, Alexandre Wagemakers, S. Rajasekar Miguel A. F. Sanjuán
  Lugar y Fecha: Univ. Rey Juan Carlos, Móstoles, Madrid, Spain, 4 June 2014

- **Seminario**: Seminars on the visit of Prof. Sanz-Serna to the URJC
  Presentación oral: Basin entropy
  Autores: Álvar Daza, Alexandre Wagemakers, Miguel A. F. Sanjuán
  Lugar y Fecha: Univ. Rey Juan Carlos, Móstoles, Madrid, Spain, 22 April 2015

- **Seminario**: Seminars on the visit of Prof. Yorke to the URJC
  Presentación oral: Basin entropy
  Autores: Álvar Daza, Alexandre Wagemakers, Miguel A. F. Sanjuán
  Lugar y Fecha: Univ. Rey Juan Carlos, Móstoles, Madrid, Spain, 19 May 2015

- **Seminario**: Máster en Modelización y Física de Sistemas Complejos
  Presentación oral: Resonancia en sistemas biestables con retardo
  Autores: Álvar Daza, Alexandre Wagemakers, Miguel A. F. Sanjuán
  Lugar y Fecha: Univ. Rey Juan Carlos, Móstoles, Madrid, Spain, 18 April 2013

- **Seminario**: Máster en Modelización y Física de Sistemas Complejos
  Presentación oral: Propiedad de Wada y sistemas con retardo
  Autores: Álvar Daza, Alexandre Wagemakers, Miguel A. F. Sanjuán
  Lugar y Fecha: Univ. Rey Juan Carlos, Móstoles, Madrid, Spain, 12 March 2014

- **Seminario**: Máster en Modelización y Física de Sistemas Complejos
  Presentación oral: Basin entropy
  Autores: Álvar Daza, Alexandre Wagemakers, Miguel A. F. Sanjuán
  Lugar y Fecha: Univ. Rey Juan Carlos, Móstoles, Madrid, Spain, 16 March 2015

Proyectos de investigación

- **Título del proyecto**: Dinámica No Lineal de Sistemas Complejos y Aplicaciones Interdisciplinares (FIS2009-09898)
  Entidad financiadora: Ministerio de Ciencia e Innovación
  Duración desde: 1 de enero 2010 **hasta**: 31 de diciembre 2013
  Investigador principal: Miguel Angel Fernández Sanjuán
  Tipo de paticipación del doctorando: Miembro investigador
  Cuantía de la subvención: 194.810, 01 euros

- **Título del proyecto**: Dinámica No Lineal de Sistemas Complejos (FIS2013-40653-P)
  Entidad financiadora: Ministerio de Economía y Competitividad
  Duración desde: 1 de enero 2014 **hasta**: 31 de diciembre 2016
  Investigador principal: Miguel Angel Fernández Sanjuán
  Tipo de paticipación del doctorando: Miembro investigador
  Cuantía de la subvención: 54.000 euros

Estancias de investigación

- **Lugar**: Toulouse, Francia
  Centro y Departamento: Université Paul Sabatier, Institut de Recherche

sur les Systèmes Atomiques et Moléculaires Complexes
Fecha: 8 septiembre-8 diciembre 2015
Financiación: Programme Investissements d'Avenir ANR-11-IDEX-0002-02 y ANR-10-LABX-0037-NEXT

- **Lugar**: Toulouse, Francia
  Centro y Departamento: Université Paul Sabatier, Institut de Recherche sur les Systèmes Atomiques et Moléculaires Complexes
  Fecha: 20 marzo-26 marzo 2016
  Financiación: Programme Investissements d'Avenir ANR-11-IDEX-0002-02 y ANR-10-LABX-0037-NEXT

Resumen

En esta sección se resumen los objetivos y las principales conclusiones de la presente tesis. Al final se incluye también una breve exposición de la metodología utilizada.

Introducción

Esta tesis constituye un estudio sobre distintos aspectos de la impredecibilidad en sistemas caóticos. Tanto la forma como el fondo de la misma es eminentemente no lineal, lo cual quiere decir que los temas tratados en los diferentes capítulos se entremezclan los unos con los otros alimentándose mutuamente. Es conveniente entender el contexto en que se sitúa la dinámica no lineal para comprender mejor el espíritu y metodología empleados en esta tesis.

Puede decirse que ha habido tres grandes revoluciones a lo largo de la Física del siglo XX: la teoría de la relatividad, la mecánica cuántica y la teoría del caos. Cada una de estas revoluciones ha traído consigo avances impresionantes en el conocimiento del universo que nos rodea. No obstante, al mismo tiempo, han impuesto restricciones insalvables -según la ciencia actual- a los límites de dicho conocimiento. La relatividad impuso un límite a la velocidad de transmisión de la información, la mecánica cuántica impuso un límite a la precisión en las medidas y la teoría del caos puso de manifiesto las dificultades de la predicción en sistemas no lineales. Son precisamente estos límites al conocimiento los que se investigan en esta tesis, especialmente los relativos a la predicción del comportamiento a largo plazo de los sistemas dinámicos no lineales.

El estudio de la llamada dinámica no lineal comporta diversos conceptos ligados íntimamente entre sí, que son invocados y utilizados repetidamente en el transcurso de la presente tesis. La teoría del caos comenzó a finales del siglo XIX con los trabajos pioneros de Poincaré sobre los tres cuerpos. Sin embargo, hubo que esperar al desarrollo de los ordenadores para que la disciplina floreciese de la mano de Edward Lorenz, Steven Smale, James A. Yorke y otros científicos. Aunque la definición de caos sigue siendo tema de debate, hay una idea fundamental que todas las definiciones comparten: la dependencia sensible a las condiciones iniciales. Esto significa que una pequeñísima incertidumbre en las condiciones iniciales crece exponencialmente en el tiempo, provocando la imposibilidad de predicción en el largo plazo.

La ideas de caos y dinámica no lineal están íntimamente ligadas a la idea de geometría fractal. El término fractal fue acuñado por Benoît Mandelbrot para referirse a objetos geométricos que estaban de algún modo *rotos* y presentaban *rugosidades*, en contraposición a la geometría euclidiana donde las formas son suaves. Los fractales son figuras que guardan algún grado de autosimilitud, esto es, que son complejas en todas las escalas. La aparición de estructuras fractales y su inevitable complejidad son una de las causas de impredecibilidad que se estudian a fondo en esta tesis.

Las estructuras fractales son fundamentales para comprender los sistemas disipativos en la dinámica no lineal. Los sistemas disipativos intercambian energía/materia con el entorno. Este tipo de sistemas suelen dar origen a estructuras estables conocidas como atractores. El conjunto de condiciones iniciales que lleva a uno de estos atractores se denomina cuenca de atracción, y en sistemas caóticos suelen tener estructura fractal. En los sistemas conservativos también se puede hablar de cuencas, en este caso de escape, como el conjunto de condiciones iniciales cuyas trayectorias atraviesan una cierta región del espacio de fases. El estudio de las cuencas de atracción y de escape proporciona mucha información sobre la dinámica de los sistemas no lineales y su impredecibilidad. Gran parte de la presente tesis está dedicada al estudio y caracterización de dichas cuencas.

Si la mecánica cuántica impone límites a la precisión de las medidas, provocando inevitables incertidumbres que se tornan catastróficas en los sistemas no lineales, la relatividad también juega un papel crucial en lo referente a la impredecibilidad. Concretamente, el hecho de que la información tarde un cierto tiempo en transmitirse hace obligado el uso de ecuaciones diferenciales con retardo en algunas situaciones. En estas ecuaciones, la evolución de algunos términos no depende del estado presente del sistema, sino de un estado anterior. Las inestabilidades que introduce el retardo pueden provocar la aparición de estructuras fractales que dificultan la predicción del estado asintótico al que tiende el sistema.

Esta sensibilidad de los sistemas no lineales comporta que una pequeña desviación de las condiciones iniciales puede provocar grandes cambios, por lo que es de suponer que las perturbaciones externas puedan tener también efectos importantes sobre la dinámica de dichos sistemas. En concreto, las resonancias no lineales son un tema de gran interés teórico y práctico que se aborda en esta tesis.

Aunque el origen de la dinámica no lineal sea físico-matemático, uno de sus grandes valores es su capacidad para traspasar las barreras entre disciplinas científicas. Desde la biología a la meteorología, pasando por la ingeniería o la astrofísica, muchos problemas de diferentes disciplinas científicas pueden estudiarse bajo el prisma único que proporciona la dinámica no lineal. Esta tesis comienza con el estudio de un interruptor genético y termina con la propagación de ondas de materia. Aunque el estudio de estos sistemas es interesante *per se*, el espíritu de mis investigaciones es más ambicioso. No sólo se pretenden estudiar sistemas dinámicos de interés, sino que se intentan desarrollar técnicas útiles en el contexto de la dinámica no lineal, y por lo tanto útiles en la resolución de multitud de problemas en diversas áreas del conocimiento científico.

Resonancia vibracional en un interruptor genético con retardo

En este capítulo se investigan los efectos de dos perturbaciones periódicas de frecuencias muy diferentes en un sistema de interés biológico conocido como interruptor genético. Los principales hitos desarrollados en este capítulo son los siguientes:

- Demostramos que una perturbación periódica de alta frecuencia puede optimizar la respuesta de un interruptor genético con retardo a otra perturbación

externa de baja frecuencia. En otras palabras, demostramos que un interruptor genético con retardo puede mostrar el fenómeno conocido como resonancia vibracional.

- Mediante simulaciones numéricas, mostramos el efecto sobre la resonancia de la variación de diferentes parámetros. Cabe destacar la aparición de la denominada *resonancia sin ajuste* cuando se varían los parámetros de la perturbación lenta, y sobre todo la posibilidad de modificar la amplitud de la perturbación rápida al modificar su frecuencia. Este resultado permite obtener resonancias equivalentes empleando perturbaciones menores.

- Debido al tiempo empleado por los procesos biológicos de traducción, ensamblaje de las proteínas y degradación, aparecen retardos en el sistema dinámico. Aunque los retados en la traducción y acoplamiento son relevantes desde un punto de vista biológico, desde el punto de vista de la dinámica el más interesante es retardo en la degradación. Demostramos que el retardo en la degradación puede inducir inestabilidades en el sistema a través de una bifurcación de Hopf, provocando un aumento de su sensibilidad ante las perturbaciones externas.

Resonancia vibracional ultrasensible

La resonancia vibracional tiene el inconveniente de que frecuentemente necesita perturbaciones muy grandes para producirse. Presentamos un nuevo tipo de resonancia vibracional llamada resonancia vibracional ultrasensible, que aprovechando la sensibilidad de los sistemas no lineales, provoca la resonancia vibracional mediante perturbaciones mínimas.

- Analizamos algunos de los problemas conceptuales de la resonancia vibracional. Intentamos buscar un tipo de resonancia que esté en consonancia con el concepto original de Galileo, en el que una pequeña perturbación de características particulares es capaz de inducir oscilaciones de gran amplitud.

- Demostramos cómo la sensibilidad que induce el retardo en un sistema dinámico puede provocar que pequeñas perturbaciones de la frecuencia adecuada hagan entrar al sistema en resonancia.

- Las curvas de resonancia en presencia de estas inestabilidades son muy diferentes de las curvas de resonancia vibracional habituales. La resonancia ultrasensible muestra curvas de resonancia fractales, donde es posible encontrar picos de resonancia arbitrariamente juntos.

- Indagamos la razón última de este tipo de resonancia y mostramos su relación con la aparición de estructuras fractales en el espacio de fases. Esta situación no tiene que ser inducida necesariamente por un término de retardo, sino que el fenómeno de la resonancia ultrasensible es más general: basta con que

el sistema presente varios atractores de diferente amplitud cuyas cuencas de atracción tengan fronteras fractales.

Test para cuencas de Wada

Los fractales presentan a menudo propiedades sorprendentes. Muestra de ello son las cuencas de Wada, en las que tres o más conjuntos comparten una misma frontera. Esta topología tan contraintuitiva provoca que los sistemas dinámicos con la propiedad de Wada tengan una impredecibilidad única. A continuación presentamos una lista de los resultados y conclusiones de este capítulo sobre la propiedad de Wada:

- Repasamos el origen matemático-topológico de la propiedad de Wada y su conexión con los sistemas dinámicos. En particular, prestamos atención a lo que denominamos la propiedad de Wada disconexa, en la que tres o más conjuntos disconexos comparten una misma frontera. El método clásico para probar que un sistema posee la propiedad de Wada no funciona en este tipo de sistemas, ni en otros casos como el espacio de parámetros o el espacio de historias en los sistemas con retardo.

- Desarrollamos un método para comprobar la propiedad de Wada en cualquier tipo de sistema. El algoritmo consta de varios pasos: se coloca una malla sobre las cuencas, se identifican los puntos de la malla que son frontera de dos o más cuencas, y se procede mediante un método iterativo hasta que se demuestra que todos los puntos en la frontera hacen frontera con todos los conjuntos, o bien se supera el número de pasos permitido.

- El método es ilustrado mediante simulaciones numéricas con el oscilador de Duffing forzado y con el método de Newton para encontrar raíces complejas de la unidad. Mostramos la eficiencia tanto en casos de Wada conexo como disconexo, y para cualquier número de atractores (cuencas) del sistema.

- Proponemos un indicador numérico del grado de Wada del sistema. Este indicador es especialmente útil para los casos denominados parcialmente Wada, en los que algunos puntos presentan la propiedad de Wada pero no todos.

Propiedad de Wada en sistemas con retardo

En los primeros capítulos se expone la importancia del retardo en la dinámica de los sistemas no lineales. En éste, nos proponemos estudiar la propiedad de Wada en sistemas con retardo, gracias a la técnica desarrollada en el capítulo anterior. Estos son los hechos más notables presentados a lo largo del capítulo:

- Estudiamos el sistema llamado oscilador de acción retardada, utilizado en la modelización del fenómeno climático de El Niño. Es un sistema de una única variable en la que el retardo hace posible la aparición de oscilaciones. Es más,

demostramos que en el espacio de las historias de este sistema aparece lo que denominamos una línea de Wada, es decir, una curva en la que todos sus puntos separan tres cuencas de atracción.

- Debido a la similitud entre la topología del oscilador de acción retardada y el oscilador de Duffing, incluimos un forzamiento periódico en el sistema retardado para estudiar la eventual aparición de la propiedad de Wada.

- Demostramos la aparición de caos transitorio y estructuras fractales en el oscilador de acción retardada con forzamiento periódico. Hasta donde nuestro conocimiento alcanza, es la primera vez que un retardo en un término lineal es capaz de provocar dinámica caótica. El retardo otorga al sistema las dimensiones necesarias para poder desplegar caos.

- El oscilador de acción retardada con forzamiento periódico muestra cuencas de atracción fractales que dan cuenta de una gran impredecibilidad. No obstante, el test de Wada muestra que estas cuencas tienen únicamente la propiedad de Wada parcial.

- Analizamos las diferencias entre el oscilador de acción retardada y el oscilador de Duffing, y decidimos modificar el sistema retardado incluyendo el retardo en el término cúbico. Éste sistema es capaz de mostrar la propiedad de Wada en base a nuestro test.

- Por vez primera comprobamos la propiedad de Wada en un sistema con retardo. De esta forma, podemos afirmar que el retardo no sólo es capaz de inducir dinámica caótica, sino también la propiedad de Wada, que dota a los sistemas de una impredecibilidad única.

- Puesto que los sistemas con retardo poseen infinitas dimensiones, es la primera vez que se encuentra la propiedad de Wada en infinitas dimensiones. Simplemente cambiando el número de parámetros con los que se definen las funciones historia, podemos conseguir cuencas de dimensión arbitraria y siempre muestran la propiedad de Wada.

Entropía de las cuencas

En el estudio de la impredecibilidad asociada a las cuencas de atracción, a menudo se realizan afirmaciones vagas cuando se compara la *fractalidad* de un sistema para distintos parámetros o determinadas situaciones particulares como la anteriormente estudiada propiedad de Wada. En este capítulo, presentamos el concepto de entropía de las cuencas, una forma natural de cuantificar dicha impredecibilidad. Estos puntos resumen lo esencial de la investigación:

- Dividimos las cuencas de atracción en *cajas* y consideramos cada una de estas cajas como una variable aleatoria, siendo sus posibles valores los atractores

que contenga. Aplicamos la entropía de Gibbs para cada caja y definimos la entropía de las cuencas promediando el valor de la entropía de todas las cajas. Este procedimiento también es válido para cuencas de escape en sistemas conservativos. El algoritmo para calcular la entropía de las cuencas es rápido y sencillo, y permite asociar a cada cuenca un número que cuantifica su impredecibilidad.

- Realizando algunas hipótesis extra para facilitar los cálculos, podemos identificar los distintos factores que contribuyen a la entropía de las cuencas. Estos factores son: el tamaño de la frontera, la dimensión de incertidumbre y el número de atractores. Además, analizamos la propiedad de Wada desde la perspectiva que nos otorga esta nueva herramienta.

- Mediante diversos sistemas dinámicos paradigmáticos, comprobamos la dependencia de la entropía de las cuencas con cada uno de los factores anteriormente señalados. Aunque aislar el efecto de cada contribución es prácticamente imposible, los resultados computacionales avalan las predicciones teóricas.

- Aplicando la metodología de la entropía de las cuencas únicamente a las cajas que se encuentran en la frontera, encontramos una condición suficiente para determinar si una frontera es fractal. Si el valor de la entropía en la frontera es mayor que $\log 2$, entonces la frontera es fractal. Ésta es una condición suficiente pero no necesaria, ya que de hecho sólo se puede cumplir en sistemas con tres o más atractores.

- Mostramos ejemplos de aplicación utilizando el oscilador de Duffing forzado. Variando la amplitud y la frecuencia del forzamiento realizamos un mapa de la entropía del sistema. Este mapa nos muestra los valores de los parámetros para los cuales es más difícil determinar el estado final del sistema.

- Proponemos un método tipo Monte Carlo para calcular la entropía de las cuencas que proporciona valores bastante precisos de la entropía de las cuencas con un costo computacional mucho menor. Este procedimiento puede utilizarse para sondear las regiones de parámetros donde un sistema dinámico presenta cuencas de atracción más interesantes.

- Aplicamos el criterio del $\log 2$ en el oscilador de Duffing forzado y comprobamos su validez. La gran ventaja de este método es que permite demostrar que un sistema tiene fronteras fractales a una determinada resolución, lo cual abre nuevas puertas para encontrar estructuras fractales experimentalmente.

Dinámica caótica en ondas de materia

En los últimos años, el scattering de átomos ultrafríos ha abierto nuevas posibilidades en interferometría. A pesar de la naturaleza cuántica de este tipo de experimentos,

algunas técnicas de la dinámica no lineal pueden emplearse para comprender y caracterizar mejor el sistema. Concretamente, el concepto de la entropía de las cuencas tiene gran parecido con el procedimiento experimental en estos dispositivos. He aquí los principales resultados y conclusiones presentados en este capítulo:

- Se presenta un sistema de dos láseres cruzados empleado comúnmente en este tipo de experimentos y que permite obtener diferentes regímenes (interruptor, separador). La mayor parte de los resultados experimentales pueden reproducirse empleando una aproximación clásica en dos dimensiones.

- El cómputo de la entropía de las cuencas presenta semejanzas con el procedimiento experimental. En ambos casos se consideran conjuntos de trayectorias y se tiene acceso a su estado asintótico, es decir, se sabe la proporción de átomos/trayectorias que escapa por cada una de las ramas del doble haz.

- Proponemos un procedimiento por el cual se puede calcular la entropía de las cuencas a partir de las medidas experimentales directamente. Las simulaciones numéricas indican que si la velocidad con la que inciden las partículas es suficientemente baja, se puede detectar la presencia de fronteras fractales haciendo uso del criterio del $\log 2$ expuesto en el capítulo anterior. Es decir, se puede probar experimentalmente la presencia de estructuras fractales en el espacio de fases de este sistema.

- Otras herramientas de la dinámica no lineal, como la estabilidad de las cuencas y los tiempos de escapes se pueden utilizar para caracterizar la dinámica caótica del sistema. En concreto, la estabilidad de las cuencas sirve para calcular la eficiencia de los regímenes de interruptor y separador del sistema, y los tiempos de escape permiten acceder a información relativa a la dimensión de la silla caótica.

Metodología

La metodología utilizada para elaborar esta tesis ha sido fundamentalmente de carácter teórico-computacional. Se han utilizado diversos modelos matemáticos no lineales de orígenes dispares, que muchas veces han servido para desarrollar y probar métodos generales, aplicables a otros sistemas dinámicos.

La formulación matemática de estos modelos ha sido en forma de mapas discretos, ecuaciones diferenciales ordinarias y ecuaciones diferenciales con retardo. Para su resolución se han empleado métodos tipo Runge-Kutta en la mayoría de las ocasiones, ajustando las características del integrador a cada caso, de tal modo que se obtuviera el mejor compromiso posible entre fiabilidad de los resultados y tiempo de cómputo. Además, para realizar los cálculos más pesados se han utilizado los recursos del Grupo de Dinámica No Lineal, Teoría del caos y Complejidad de la URJC: varios

servidores de alto rendimiento[2] y un cluster[3] que permite paralelizar los procesos obteniendo un poder de computación superior. La programación se ha realizado fundamentalmente en Matlab, C, C++, Fortran y MPI para los procesos en paralelo.

[2]Dell PowerEdge 2900 (2 unidades), PowerEdge T710 (2 unidades) y PowerEdge T620 (1 unidad)

[3]El cluster está basado en sistemas PowerEdge R410, R510 y R720 de Dell, posee cerca de 100 cores y 180 GB de memoria RAM.